2021

PHARMACOLOGICAL EFFECTS OF EBSELEN AND OTHER NOVEL ORGANOSELENIUM COMPOUNDS IN VITRO AND IN THE MOUSE MODEL OF VULVOVAGINAL CANDIDIASIS

Suvidha M. Menon

PHARMACOLOGICAL EFFECTS OF EBSELEN AND OTHER NOVEL ORGANOSELENIUM COMPOUNDS *IN VITRO* AND IN THE MOUSE MODEL OF VULVOVAGINAL CANDIDIASIS

A dissertation submitted in partial fulfillment of the

requirements for the degree of

DOCTOR OF PHILOSOPHY

to the faculty of the

DEPARTMENT OF GRADUATE DIVISION

of

COLLEGE OF PHARMACY AND HEALTH SCIENCES

at

ST. JOHN'S UNIVERSITY

New York

by

SUVIDHA M. MENON

Date Submitted: _____ Date Approved: _____

_____ _____

SUVIDHA M. MENON Dr. BLASE BILLACK

ABSTRACT

PHARMACOLOGICAL EFFECTS OF EBSELEN AND OTHER NOVEL ORGANOSELENIUM COMPOUNDS IN VITRO AND IN THE MOUSE MODEL OF VULVOVAGINAL CANDIDIASIS

Suvidha M. Menon

The current era is witnessing the emergence of virulent and resistant *Candida* and other pathogenic strains that has led to high morbidity and mortality rates on a global scale. Drug resistance has rendered once proven potent and commonly used antifungal drugs ineffective, especially in immunocompromised patients. These reasons justify the need for identifying novel antifungal targets and thereby building the antifungal armamentarium.

Our lab has previously investigated and studied Ebselen (EB), an organoselenium compound for its antifungal mechanism and activity against *Candida* strains. *In vitro* studies have shown the growth inhibitory activity (IC_{50} ~ 15 μM) for various *C. albicans* strains. Furthermore, EB inhibits a novel fungal target H^+-ATPase unlike the standard drugs available on the market. However, EB interacts with critical thiol residues of enzymes and exhibits numerous off-target effects. Also, EB is a poorly aqueous soluble drug and hence it is difficult to use for *in vivo* studies. For these reasons, the present study was carried out with two complementary strategies: Firstly, we have carried out an *in vitro* study intending to address the drug-resistance issue by building the antifungal library. Secondly, we molded EB into a topically acting nanoformulation for vulvovaginal candidiasis (VVC).

Given the current interest in organoselenium inhibitors of the plasma membrane H+ -ATPase, the first part of the study characterized the antifungal activity of forty novel organoselenium compounds (G1-G40) in S1 (fluconazole (FLU) sensitive) and S2 (FLU

resistant) strains. Amongst the test compounds, G4, G13, G20 and G30 showed equivalent or better antifungal activity than EB in both the strains. Compound G20 was the most potent with a MIC of 3.125 μM in both strains while EB displayed a MIC of 25 μM and FLU-treated wells showed MIC >100 μM in both strains. In addition, medium acidification assays revealed that these selected EB analogs, indeed, act on the fungal membrane H^+ -ATPase pump. Taken together, these *in vitro* results indicate that modified EB analogs should be investigated further for use as antifungal agents in FLU-resistant as well as other *C. albicans* strains.

Next, we developed a nanoformulation of EB (EBN) as an intervention to treat VVC, the most common infection caused by *Candida albicans* in women. EB loaded self-nanoemulsifying preconcentrate (EB-SNEP) was developed, characterized *in vitro*, and tested in a mouse model of VVC. *In vivo* studies carried out with intravaginal administration of EB-SNEP (12.5 mg/kg) showed a remarkable decrease in infection by ~ 800-fold compared to control (infected, untreated animals). *In vitro* studies of EBN formulation on mammalian cells and probiotic organisms and histological sections of EB-SNEP-treated mouse vaginal tissues did not demonstrate any signs of toxicity. To conclude, the present results indicate that EBN (12.5 mg/kg) should be investigated further for use as an antifungal agent in FLU-resistant as well as other *Candida* strains.

To recapitulate, organoselenium compounds proved to be effective and promising antifungal agents. Furthermore, EB nanoformulation provides a robust intravaginal delivery approach that overcomes issues related to poor-solubility drugs and simultaneously acting as a novel solution for drug-resistant strains.

DEDICATION

I would like to dedicate this thesis to my beloved parents Mohanakrishnan and Sita Menon, my sister Sunita Menon, my husband Aditya Menon, my extended family V K Gireesan and Chandrakala Menon, and my pets Cookie and Niko.

ACKNOWLEDGEMENTS

Firstly, I would like to thank Almighty God for giving me endurance and wellness to achieve my goal.

I would like to extend my deepest gratitude to my mentor, Dr. Blase Billack, who expertly guided me through my entire Ph.D. project. I truly admire your inquisitive nature to learn more about research and Ebselen as well as always willing to make time for your students.

I would like to sincerely thank my Ph.D. thesis committee members, Dr. Cantor, Dr. Reznik, Dr. Schanne and Dr. Patel, for their valuable suggestions, patience and support.

Special thanks to Dr. Patel and Richa for helping us move forward this project with their expertise.

I must also express my deep appreciation to the following people:

- Dr. M. Piętka-Ottlik, and Dr. J. Młochowski (Department of Organic Chemistry, Wroclaw University of Technology, Wroclaw, Poland).
- Dr. J. Morchhäuser *(In*stitut für Molekulare Infektionsbiologie, University of Würzburg, Würzburg, Germany).
- Members of PHS department (Dr. Vijaya Korlipara, Dr. Carvalho, Joyce Festa, Susana Solis, Luz Mery Benitez, Helen Scaramell, Eileen Hussey and Ernie) for their support.
- I would like to thank St. John's University and the Pharmaceutical Sciences Department for funding my research throughout my Ph.D. program.

I would like to express my sincere gratitude and love to my fellow lab mates Trishaal, Ganming, Vera, Hemanth, Benedette and Maria for their invaluable assistance and suggestions.

Special thanks to my dear friends Khushboo, Anuja, Nikkita, Ankit, Wow, Derrick for all the wonderful memories shared together.

Above all I would like to thank my husband, Aditya Menon for his constant support always for which my mere expression of thanks does not suffice.

I am grateful towards my family for their prayers and incredible support throughout this journey.

Lastly, I would like to thank all my friends at St. John's University.

TABLE OF CONTENTS

LIST OF TABLES

LIST OF FIGURES

ABBREVIATIONS

CFU	Colony forming units
DMA	Dimethylacetamide
DMSO	Dimethyl sulfoxide
EB	Ebselen
EBN	Ebselen nanoemulsion
FLU	Fluconazole
H & E	Hematoxylin and Eosin
HeLa	Henrietta Lacks
HRP	Horseradish peroxidase
IACUC	Institutional Animal Care and Use Committee
IC50	Half maximal inhibitory concentration
IHC	Immunohistochemistry
LDH	Lactate dehydrogenase
LP	Lamina propria
MIC	Minimal inhibitory concentration
MICO	Miconazole
MPO	Myeloperoxidase
NAC	Non *albicans Candida*
OPC	Oropharyngeal candidiasis
PMN	Polymorphonuclear leukocytes
Pma1p	Plasma membrane H^+-ATPase
PAS	Periodic acid Schiff

PRR	Pattern recognition receptors
SAP	secreted aspartyl proteinases
SAR	Structure activity relationship
SC	Subcutaneous
SEM	Scanning electron microscopy
SM	Submucosa
SNEDDS	Self-nanoemulsifying drug delivery system
SNEP	Self-nanoemulsifying preconcentrate
TTO	Tea tree oil
VEC	Vaginal epithelial cells
VL	Vaginal lumen
VM	Vaginal mucosa
VVC	Vulvovaginal candidiasis

CHAPTER I

INTRODUCTION

1. Impact of yeast on human life

Yeast have played a vital role in human civilization for baking, brewing, distilling and, winemaking for ages (Duan *et al.*, 2018). In fact, the history of yeast for human use goes back to centuries ago, but it was not until the nineteenth century, that the French scientist Louis Pasteur established the key role of yeast as microorganisms in the fermentation process (Barnett, 1998, 2000). The substantial evidence, thus, obtained from the experiments on the leading model organism has paved a way to infer gene and protein interactions as well as understand the complex patterns of inheritance in eukaryotes including humans (Botstein and Fink, 2011). In addition, a worldwide effort of hundreds of researchers with pioneering works led to the first eukaryote, *Saccharomyces cerevisiae* with a completely sequenced genome (Botstein *et al.*, 1997).

The fact that there are genes in yeast and mammals that encode fundamentally similar proteins seemed intriguing and steered the researchers to conduct numerous experiments in cellular biology and biotechnology. Several studies with yeast genes have provided great insights in understanding various diseases such as colon cancer and aging due to mutations in human homologs (Botstein *et al.*, 1997). With such progress, recombinant yeast was used for development of vaccine for human hepatitis B virus infection (McAleer *et al.*, 1984). Being the most facile organism, yeast has also been exploited to produce biofuels and serves as a valuable commodity for animal feed (Botstein and Fink, 2011). With advent of gene technology, yeast, more than any other organism, has provided profound understanding in protein-protein interaction and gene networks.

Of the estimated 1.5 million fungal species inhabiting the earth (Blackwell, 2011), human interactions with some fungi proves to be detrimental. The molds *Aspergillus* and *Penicillium* spp. are common contaminants of stored food grains, rendering it unfit for human consumption. These fungi stand out for producing mycotoxins including aflatoxin, one of the most carcinogenic compounds known (Mannaa and Kim, 2018). In addition, *Aspergillus* is one of the well documented and life-threatening airborne fungal pathogens known to cause diseases such as invasive pulmonary aspergillosis, aspergilloma, and hypersensitive reactions, particularly common among immunocompromised hosts (Mousavi *et al.*, 2016).

2. *Candida albicans*: The commensal & opportunistic pathogen

Candida albicans, the eukaryotic organism from the *Candida* genus is a remarkably variable and adaptable fungus. This pleomorphic fungus exists as a common colonizer in various human niches (gut, oral mucosa, vagina, skin) without causing disease and as a fungal pathogen in immunocompromised or immunosuppressed or patients in which barriers that prevent dissemination have been disrupted (Nobile and Johnson, 2015). While *Candida* is associated with major cases of infections, there is a recent reported rise in diseases related to non-*albicans Candida* or NAC (*C. glabrata, C. parapsilosis, C. tropicalis, and C. krusei*).

2.1 Types of diseases and their risk factors

Although *C. albicans* are commensal organism thriving majorly in gastrointestinal and genitourinary tract, they are known to cause a myriad of diseases as an opportunistic pathogen. *Candida* can cause superficial (dermal/cutaneous infection), or mucocutaneous

(oral or vaginal cavity), or disseminated or invasive candidiasis (Spampinato and Leonardi, 2013).

- **Cutaneous Candidiasis**: Skin is a complex and dynamic ecosystem inhabited by wide varieties of microbes. Among the 200 *Candida* species, only a few commensals (*C. tropicalis, C. parapsilosis, C orthopsilosis*) that are found on a healthy skin, can be pathogenic. This type of infection usually affects intertriginous and interdigital areas, and the clinical manifestation includes erythema, thickening of skin, hyperkeratosis, or pustules. The initial Candida recognition by innate immune receptors, such as pattern recognition receptors (PRRs) including Toll-like receptors and C-type lectin initiates an efficient immune response as a way of skin defense (Kühbacher *et al.*, 2017; Watts *et al.*, 2009).

- **Oropharyngeal candidiasis (OPC)**: Oropharyngeal candidiasis is an opportunistic mucosal infection affecting the oral cavity characterized with thrush (curd-like discrete plaques) or erythematous patches. *Candida* is found in ~60% of oral cavity of healthy individuals. This type of infection can have a severe impact on fluent speech, nutritional intake, and quality of life. Risk factors predisposing to this infection includes immunosuppression, hematological disorders, broad-spectrum antibiotic use, diabetes, wearing dentures, and smoking. OPC has been shown to be a predictive marker in HIV-infected individuals (Conti *et al.*, 2014; Pankhurst, 2009).

- **Vulvovaginal candidiasis (VVC)**: Vulvovaginal candidiasis (VVC) is the most common opportunistic mucosal infection among women caused predominantly by *C. albicans* (90%) and the remaining cases caused by *C. glabrata* (Fidel *et al.*, 1999). VVC can be characterized by clinical features such as vaginal discharge, pruritus, dysuria, and

redness of vulva and vaginal mucosa (Figure 1). It is estimated that approximately 75% of women experience VVC once in their lifetime with ~5-8 % of them suffering from recurrent VVC. Vaginal thrush is a common manifestation among immunocompromised patients, especially HIV-infected women (Ray *et al.*, 2011; Yano *et al.*, 2018). The etiological factors that precipitate the onset of symptomatic VVC are chronic use of broad-spectrum antibiotics, diabetes mellitus, elevated estrogen levels such as during pregnancy, oral contraceptive use or hormone replacement therapy, and genetic factors such as variants in gene *MBL2*, *SIGLEC15*, *TLR2*, and *NLRP3* (Merkhofer and Klein, 2020; Yano *et al.*, 2018). Moreover, perturbations in physiological factors such as increase in vaginal pH > 4.5 and elevated glycogen content help *Candida* adhere to vaginal epithelial cells (VEC), thereby disturbing the vaginal microbiome (Cassone, 2015; Donders *et al.*, 2020). In other words, a healthy vagina is a balance between *Candida* spp. and *Lactobacilli* spp. which can alleviate the phenotypic switching of *Candida* from commensal form to pathogenic form (hyphae) (Bradford and Ravel, 2016).

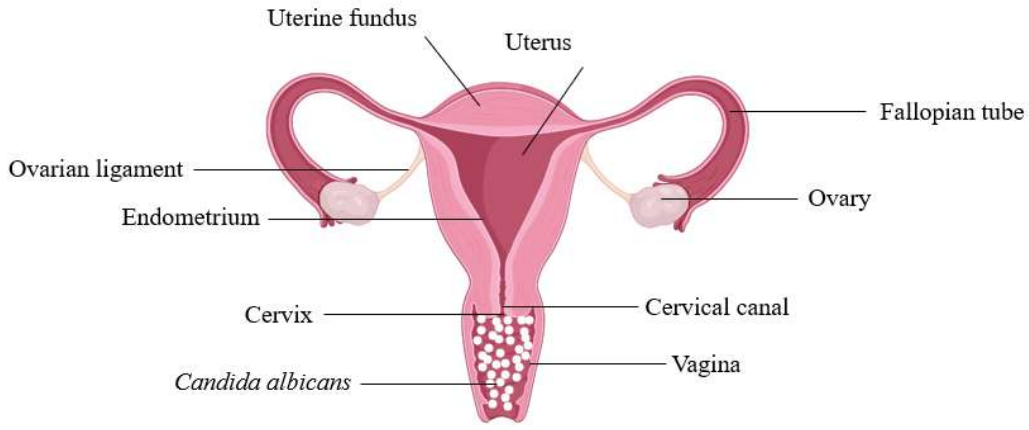

Figure 1:Female reproductive system with vulvovaginal candidiasis (adapted from https://www.std-gov.org/); Drawn using Biorender.

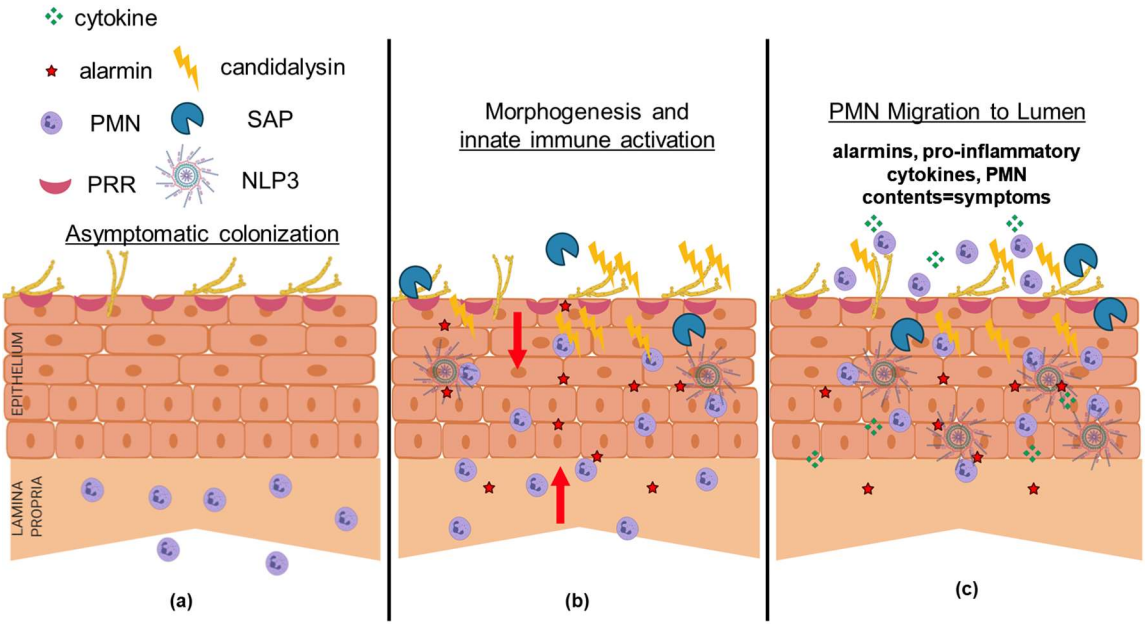

Figure 2: A working model of immunopathogenesis of *C. albicans* vaginitis adapted from (Willems et al., 2020). Drawn using Biorender.

Figure 2a depicts the asymptomatic environment in the vagina with yeast forms of *C. albicans* despite the presence of numerous pattern recognition receptors (PRR) on the epithelial surface, while Figure 2b describes the yeast-to-hypha switch under morphogenesis-inducing conditions such as increase in estrogen, elevated vaginal pH, and microbiome disruption). Augmented recognition by PRRs, increased hyphal biomass, expression of hypha-associated virulence factors (candidalysin, secreted aspartyl proteinases (SAPs)) activates NLRP3 inflammasome signaling, eliciting inflammatory cytokines and chemokines (e.g., IL-1β, S100A8/9 alarmins) in the vaginal epithelium, resulting in initial migration of polymorphonuclear leukocytes (PMNs) from the lamina propria (L.P) to the vaginal lumen. Figure 2c illustrates the continued expression of innate immune effectors by the vaginal epithelium as a result of failure to adequately reduce immunopathological triggers. These initial signals, coupled with the secondary

amplification of immune effectors by recruited PMNs, contribute to symptomatic infection and characteristic immunopathology.

- **Invasive candidiasis**: Towards the end of twentieth century, there was an upsurge of hospital-acquired infections. Blood-borne candidiasis is a serious problem in hospital settings where the *Candida* breaches the skin barrier with the use of medical implants or catheters or after a surgery. *Candida* is the major species causing invasive candidiasis (46.3%), followed by *C. glabrata* (24.4%) and *C. parapsilosis* (8.1%). Disseminated candidiasis often causes death with a mortality rate as high as 40% (Conti *et al.*, 2014; Yang and Rao, 2018). The delays related to early recognition and establish a diagnosis with proper systemic antifungal leads to much worse clinical outcomes such as the fungi disseminating to different organs.

2.2 Mechanisms of pathogenicity

C. albicans are dimorphic and can switch phenotypically from yeast cells to hyphal form in response to change in temperature, pH, CO_2, nutrient starvation. It is this transition from yeast to hyphae that conditions its virulence. Other virulence factors of *Candida* spp. include biofilm formation, expression of adhesins on cell surface, hydrolytic enzyme secretion, secretory cytolytic peptides (candidalysin) that damage host cells, phenotypic switching resistant to neutrophil engulfment, and evasion from host immune system. These evolutionary adaptive traits helps *Candida* survive in harsh conditions and evade from host immunity (Dadar *et al.*, 2018; da Silva Dantas *et al.*, 2016).

2.3 Other emerging pathogens

- ***Candida glabrata*:** *C. glabrata* is the second most common cause of nosocomial and mucocutaneous candidiasis infections after *C. albicans*. They are commensal organisms

like *C. albicans*, however, *C. glabrata* are not dimorphic and so exists as blastoconidia under both commensal and pathogenic state. They are known to cause mucocutaneous or systemic infections, particularly in immunocompromised or diabetic patients. Even though it has few virulence attributes than albicans, *C. glabrata* infection spreads rapidly and its high resistance towards azole and less susceptibility towards other antifungal agents including amphotericin makes it difficult to treat (Pappas *et al.*, 2018; Yang and Rao, 2018). Previous studies have shown the drug resistance mechanisms due to changes in CYP-450 lanosterol demethylase enzyme, changes in Δ^{5-6}-sterol desaturase, and energy-dependent drug efflux mechanism (Fidel *et al.*, 1999; Hitchcock, 1993). In comparison to *C. albicans*, it has been difficult to develop an *in vivo* model with *C. glabrata* infection due to lack of state of colonization or infectivity which contradicts the high mortality rate seen in the clinical scenario (Fidel *et al.*, 1999).

- ***Candida auris***: There has been a steady increase in the global prevalence of NAC spp. One such fungal pathogen that gained international attention is *C. auris,* a multidrug-resistant and implicated in critical hospital-acquired infections. Originally isolated from the ear canal infection of a Japanese patient, the Center for Disease Control and Prevention published an alert as soon as *C. auris* was detected as the cause for the contemporaneous outbreaks in different regions of the world (Fisher *et al.*, 2020). A research study showed that the ability of *C. auris* isolates to produce virulence factors such as phospholipase, proteinase, and biofilms are much weaker than *C. albicans* (Larkin *et al.*, 2017). Recent findings from a study indicate that these isolates are well adapted to temperature stress and maintain their pathogenicity at higher temperatures (Wang *et al.*, 2018). Since the complete genome sequence was recently studied, we are only now beginning to understand the role

played by different genes in the pathogenicity and virulence of this emerging pathogen (Rossato and Colombo, 2018).

With the growing emergence of multiple-drug resistant strains and incidence of infections with high mortality rate, investigation and identification of novel agents that are effective against these strains is critical.

3. Conventional antifungals and their limitations

Currently available antifungal agents used in clinical treatments belong to diverse classes, however, only a few can be used to treat mucosal or systemic infections with *Candida* spp.

3.1 Azoles: Inhibition of ergosterol biosynthesis pathway

Ergosterol, analogous to cholesterol in mammalian cells, is vital for maintaining membrane integrity in fungal cells. Lanosterol demethylase (Erg11p) is a cytochrome P-450 enzyme mediating rate-limiting step in ergosterol biosynthesis. By binding the heme moiety in Erg11p, azoles inhibit activity of this enzyme and therefore disturb ergosterol biosynthesis. Conversion of Erg11p substrate into toxic methylated sterols leads to growth inhibition. The azole family includes imidazoles (miconazole, econazole, clotrimazole, and ketoconazole) and triazoles (fluconazole, itraconazole, voriconazole and posaconazole). Many azoles are effective both for topical use and for the treatment and prophylaxis of invasive fungal infections. The primary mechanisms for the azole resistance in *Candida* include mutations or overexpression of *ERG11*, reduced uptake of azole, efflux via ABC transporters, tolerance to methylated sterols via *ERG3*, biofilm formation, and import of host cholesterol (Bondaryk *et al.*, 2013).

3.2 Echinocandins: Inhibition of 1,3-D-glucan synthesis

The cell wall represents an ideal potential target for antifungal agents, as this structure is absent in mammalian cells. Echinocandins disturb cell wall structural integrity by inhibition of 1,3-β-glucan synthase, an enzyme responsible for synthesis of 1,3-β-glucan that strengthens the yeast cell wall. Lack of the glucan component in the cell wall makes the cell vulnerable to osmotic lysis. All three agents (caspofungin, micafungin, and anidulafungin) exhibit concentration-dependent fungicidal activity against most species of *Candida* for the treatment of esophageal and invasive candidiasis, including candidemia. Resistance to echinocandins is linked to a mutation in 1,3-β-glucan synthase complex (*FKS* gene) or lack of 1, 3-β-glucan in the fungal cell wall (Bondaryk *et al.*, 2013; Spampinato and Leonardi, 2013).

3.3 Polyenes: Binding to Ergosterol

As discussed above, ergosterol is another perfect target for antifungal agents. Drugs belonging to polyene class (nystatin and amphotericin B both isolated from *Streptomyces* spp.) disrupt the major lipidic component of the fungal cell membrane resulting in the production of aqueous pores. Consequently, these pores permit the efflux of cations resulting in the oxidative damage and fungal cell death (Cannon *et al.*, 2009). The slight affinity of polyenes for cholesterol (human counterpart of ergosterol) explains the high toxicity along with adverse effects, limiting the use of amphotericin B systemically (Vandeputte *et al.*, 2012).

3.4 Nucleoside analogs: Inhibition of nucleic acids synthesis

Flucytosine is a pyrimidine analogue and is transported into fungal cells by cytosine permeases. Then, it is deaminated to 5-fluorouracil and phosphorylated to 5-

fluorodeoxyuridine monophosphate. This fluorinated nucleotide inhibits DNA synthesis by targeting thymidylate synthetase. The 5-fluorodeoxyuridine monophosphate further gets phosphorylated into 5-fluorouridine triphosphate, affecting RNA and protein synthesis by and incorporating to RNA. Rapid development of resistance in *Candida* spp. and adverse effects such as skin rash, bone marrow suppression, liver dysfunction limits its use as monotherapy. (Bondaryk *et al.*, 2013; Spampinato and Leonardi, 2013).

3.5 Inhibition of squalene-epoxidase

Terbinafine and naftifine are two common allylamines used in the treatment of fungal infections of skin, nails, and hair. These drugs inhibit ergosterol biosynthesis independent of CYP-450 enzymes, by binding to squalene epoxidase (Erg1p) resulting in accumulation of squalene in high amounts inside the cell. This leads to increased membrane permeability, perturbation of cell organization and ultimately to cell death. The mechanism of fungal resistance to terbinafine are due to a single amino acid substitution in Erg1p, upregulation of genes (*CDR1*, *AGP2*, and *HOL3*) that extrudes the antifungal agent accumulated inside the cell, detoxification and stress tolerance (Bondaryk *et al.*, 2013 Zeng *et al.*, 2007).

4. Strategies to overcome antifungal drug resistance

Management of fungal infections has become increasingly difficult and represents a serious threat to modern society, mostly since current antifungal drug therapy is highly skewed towards drugs targeting ergosterol while the fungi are evolving to evade the drug. The characteristics of an ideal antifungal agent, in addition to meeting pharmacological requirements, would not be susceptible to the development of resistance due to efflux

mechanisms. Following are the four principal approaches to negating the impact of efflux, all of which depend on maintaining a high concentration of the antifungal agent at its site of action (Burghoorn *et al.*, 2002; Cannon *et al.*, 2009; Chan *et al.*, 2007).

- The simplest would be to use antifungals that are not substrates of efflux pumps. Studies have shown that designing compounds such as polyenes and echinocandins with such size and hydrophobicity constraints could avoid being ABC transporter substrates. Again, designing such compounds are challenging as the efflux pumps have evolved large with flexible drug-binding sites to protect cells against a wide variety of toxic compounds.
- Another approach would be to developing treatments that prevent efflux while maintaining antifungal efficacy. These inhibitors could affect the pump directly either by binding as a pseudosubstrate competitively or noncompetitively, and blocking access to the binding site, or by locking the pump in a conformation that prevents the transport reaction cycle.
- A third approach would be to inhibit the plasma membrane H^+ ATPase. The yeast plasma membrane H^+-ATPase (Pma1p), a member of the P-type ATPase family, is an electrogenic proton pump that couples ATP hydrolysis to proton (H+) transport. Pma1p is encoded by the PMA1 gene and found to be vital for the normal growth of yeast, and its deletion in haploid strains of yeast is lethal (Chan *et al.*, 2007). Pma1p drives a range of secondary transporters, such as those involved in ionic balance and nutrient uptake required for ATP synthesis, so it indirectly affects drug efflux by ABC transporters. A previous study demonstrated that inhibitors of C. albicans Pma1p also inhibit azole resistance at concentrations below the MIC (Monk *et al.*, 2005). Previous research work has shown ebselen (EB), an organoselenium compound blocks the H^+-ATPase pump (Chan *et al.*,

2007). The fungal membrane comprises of 70% of Pma1p, however, shows only 25% similarity with analogous mammalian ATPases. Therefore, novel Pma1p inhibitors should possess low potential for adverse effects in humans (Burghoorn *et al.*, 2002).

- Alternatively, it might be possible to design drugs with an enhanced rate of uptake and thus shift the balance between uptake and efflux so that a high intracellular concentration of the drug is maintained despite any upregulation of efflux (Cannon *et al.*, 2009).

In the present work, the effect of EB and novel analogs of it on Pma1p activity has been explored (the third approach listed above).

5. Organoseleniums

The biochemistry and pharmacology of organoselenium compounds are subjects of intense current interest. Selenium is an essential trace element and is a vital component of glutathione peroxidase enzyme (Radhakrishna *et al.*, 2010). It is well known that the nucleophilic reactivity and radical scavenging properties of selenium contribute to the biological activity of selenium compounds (Mouithys-Mickalad *et al.*, 2004). The essentiality and toxicity of selenium in vertebrates generate the remarkable scientific research interest in this element (Alam *et al.*, 2016). With the growing emergence of resistant strains, there is a need for immediate development of novel antifungal treatments.

5.1 *In vitro* and *in vivo* and clinical studies related to Ebselen (EB)

EB (2-phenyl-1,2-benzisoselenazol-3(2H)-one), is a broadly studied organoselenium compound both in research laboratories as well as clinical settings for indications such as atherosclerosis (Chew *et al.*, 2010), bacterial and fungal infection (Nozawa *et al.*, 1996), inflammation (Cotgreave *et al.*, 1988), ischemic stroke (Yamaguchi

et al., 1998), cerebral ischemia (Parnham and Sies, 2000), bipolar disorder (Singh *et al.*, 2013), and noise induced hearing loss (Kil *et al.*, 2007). Noticeably, studies have also highlighted EB as a promising drug against SARS-CoV-2 (Menéndez *et al.*, 2020). Moreover, pre-clinical and clinical studies have shown its safety profile and lack of immunogenicity which underscores the reason for drug repurposing (Nozawa *et al.*, 1996). Due to its ability to interact with endogenous thiol groups, EB is a multi-faceted compound exhibiting various mode of actions such as mimicking the glutathione-peroxidase activity, inhibiting the yeast plasma membrane H^+-ATPase pump (Chan *et al.*, 2007) (Nakamura *et al.*, 2002), and mimicking peroxiredoxin via thioredoxin and thioredoxin reductase (Ren *et al*., 2018). *In vitro* studies have shown that EB possesses antifungal activity against both FLU- sensitive and resistant strains of *C. albicans.* In addition, we (Billack *et al.*, 2009; Chan *et al.*, 2007; Orie *et al.*, 2017) and others (Soteropoulos *et al.*, 2000) have found that EB inhibits the plasma membrane H^+-ATPase pump, a critical player in fungal cell growth and survival. Drug repurposing is a strategy to identify alternative uses of therapeutic agents which has already cleared the early hurdles of drug development thereby facilitating rapid translation of results into clinical phase (Singh *et al.*, 2016).

5.2 EB: A potential arsenal to target Pma1p and combat VVC

Although EB has shown promising results in clinical trials and has recently approved for Phase II trial in COVID-19 patients (NCT04484025), it has largely been ignored as an antimicrobial agent despite showing excellent activity against bacteria, viruses and fungi. Many of the beneficial effects of EB have been attributed to its antioxidant actions, likely attributable to its function as a glutathione-peroxidase mimetic (Griffiths *et al.*, 1992; Hayashi and Slater, 1986). EB has been implicated as a potential

blocker of H^+-ATPase function as a result of its strong reactivity with the sulfhydryl groups of cysteine residues within proteins. It appears that the strong affinity of EB towards sulfhydryl groups is necessary for its antimicrobial effects. It is noticeable that EB does not exhibit significant human toxicity, perhaps because the selenium is not bioavailable, and remains bound within the molecule (Sies, 1993).

5.3 Limitations of EB

Although EB is a distinct and multi-faceted compound, the use of EB has been impeded by a few limitations. It has been observed that *in vivo*, 90% of EB is bound to serum albumin within the plasma which makes it less bioavailable than other known antifungal agents. EB has also exhibited immunosuppression in *in vivo* experiments, predominantly via inactivation of neutrophils (Nozawa *et al.*, 1996). Although the toxicity of many selenium compounds is a limiting factor for their use in pharmacotherapy, one way to overcome the toxicity could be building the analogs with suitable substituents. Previous studies have shown that the developed analogs exhibited better antifungal activity compared to EB, while simultaneously minimizing the pharmacological deficiencies of EB (Orie *et al.*, 2017).

5.4 EB analogs

Numerous analogs of EB have been synthesized with varying structural substitutions in order to evaluate their ability to inhibit microbial growth as compared to the parent compound (EB). Different manipulations have been introduced, such as changes in lipophilicity, and chemical moieties in an attempt to find modified analog or, set of analogs with an enhanced antimicrobial activity *in vivo*. Figure 3 depicts EB and selected analogs used in this study.

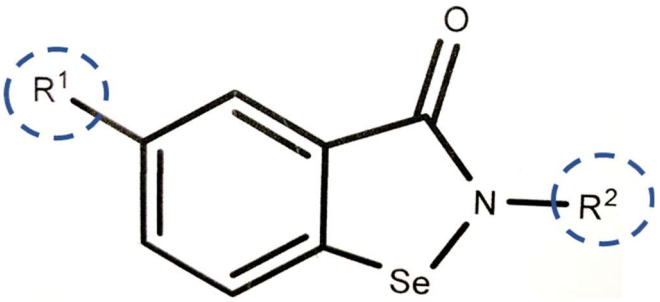

	Compounds	R1 group	R2 group
Group I	G1	5-CH_3	H
	G2		Me
	G3		Pr
	G4		t-Bu
	G5		cHex
	G6		Ph
	G7		Ph-4Cl
	G8		2Py
	G9		2Py-5Cl
	G10		N(Ph)2

	Compounds	R1 group	R2 group
Group II	G11	5-Cl	H
	G12		Me
	G13		Pr
	G14		t-Bu
	G15		cHex
	G16		Ph
	G17		Ph-4Cl
	G18		2Py
	G19		2Py-5Cl
	G20		N(Ph)2

	Compounds	R1 group	R2 group
Group III	G21	5-NO_2	H
	G22		Me
	G23		Pr
	G24		t-Bu
	G25		cHex
	G26		Ph
	G27		Ph-4Cl
	G28		2Py
	G29		2Py-5Cl
	G30		N(Ph)2

	Compounds	R1 group	R2 group
Group IV	G31	5-CH_3SO_2	H
	G32		Me
	G33		Pr
	G34		t-Bu
	G35		cHex
	G36		Ph
	G37		Ph-4Cl
	G38		2Py
	G39		2Py-5Cl
	G40		N(Ph)2

Figure 3: Chemical structure of EB and list of EB analogs

6. Development of EB nanoformulation

- **The vaginal tract as site for drug delivery**

The vagina has been studied as a favorable site for the local and systemic delivery of drugs, specifically for female-related conditions. Traditionally, the vaginal cavity has been used for the delivery of locally acting drugs such as antibacterial, antifungal, antiprotozoal, antiviral, labor-inducing and spermicidal agents, prostaglandins and steroids. Compared to the oral cavity, the vagina might serve as a better route for the delivery of antifungal treatments owing to the lack of drug interactions observed in the gastrointestinal tract (Vermani and Garg, 2000). Other advantages of this delivery route are ease of administration, avoidance of the first-pass hepatic metabolism, and the possibility of assuring local effects. Unfortunately, therapeutic outcomes can be limited by changes in the vaginal environment due to the menstruation cycle (El-Hammadi and Arias, 2020). A recent study demonstrated the use of EB vaginal film serving as a dual purpose for treating VVC and pre-exposure prophylactic (PrEP) against HIV (Vartak *et al.*, 2020a).

- **EB Nanoformulation- an ideal drug delivery approach**

In the present study, EB was repurposed with an aim to improve its aqueous solubility by developing a self-nanoemulsifying drug delivery system (SNEDDS) while retaining the antifungal activity against *Candida* strains for VVC infection. In addition, tea tree oil (TTO) was included in the nanoformulation to enhance its stability. Altogether, EB nanoformulation (EBN) is comprised of EB, Captex® 300 EP/NF, Kolliphor® ELP, and TTO, rendering a local antifungal effect intravaginally.

7. Studying EB nanoformulation in VVC model

- **Mouse model of VVC**

A popular model of VVC is a murine model, particularly that developed and adopted by Fidel and colleagues (Fidel *et al.*, 2000; Yano and Fidel, 2011). Advantages of this model over the other VVC models such as rat, pig, macaque are lower cost, easy handling, and great availability of genetically modified animals. In addition, no ovariectomy is necessary for infection, as estrogen administration alone is sufficient for pseudoestrus induction. Among the putative virulence factors, yeast dimorphism, biofilm formation, adhesins, and secretory aspartyl proteinases (SAP) have been extensively studied (Cassone and Sobel, 2016; Kumar *et al.*, 2015; Wu *et al.*, 2020). As in mice, the infection is evaluated and monitored by determination of colony-forming counts (CFU) of fungal cells in the vaginal fluid or in the tissue of excised vagina following intravaginal *Candida* administration. Fidel and colleagues showed the typical estrogen dependence of *Candida* infection, the changes of the surface vaginal epithelium caused by the pseudoestrus, the fungal biofilm on vaginal epithelium (Fidel *et al.*, 2000; Yano *et al.*, 2010). In mice, the fungal intravaginal administration causes a strong inflammatory exudate with dominance of polymorphonuclear cells (neutrophils) and the production of neutrophil-chemoattractive chemokines and cytokines by the vaginal epithelial cells (VEC) (Yano *et al.*, 2010).

- ***In vitro* model for Candidiasis: An alternative to *in vivo* model**

Developing a VVC model to investigate antifungal agents both *in vitro* and *in vivo* helps gains new insight into disease mechanism. It is ideal to test the antifungal agents *in vitro* before moving into *in vivo* phase to save both time and money. An *ex vivo* model

using mouse vaginal explant was carried out to simulate the microenvironment in *Candida* infection. This study showed that *C. albicans* was able to adhere, and form hyphae and subsequent biofilm on vaginal explants indicating that fungal growth occurs most likely by scavenging host nutrients (Harriott *et al.*, 2010). Although, there is a paucity for human-based *in vitro* models for VVC, recently a few companies have developed a reliable *in vitro* human tissue model. A product of MatTek's Life Sciences, EpiVaginal™, is a valuable *in vitro* research tool cultured from human-derived vaginal cells. The fact that it its highly differentiated structure imitates the *in vivo* tissue and therefore can be used for evaluating safety and efficacy of chemicals. Studies have validated this model as a sensitive *in vitro* method to predict vaginal irritation and inflammation caused by topically applied therapeutic agents. One advantage of using EpiVaginal™ tissue is lack of inter-species extrapolation and the findings have direct pertinence to women's health. The drawback of using mouse vaginal explant in comparison to EpiVaginal™ tissues is that the latter can be cultured for extended duration (2-3 weeks) helping researchers to carry multiple experiments (Ayehunie *et al.*, 2011).

- **Difference between mouse and the human vaginal tissue**

The female genital system is a unique and dynamic in both rodents, and the human as variation in hormone levels during menstrual/estrus cycle or pregnancy influences the varying morphological appearance. There is a considerable difference in the gross anatomy as the mouse vaginal tissue is short (~1 cm) in comparison to the human vaginal tissue (6 - 7.5 cm). Another striking difference in the bicornuate uterine horns of mouse unlike a human's single uterus. Based on the stained histological studies, mouse has a single cervix lined by stratified squamous epithelium continuous with the vaginal epithelium, while

human cervix are divided into two portions: endocervix (upper portion composed of simple columnar mucinous epithelium) and ectocervix (lower portion composed of stratified squamous epithelium similar to the vaginal tract). The stratified squamous epithelium of the ectocervix is continuous with the vaginal squamous epithelium. Like human vaginal mucosa (VM), the mouse VM is composed of stratified squamous epithelium with no glands. Unlike that of the mouse, the human vagina is not keratinized, and the morphology of the human vaginal mucosa does not change significantly during the menstrual cycle (Boyd *et al.*, 2018) Comparative studies have shown that human vaginal pH ranges from 3.8-4.5 while the mouse vaginal pH is 6.5. This salient difference can be better explained based on the vaginal microbiome. Human vaginal microbiome is dominated by *Lactobacillus* which creates an acidic environment thereby protecting from various microbial pathogens (Witkin and Linhares, 2017). Since mouse is not confronted with pathogenic microbes or harsh conditions, it lacks the probiotic organisms resulting in higher vaginal pH. Another distinctive feature is unlike humans, rodents are not a host of *C. albicans* in the vaginal tract and other mucosal areas. (Miller *et al.*, 2016; Naglik *et al.*, 2008).

- **Limitations of *in vitro* and *in vivo* model**

In vitro monolayer cultures derived from primary human vaginal epithelial cells present differences in gene and protein expression levels between monolayer cultures and vaginal epithelium. Testing aqueous incompatible formulations such as gels, films, and vaginal rings make monolayer cultures poor models for vaginal irritation or toxicity. Further, versus animal models, the human cell-based EpiVaginal tissue is directly infectible with human pathogens such as HIV-1, while animal models are infectible only with viruses

that resemble HIV-1. The use of human ectocervical tissue explant models are limited due to restricted availability of fresh surgical tissues, and is likely to be poorly reproducible due to intra-subject variability in hormonal levels, vaginal flora and infections, use of vaginal products, recent coitus, and other factors. In addition, *in vitro* studies with vaginal tissue explants have so far shown poor viability (Ayehunie *et al.*, 2006; Collins *et al.*, 2000). Since, rodents are not a host of *C. albicans*, establishment of mucosal colonization requires extraneous administration of estrogen or immunosuppressive agents. Other drawbacks of *in vivo* model that should be taken into account are the economic, scientific and ethical considerations related to the use of animals.

8. Statement of the problem

The incidence of fungal infections has increased with rise in use of broad-spectrum antibiotics and immunocompromised individuals. An increase in multidrug resistance indicates that the fungal strains are continuously evolving, leaving the commonly used antifungal agents futile. VVC is the second most common infection experienced by women after bacterial vaginosis. Emergence of drug resistant and more virulent strains as well as their fungistatic nature results in recurrent episodes of VVC, causing discomfort and affecting their social quality of life. This compels the need for investigation for novel antimycotics and new potential drug targets.

9. Hypotheses and study objectives

Our study has several hypotheses:

- **EB possesses antifungal activity against *C. glabrata* and *C. albicans* S1 (FLU-sensitive) and S2 (FLU- resistant) strains.**

This hypothesis was tested using the following approaches:

- Determination of MIC and IC_{50} values by broth microdilution assay.
- Determination of MIC values by a colorimetric assay
- Effect on medium acidification

- **Novel organoselenium compounds possess antifungal activity against S1 and S2 strains.**

This hypothesis was tested using the following approaches:

- Determination of MIC and IC_{50} values by broth microdilution assay.
- Determination of MIC values by a colorimetric assay
- Effect on medium acidification

- **EB-SNEP exhibits potential antifungal treatment for VVC *in vivo*.**

This hypothesis was tested using the following approaches:

- Implementation of mouse VVC model.
- Determination of vaginal fungal burden
- Histopathological analysis using H & E study

- Immunohistochemistry analysis

- **EBN is safe *in vitro* and effective in an *in vivo* mouse model of VVC.**

This hypothesis was tested using the following approaches:

- Evaluation of cytotoxicity of EBN using LDH assay on HeLa cells

- Evaluation of cytotoxicity of EBN formulation on *Lactobacilli* spp.

In this study, we have extended the antifungal potency of EB to demonstrate that EB is an ideal antifungal treatment for VVC.

CHAPTER II

MATERIALS AND METHODS

1. Yeast

The *C. albicans* strains S1 (fluconazole sensitive) and S2 (fluconazole resistant) were kindly provided by Dr. J. Morchhauser *(In*stitut für Molekulare Infektionsbiologie, University of Würzburg, Würzburg, Germany) (Franz *et al.*, 1999). *C. albicans* strain.

2. Chemicals, reagents, and other materials

β-Estradiol 17-valerate (cat # E1631), dimethyl sulfoxide (DMSO) (cat # D1435), Dimethyl acetamide (DMA) (cat # 271012) were obtained from the Sigma Aldrich Chemicals Company (St. Louis, MO). Eosin (cat # CA95057-848), hematoxylin (cat # CA95057-844), xylene (cat # CA95057-822), histology grade 100% ethanol (cat # 89370-084) and Paraplast X-tra (cat # 15159-486-1kg) were purchased from VWR International (West Chester, PA). Buffered formalin (1:10 dilution, already diluted) (cat # 23-245-685) was procured from Fisher Scientific (Nazareth, PA). Permount (cat # SP15-500) was purchased from Fisher Scientific (Fairlawn, NJ). Slides and cover glasses were also acquired from VWR International (Radnor, PA; cat # 16004-386 and cat # 48382-136, respectively). Sterile Phosphate buffered saline (PBS) (cat # J61196) was obtained from Thermo Fisher Scientific (Ward Hill, MA). Dextrose (cat # 90640354) was purchased from EMD Chemicals (Dermstadt, Germany). Tissue culture plates (24-well) were purchased from Sarstedt (Newton, NC; cat # 101093-445), while 96-well cell culture plates were

purchased from Eppendorf (Hauppauge, NY;cat # 13-690-076). Resazurin dye was obtained from Sigma-Aldrich (St. Louis, MO; cat # R7017).

3. Culture media

Liquid Yeast peptone dextrose (YPD) medium (pH 6.5) was prepared by adding YPD media broth powder (50.0 g) from HiMedia Laboratories (Mumbai, India; cat # M1363) to distilled water (~1000.0 mL). The medium was supplemented with adenine hemisulfate salt (0.4 g) from Sigma Aldrich Chemicals Company (St. Louis, MO; cat # A9126) and then autoclaved at 121°C for 15 min. YPD agar plates were prepared by the addition of 65 g of agar from Becton, Dickinson and Company (Nazareth, PA; cat # DF0427-17-6) to 1 L of YPD liquid medium prior to sterilization. The molten mixture was then poured into petri dishes (20 mL/dish) (cat # 73210-516). RPMI 1640 medium, buffered with 0.165 M MOPS [3-(*N*-morpholino) propanesulfonic acid] containing L-glutamine and lacking sodium bicarbonate, was purchased from Sigma-Aldrich Co. (St. Louis, MO; cat # R6504). Medium was prepared by dissolving 10.4 g of RPMI 1640 powder in 1 L of distilled water and adjusting pH to within the range of 6.8-7.0. Following final pH adjustment, the medium was sterilized using Nalgene disposable bottle top filter with polyethersulfone (PES) membrane 0.2 μm (Nazareth, PA; cat # 595-3320).

4. Equipment

An Acculab VI-350 weighing balance (Acculab, Edgewood, NY), Sartorius CP64 analytical balance (Sartorius Corporation, Edgewood, NY) and a Metler-Toledo analytical balance (Mode; AG 104, Columbia, MD) were used for weighing the required amount of

test compounds and vaginal tissue. A Vortex Maxi Mix II (type 37600 Mixer Thermolyne, New Brunswick, NJ) and Fisher Vortex Genie 2 (Scientific Industries Inc., Bohemia, NY) were used for dissolving the test compounds and uniform mixing of components in the formulations. A UV-160 spectrophotometer (Shimadzu Corp., Kyoto, Japan) was used for reading absorbances. The other equipment used for *in vitro* studies were a MaxQ A4000 shaker (Barnstead Lab-Line, Melrose Park, IL), a Sorvall TR6000B refrigerated centrifuge (Long Island Scientific, Port Jefferson, NY), an Eppendorf centrifuge 5415 (Brinkman Instruments, Westbury, NY), an Orion Star AIII pH meter (Thermo Scientific Co., Pittsburgh, PA), and a Thermolyne Type 17600 Dri-bath (Barnstead/Thermolyne, Dubuque, IA). A Reichert Jung Leica 2030 Biocut Microtome (Labequip Ltd., Markham, Ontario) was used to cut tissue sections for histological staining, scoring and immunohistochemistry. An Integrated separation system hybridization oven (Model BT 400100, Enprotech) was used to embed all the tissues in paraffin blocks. A Precision Scientific water bath (Model #182, Precision Scientific, Chicago, IL) was used to help remove wrinkles on the sections. Low profile microtome blades (Sakura Finetek, Torrance, CA; cat # 4689) were used for section cutting. A Zeiss Axio Scope A1 microscope (Micro-Optics Precision Instruments, Fresh Meadows, NY) with Zeiss Zen 2.3 software was used for obtaining light microscopy images of H & E and PAS staining.

5. Test compounds for evaluation of antifungal activity

EB (cat # V1941) was purchased from AK Scientific (Union City, CA). The other analogs of EB (compounds G1- G40) were kindly provided by Drs. M. Piętka-Ottlik, E. Wojaczynska, and J. Mlochowski (Department of Organic Chemistry, Wroclaw University

of Technology, Wroclaw, Poland). FLU (cat # B2094) was purchased from ApexBio (Boston, MA). MICO was purchased as Monistat 7 (Miconazole Nitrate Cream 2%) from Insight Pharmaceuticals (Tarrytown, NY). See Table 1 for a complete description of the preparation and the stock concentration of EB and test compounds.

5.1.Test compound solutions-

The table below describes the preparation and the stock concentrations of EB and EB analogs:

Table 1:Description, molecular weights, and working concentration of EB and its analogs (G1- G40)

Compound with description	**Mol. wt. of compounds**	**Amount of compound + volume of DMSO**	**Stock concentration**
G1 (white crystals)	212.11 g/mol	3.9 mg in 184 µL	100 mM
G2 (white/pale green crystals)	226.13 g/mol	8.6 mg in 380 µL	100 mM
G3 (white crystals)	254.19 g/mol	7.4 mg in 291 µL	100 mM
G4 (fine white crystals)	268.21 g/mol	9.7 mg in 362 µL	100 mM
G5 (white crystals)	294.25g/mol	7.9 mg in 536 µL	25 mM
G6 (pale green yellow crystals)	288.20 g/mol	6.7 mg in 232 µL	100 mM
G7 (white/ pale green crystals)	322.65 g/mol	7.1 mg in 220 µL	100 mM
G8 (off white crystals)	289.19 g/mol	5.1 mg in 352 µL	50 mM

G9 (white/pale green crystals)	323.64 g/mol	5.9 mg in 546 µL	3.3 mM
G10 (pale green crystals)	379.31 g/mol	4.1 mg in 108 µL	100 mM
G11 (off white crystals)	232.53 g/mol	6.2 mg in 267 µL	100 mM
G12 (brownish crystals)	246.55 g/mol	4.6 mg in 352 µL	100 mM
G13 (white crystals)	274.61 g/mol	14.2 mg in 517 µL	100 mM
G14 (white crystals)	288.63 g/mol	8.5 mg in 294 µL	100 mM
G15 (white crystals)	314.67 g/mol	13.5 mg in 1287 µL	37.5 mM
G16 (pale green crystals)	308.62 g/mol	8.1 mg in 786 µL	25 mM
G17 (white crystals)	343.07 g/mol	6.2 mg in 543 µL	37.5 mM
G18 (white/pale green crystals)	309.61 g/mol	7.5 mg in 970 µL	25 mM
G19 (off white crystals)	344.05 g/mol	5.8 mg in 338 µL	2.1 mM
G20 (light yellow/green crystals)	399.73 g/mol	6.0 mg in 150 µL	100 mM
G21 (sharp yellow crystals)	243.08 g/mol	5.9 mg in 243 µL	100 mM
G22 (sharp orange crystals)	257.10 g/mol	12.3 mg in 338 µL	50 mM

G23 (bright orange crystals)	285.16g/mol	11.7 mg in 410 µL	100 mM
G24 (yellow crystals)	299.18 g/mol	10.7 mg in 358 µL	50 mM
G25 (yellow crystals)	325.22 g/mol	3.4 mg in 105 µL	100 mM
G26 (orange crystals)	319.17 g/mol	4.8 mg in 150 µL	100 mM
G27 (red crystals)	353.62 g/mol	5.6 mg in 158 µL	50 mM
G28 (orange crystals)	320.16 g/mol	4.7 mg in 147 µL	3.5 mM
G29 (white/pale green crystals)	354.61 g/mol	8.7 mg in 245 µL	3.8 mM
G30 (brown/green crystals)	410.28 g/mol	9.6 mg in 234 µL	100 mM
G31 (white crystals)	376.17g/mol	15.0 mg in 543 µL	50 mM
G32 (white crystals)	290.20 g/mol	7.6 mg in 262 µL	100 mM
G33 (white crystals)	318.25 g/mol	4.3 mg in 135 µL	100 mM
G34 (white crystals)	332.28 g/mol	7.2 mg in 217 µL	100 mM
G35 (white crystals)	358.31 g/mol	7.2 mg in 201 µL	50 mM
G36 (white/pale green crystals)	352.27 g/mol	11.0 mg in 312 µL	100 mM
G37 (white/pale green crystals)	386.71 g/mol	12.8 mg in 332 µL	100 mM
G38 (white crystals)	353.26 g/mol	4.6 mg in 130 µL	100 mM
G39 (white/pale green crystals)	387.70 g/mol	8.7 mg in 224 µL	3.9 mM

G40 (yellow/green crystals)	444.38 g/mol	10.1mg in 228 µL	100 mM
G59	274.18 g/mol	12.2 mg in 445 uL	100 mM
EB-1	274.18	16.5mg in 602 uL	100 mM

5.2. Log P determination for EB and its analogs

The partition constant of a compound or Log P, between n-octanol and water, is a critical tool for expressing the lipophilicity of a molecule. The binary phase of n-octanol/water provides a potential model of lipid constituents of biological membranes. (Amézqueta *et al.*, 2020). The ability to predict log P values based on molecular characteristics is currently widely used in the field of drug discovery, in order to estimate properties such as absorption, bioavailability, metabolism, and toxicity (Ghose *et al.*, 1998). In this study, log P was evaluated to determine whether the degree of lipophilicity of EB and its analogs (G1- G40) would have an impact on plasma membrane penetration and fungal cell death. All predicted log P values were obtained using the milogP calculator provided by the Molinspiration Property Calculation Service (www.molinspiration.com).

6. *In vitro* assessment of antifungal activity of EB and its analogs against S1 and S2 strains of *C. albicans*

6.1. Evaluation of the minimal inhibitory concentration (MIC) of EB and its analogs in the yeast strains (S1 and S2) of *C. albicans* strains

Yeast test suspensions (S1 and S2) were prepared by the broth microdilution method (Koga-Ito *et al.*, 2008) with small modifications, following CLSI document M27-A guidelines (NCCLS, 2002). In brief, three to five colonies of the appropriate *C. albicans* strain greater than 1.0 mm in diameter were selected from stock YPD agar plates and suspended in 1 mL of RPMI 1640 medium. A 1:11 dilution in RPMI 1640 (1 mL) was then prepared and the turbidity was measured spectrophotometrically. The original 1 mL solution was then diluted in 50 mL of fresh RPMI 1640 to achieve an initial inoculum with an $Abs_{600\ nm}$ of 0.010. The stock solutions of FLU, EB and the other EB analogs were diluted in RPMI 1640 medium to achieve the drug concentration (200 µM) unless otherwise specified. These test compounds were then 1:2 serially diluted in RPMI 1640 medium to obtain a concentration range of 100, 50, 25, 12.5, 6.25, 3.125, 1.56, 0.78 µM as per the starting concentration. Growth inhibition assay was performed in triplicate for all EB analogs against S1 and S2 strains. Each test well was filled with 200 µL of the cell suspension followed by 200 µL of the appropriate 2x-concentration test compound. Final drug concentrations within test wells ranged from 3.125-100 µM, with exception for compounds G8, G22, G24, G27, G31, G35 (1.56 - 50 µM); G-15 and G17 (1.17 - 37.5 µM);); G5, G18, (0.78 - 25 µM); G39 (0.121 - 3.9 µM); G29 (0.118 - 3.8 µM); G28 (0.109 - 3.5 µM); G9 (0.103 - 3.3 µM); G19 (0.065 - 2.1 µM) and G20 (0.78 - 25 µM). The concentration of vehicle did not affect yeast growth and did not exceed 0.4 % (vol/vol) in any of the wells. The growth control wells contained 200 µl of the inoculum suspension and 200 µl of RPMI 1640 medium. Sterility control wells contained 400 µl of RPMI 1640 only. All plates were incubated at 30°C for 48 ± 4 h and MIC values were recorded at 24 and 48 h (MIC_{24h}, and MIC_{48h}, respectively) following a visual observation of turbidity as

compared to drug-free growth medium. The MIC was defined as the lowest concentration showing complete inhibition of growth after 48 h, when inspected by eye, in all three wells of a given treatment.

6.2. Evaluation of the IC_{50} of EB and its analogs in the S1 and S2 strains of *C. albicans*

In studies assessing the IC_{50} of EB and compounds G1- G40, cells were treated and incubated for 48 h as described in 6.1. Immediately following MIC_{48hr} assessment, 800 µL of distilled water was added to all wells and the turbidity of each well measured spectrophotometrically to determine the $A_{600\ nm}$. A mixture of 400 µL of sterile RPMI culture medium and 800 µL of distilled water served as the blank. For each test compound, the average of the triplicate measurements was then plotted as a function of the respective drug concentration (semilog plot). IC_{50} values were then determined from the graph.

6.3. Confirmation of MIC using a colorimetric assay

Resazurin assay is a colorimetric assay that is extensively used to assess the cell viability. The blue dye, resazurin (7-hydroxy-3H-phenoxazin-3-one 10-oxide) is nonfluorescent and reduced to pink, highly red fluorescent resorufin (7-hydroxy-3H-phenoxazin-3-one) by the living cells (Vasconcelos *et al.*, 2014) (Walzl *et al.*, 2014). The yeast cells were seeded at an $Abs_{600\ nm}$ of 0.010 and incubated with the respective compounds in a total volume of 200 µL in a 96-well plate. After obtaining MIC from the broth microdilution method, ~20 µL resazurin (0.02%, 2 mg diluted in 10 mL) were added to each well and mixed with the well contents. The plates were sealed with plastic paraffin film and re-incubated for further 1 h before visual reading. Wells with pink-violet or pink color indicated fungal activity with chemical reaction of oxidation-reduction of resazurin

into resorufin, therefore the last blue well (left to right) on the 96-well plate served as the MIC. Resazurin assay was carried out with the most active compounds from the four groups (G4, G13, G23, G20, and G30). All the experiments were performed in triplicate

7. Evaluation of the effect of EB and compounds G4, G13, G20 and G30 upon medium acidification by S1 and S2 strains of *C. albicans*

(a) Chemicals- KC1 (2.98 g) was dissolved in distilled water (40.0 mL) to give a 1.0 M solution. Dextrose was dissolved in distilled water to a final concentration of 40.0 % (wt/vol).

(b) Test compound solutions- Based on the trend of IC_{50} values observed for the EB analogs, it was decided that representative compounds with no (FLU), low (G4), medium (G13 and EB), or high (G20 and G30) growth inhibition activity would provide a balanced sample set in order to test the link between inhibition of medium acidification and fungal toxicity. Therefore, compounds G4, G13, G20, and G30 were selected for further studies. This set of compounds also provided a sample set with an appealing distribution of structural substitutions to analyze. EB, a known Pma1p inhibitor in yeast, was selected to serve as a positive control, while FLU was selected to serve as a negative control.

FLU (5.0 mg) was dissolved in DMSO (163.4 µL) to give a 100.0 mM solution. EB and its analogs were prepared from their stock solutions and were diluted in 100% DMSO to yield stock concentrations of 1.0, 10.0, 20.0, and 30.0 mM.

(c) Method- Medium acidification assays were carried out using a modification of a procedure described by (Perlin *et al.*, 1988). To this end, yeast cells (S1 & S2 strains) were suspended in 1.0 mL of YPD medium and the $Abs_{600\,nm}$ of the cell suspension was adjusted to within the range of 0.5 - 2.0. A 10 µL aliquot of this inoculum was then added to 50 mL

of YPD medium in a 250 mL Erlenmeyer flask. The yeast cells were then placed in a shaking incubator set at 30°C and 200 rpm for approximately 12 h ($Abs_{600\ nm}$~1.0), and then adjusted to mid-log phase ($Abs_{600\ nm}$= 0.8). Following this standardization, 50 mL of the mid-log phase cell suspension was centrifuged at 2000 x g for 5 min to obtain a pellet. The supernatant was discarded, and the pellet was resuspended in 40 mL of distilled water (dH_2O). The 40 mL sample was then centrifuged at 2000 x g for 5 min, after which the supernatant was again discarded. This wash step was then repeated once more. Following the second wash, the pellet was resuspended in 10.0 mL of dH_2O wherein 9 mL sample was then added to 41 mL of dH_2O. The sample was then aliquoted into 5 separate 50 mL conical tubes, with each tube receiving 9 mL of cells. The cell samples were then placed in a shaking incubator at room temperature and 200 rpm for 2 h. Following the 2 h incubation period, the test sample received 21 mL of dH_2O and 750 µL of KCl solution. The samples were then transferred to 40 mL beaker and stirred briskly using a magnetic stir bar. The pH of the mixture was adjusted to ~6.0 using drop wise addition of either 0.1 N HCl or 0.1 N NaOH (as required). Once the pH stabilized (~15 min on average), samples received 1.5 mL of 40% (wt/vol) dextrose solution. Note that samples were then pre-incubated with 32.3 µL of each test compound 2 min prior to addition of dextrose, to give treatment concentrations (0.1, 0.3, 10 & 30 µM). Following administration of dextrose, the pH of each sample was recorded every minute for 30 min. For each treatment compound, the pH values were plotted as a function of time. All the experiments were performed at least three times using the same test concentrations of each drug. The concentration of test compound required to inhibit medium acidification by 50% (IC_{50MA}) was then determined from a plot of the change in pH vs. the concentration of test compound at 30 min, as

compared to untreated cells. The change in pH for untreated cells at 30 min was assigned the value of 100%.

8. Scanning Electron Microscopy

A scanning electron microscope (SEM) scans a focused electron beam over a surface to create an image and obtain information about the surface topography and composition. S1 & S2 cells were separately cultured in the absence (control) or presence of EB, FLU or G30 (30 μM) in YPD media in a 50 ml conical tube on the shaker at 200 rpm. After 14 h incubation, yeast cells were pipetted onto filter paper with the aid of suction, washed with PBS, and fixed in phosphate-buffered glutaraldehyde (1.5 %) for 1 h at 4 ℃. Dehydration of the samples was achieved through a series of increasing concentration of alcohol transfer steps. Cells were dried in a Tousimis' Autosamdri-815 critical point dryer using bone-dry carbon dioxide as a transition fluid. Samples were sputter-coated for 120 s with Pt/Pd. Samples were viewed on a JEOL JSM-6010LA scanning electron microscope with an accelerating volt at 20kV.

9. Formulation

Ebselen nanoemulsion: EB is a difficult drug to use *in vivo* due to its high hydrophobicity and tendency to precipitate into watery components of tissues. In collaboration with Dr. Ketan Patel (St. John's University), a self-nanoemulsifying drug delivery system (SNEDDS) was formulated. Nanoemulsion are kinetically stable colloidal systems which comprises of two immiscible liquids like water and oil, stabilized by an interfacial film consisting of a suitable surfactant and co-surfactant to form a single phase (Gurpreet and

Singh, 2018). EB in a nanoemulsion delivery system makes it feasible to be incorporated in hydrophilic environment thereby alleviating the precipitation of the drug & providing high stability to the formulation. A preconcentrate is an anhydrous homogenous mixture of all the components of a formulation and in contact with water forms SNEDDS. In other words, a self-nanoemulsifying preconcentrate of EB (EB-SNEP) will help in releasing the drug intravaginally over a controlled release rate by forming a nanoemulsion (EBN) intravaginally. The rationale for testing 0.10 mg and 0.25 mg dose of EB is based on the previous studies from our lab which showed efficacy against chemical-induced cutaneous injury.

9.1 Preformulation studies

a) Preparation of EB loaded-self nanoemulsifying preconcentrate (EB-SNEP): Based on the preformulation studies (Vartak *et al.*, 2020b) excipients and co-solvents were selected for preparation of EB loaded preconcentrate (EB-SNEP). The ternary phase diagram was plotted by varying the following parameters i.e. TTO, oil: surfactant and DMA as co-solvent. Pre-concentrates were thoroughly dispersed in fixed quantity of water to form nanoemulsion. The optimized preconcentrate was selected based on visual assessment (transparent with no phase separation), particle size and long-term stability of the nanoemulsion (EBN) formed.

b) Preparation of EBN formulation: For the preparation of medium chain triglyceride (MCT) Captex® 300 EP/NF and tea tree oil constituted the oily phase, whereas Kolliphor® ELP served as the surfactant. Together, the MCT and the surfactant were mixed in 5:7 ratio. EB-SNEP was prepared by adding EB in DMA (2 mg EB) to the MCT-surfactant mixture and tea tree oil in 1:5:2.5 ratio. Altogether, when EB-SNEP is brought in contact

with simulated vaginal fluid (SVF) or intravaginal fluid in a pre-clinical setting, a nanoemulsion (EBN) will form.

c) Optimization and characterization of TTO in EBN: Firstly, EB preconcentrates with varying TTO concentration of 0, 10, 20, and 30% v/v were visually assessed for any signs of agglomeration or haziness by dispersing 150 µL of each preconcentrate in 5 mL of distilled water. A stable nanoemulsion formation was confirmed by a clear homogenous system and presence of a blue tinge confirming the nanosized system.

The preconcentrates with varying concentrations of TTO (0, 10, 20, and 30%) were also dispersed in simulated vaginal fluid (SVF) prior to particle size analysis. A precipitation study was carried out for 4 h primarily to optimize the TTO concentration and assess the effect of TTO concentration on the stability of EB in nanoemulsion. Briefly, an increasing concentration of TTO from 0-30 % was added to a fixed ratio of EB in DMA and oil:surfactant mixture. All the samples were dispersed in purified water such that a nominal concentration of 1 mg/mL of EB was achieved. An equivalent concentration of EB in DMA stock dispersed in water was also assessed for precipitation. The resultant dispersions were constantly agitated on a thermostatically controlled shaker at 37℃. Aliquots from each sample were withdrawn and added to different centrifuge tubes at time points of 1, 2, 3 and 4 h and centrifuged at 2000 rpm for 10 mins. The resulting supernatant of each sample was withdrawn and diluted with acetonitrile and further analyzed using HPLC (Appendix 1). All the samples were analyzed in triplicates.

To optimize the final TTO concentration, each preconcentrate batch was assessed for particle size and polydispersity index (PDI) in triplicates by dynamic laser light scattering method using Malvern Zetasizer Nano (Malvern Panalytical, UK). The detailed

composition of EBN formulation used in the intervention *in vivo* study are described in (Appendix 2).

9.2 Antifungal susceptibility testing of EBN formulation

The MICs of the EBN formulation for yeast test suspensions (S1, S2, and *C. glabrata*) were prepared by the broth microdilution method (Koga-Ito *et al.*, 2008) with small modifications (Orie *et al.*, 2017), following CLSI document M27-A guidelines (Clinical and Laboratory Standards Institute, 2008) and determined by resazurin colorimetric assay. Approximately five colonies of the appropriate *C. albicans* strain ≥ 1.0 mm in diameter were selected from stock YPD agar plates and suspended in 1 mL of RPMI 1640 medium. An inoculum was prepared with an Abs_{600} nm of 0.010. The test drugs (EB in DMA, EBN, FLU, and MICO) were 1:2 serially diluted in RPMI 1640 medium with L-glutamine to obtain a concentration range of 12.5 – 200 µM and the final concentrations of all the test drugs ranged from 6.25 to 100 µM. Similarly, the Blank + TTO was serially diluted to obtain a TTO concentration of (0.0125% - 0.4% v/v). Sterility control wells included RPMI only, vehicle (DMA only). The plates were incubated for 48 h at 30℃. ~20 µL of 0.02% w/v of resazurin) To confirm the growth inhibitory effects of the test drugs, the resazurin viability assay was carried out. The MIC was recorded by visually assessing the turbidity and was classified as the lowest concentration that prevented the change in color from blue to pink (last blue well from left to right) indicating no cell growth. All experiments were carried out in triplicate wells and repeated thrice.

9.3 *In vitro* cytotoxicity assay

a) Lactate dehydrogenase (LDH) assay: LDH assay is a colorimetric analysis to determine the amount of LDH enzyme released which is directly related to cytotoxicity

level produced when exposed to toxic agents. The cytotoxicity of EBN with and without TTO was evaluated in HeLa cell line using the LDH cytotoxicity assay kit as previously described (Vartak, *et al.*, 2020b). All the reagents were prepared based on manufacturer's protocol. Cells cultured in 96- well plates were treated with highest concentration of EBN (100 µM) with and without 30% TTO and incubated for 3 h. Control cells without treatment served as negative control for this assay. After incubation, plate was centrifuged and 100 µL of supernatant from each well was transferred to another 96- well plate and further incubated with 100 µL of LDH for 30 min at 37 ℃ and 5% CO_2. Intensity of color in each well was compared with control by measuring the absorbance at 490 nm wavelength using a microplate reader (Bio-Tek Instruments, Inc). These data are shown as % LDH activity compared to the control for both EBN with and without TTO.

b) Evaluation of cytotoxicity of EBN formulation on *Lactobacilli*: The bacterial culture in the exponential growing phase were used to study the cytotoxicity of EBN and its components on *Lactobacillus* population using a resazurin based colorimetric assay. Three-five colonies of *L. acidophilus* were seeded in 10 mL MRS broth at 37 ℃ shaking at 200 rpm for 16-18 hours. In brief, bacterial cells were adjusted to 0.5 McFarland standard density i.e. (~10^8 CFU/ml). Treatment groups (Blank, Blank + TTO, and EBN) were tested at concentrations ranging from 1.56 - 100 µM of EB in 96-well plates along with 50 µl of bacterial suspension to make a total volume of 100 µl using MRS broth. Negative control wells included MRS broth only while positive control wells included cells only and ampicillin (0.1 mg/ml) as a reference control. After incubation for 24 h at 37°C, 20 µl of resazurin dye (0.02 % w/v) was added to each well and observed for change in dye color to determine cell viability.

10. Animals

The Institutional Animal Care and Use Committee (IACUC) of St. John's University reviewed and approved protocol # 1369 for the pilot study to establish the mouse model of VVC whereas the protocol # 1949 was approved for the intervention study in the established mouse model of VVC. The animal care was taken in accordance with the guidelines established by the U.S. Department of Agriculture.

a) Source of Animals:

Female BALB/c mice 18-22 g were purchased from Taconic Biosciences (Germantown, NY). All animals were housed and handled according to AAALAC-accredited Animal Care Center (ACC) at St. John's University (Queens, NY). Animal were allowed to acclimatize for a week in the ACC.

b) Animal Housing:

All animals were housed singly during the study in temperature and humidity regulated rooms with 12 hour-day and 12 hour-night cycles.

c) Number of animals:

In vivo studies were carried out first with pilot studies for establishing the mouse VVC model with two strains, S1and 10231. The number of animals that accounted for the pilot study were 12/strain (Table 2 and Figure 4). The intervention study with S1 strain comprised of 11 experimental groups (Table 3 and Figure 5) with an n=7-9 per group which equals 79 in total. On the day of an experiment, ~ seven mice were randomly selected from among the different groups by a random generator. All the animal details including body weight, codes, randomization number, euthanization date are included in the Appendix 3.

11. Animal Studies

A mouse model of VVC was used in the current study (Junko Yano and Fidel, 2011). This experimental mouse model has been established to study the pathogenesis of *Candida* infection as well as to test potential antifungal therapies *in vivo.* Vaginal fungal burden and immunohistological responses are commonly studied using this model. The advantage of this model is that it can be used to test novel interventions *in vivo* and can be adapted to test potential antifungal agents that work against drug-resistant strains (Junko Yano *et al.*, 2012; Bruno *et al.*, 2015).

11.1. A pilot study to establish a mouse model of vulvovaginal candidiasis (VVC)

a) *C. albicans* strains: The pilot study was carried with intravaginal inoculation of both the strains of *C. albicans*, S1, a clinical isolate (5.5 x 10^5 CFU/20 µl) and ATCC 10231 (5.5 x 10^6 CFU/20 µl). Each strain of *C. albicans* were added to YPD media and adjusted spectrophotometrically to an Abs_{600nm} of 0.010. The broth culture was incubated in YPD broth for ~11 h at 30°C with shaking at 200 rpm to reach a stationary phase culture. Following incubation, the broth culture was spun in a centrifuge at 800 x g for 5 min. The resulting pellet was washed twice with sterile PBS. The pellet was suspended in a fresh YPD media and adjusted to obtain a concentration of 5.5 x 10^5 or 10^6 CFU in 20 µL, respectively. This inoculum was enumerated on a YPD agar plate to confirm the colony forming units (CFUs/20 µl).

b) Vaginal inoculation*:* As depicted in Figure 4, mice were administered with 0.2 mg of β-estradiol 17-valerate dissolved in 100 µl sesame oil by subcutaneous injection 72 h prior to inoculation (day -3). Nine mice were inoculated with test strain 10231 and the other nine with test strain S1. An additional three mice per test strain were inoculated with yeast but

not exposed to estrogen and these mice served as the controls for this study (Table 2). In order to reduce the number of animals for the pilot study, naive or estradiol valerate only groups were excluded, as mice do not harbor *C. albicans*, like humans do (Segal and Frenkel, 2018).

Table 2: Tabular representation of the groups involved in the pilot study

S1 (clinical isolate) at 5.5 x 10^5/20 µl and 10231 (ATCC strain) at 5.5 x 10^6/20 µl

Groups	**Day 0**	**Day 3**	**Day 6**	**Day 9**
Group 1 (with estrogen) n per strain	Yeast (5.5 x 10^5 or 10^6) in PBS (20 µl) + estradiol valerate in sesame oil (2mg/ml)	n=3	n=3	n=3
Group 2 (without estrogen) n per strain	Yeast (5 x 10^5 or 10^6) in PBS (20 µl)	n=1	n=1	n=1

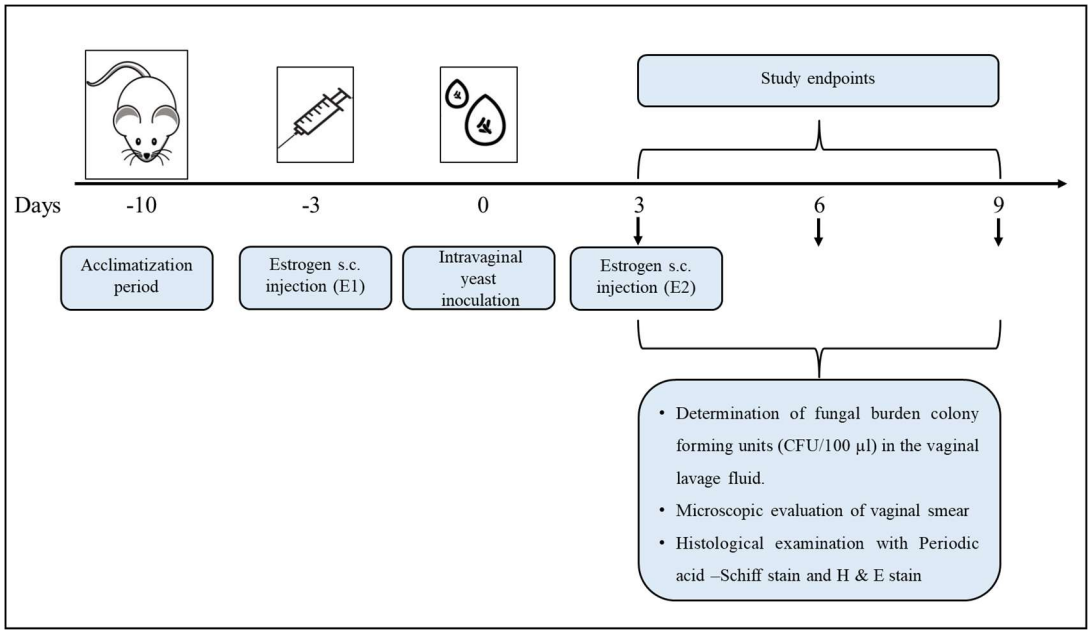

Figure 4:Schematic representation of experimental setup and timeline for the *in vivo* pilot study for construction of mouse VVC model. Day -10 to -3 indicates acclimatization, day -3 indicates subcutaneous s.c. estrogen injection, day 0 indicates intravaginal yeast inoculation, day 3 indicates second s.c. estrogen injection and day 3, 6, and 9 indicates study endpoints for the respective groups.

To test the utility of the 10231 and the S1 strains in the VVC model, estrogen-treated (estrogenized) mice were intravaginally inoculated by introducing 20 µl of YPD containing *C. albicans* (S1 or 10231 blastoconidia (5.5×10^5 or 10^6 CFUs) into the vaginal lumen (day 0) and the infection was allowed to progress for an additional nine days. A gel loading tip (highly flexible unlike sturdy pipette tips) was gently inserted not more than 5 mm deep into the vaginal lumen of 12 mice. The duration of the pilot study accounts for 12 days after the acclimatization period. Vaginal fungal burden was evaluated terminally at designated time points post-inoculation (day 3, 6, and 9) day post-inoculation (dpi) (Bruno *et al.*, 2015; Kovács *et al.*, 2014; Yano and Fidel, 2011). On day 3, mice were given a 2nd estrogen injection to maintain pseudoestrus phase throughout the study period.

c) Vaginal lavage and fungal burden: After euthanization, vaginal lavages were collected from sacrificed mice using 100 µl of sterile PBS. The fluid was serially diluted (1:10) and plated on YPD agar plates supplemented with ampicillin. The colony-forming units (CFU) were enumerated 48 h after incubation at 30°C. Vaginal lavages were also examined microscopically for the presence of leukocyte infiltration and hyphae as evidence of infection.

d) Histological evaluation by PAS stain: Periodic acid–Schiff (PAS) stain is recommended for observing fungi in tissues and smears. Fungi stain specifically by virtue of the presence of polysaccharides and chitin in the fungal cell wall. Fixed and paraffin embedded vaginal tissues were immersed in xylene to deparaffinize followed by quick dips in 100% ethanol and then in distilled water. The slides were then immersed in 1% periodic acid for 10 min and rinsed in tap water for 5- 10 min. Later, the slides were immersed in fucshin solution for 2 min, rinsed in tap water for 30 sec, and then immersed in sodium metabisulfite solution for 30 min. The slides were then rinsed in tap water for 3-5 min and immersed in light-green stain for 2 mins, followed by a brief rinsing and a set of dehydration steps (10 sec in 95% ethanol, 1 min in 100% ethanol, and twice for ~ 1 min xylene. The slides were mounted and observed under light microscopy.

11.2. An intervention study was carried out to assess the antifungal activity of EBN, FLU, and MICO in the mouse model of vulvovaginal candidiasis (VVC)

a) *C. albicans* strains: Since ATCC 10231 did not provide a sustained infection over 6 days, the intervention study was carried out using S1 strain with 5.5 x 10^5 CFU/20 µl. All strains of *C. albicans* were grown in yeast extract-peptone-dextrose (YPD) broth for ~11 h at 30°C with shaking at 200 rpm to reach a stationary phase culture. Following incubation,

the *C. albicans* culture was washed in sterile YPD and enumerated on a YPD agar plate to determine the colony forming units (CFUs/100 µl).

b) Vaginal inoculation*:* Briefly, mice were administered with 0.2 mg of β-estradiol 17-valerate dissolved in 100 µl sesame oil by subcutaneous injection 72 h prior to inoculation (day -3). To establish a robust model of VVC (Figure 5), estrogen-treated (estrogenized) mice were intravaginally inoculated by introducing 20 µl of YPD containing *C. albicans* S1 strain blastoconidia (5.5×10^5 CFU/20 µl) into the vaginal lumen (day 0) and the infection was allowed to progress for an additional three days (day 3). A gel loading tip (highly flexible unlike sturdy pipette tips) is gently inserted not more than 5 mm deep into the vaginal lumen Groups of 13 mice were evaluated terminally at designated time points post-inoculation (3^{rd} & 6^{th} day post-inoculation (dpi)) (Bruno *et al.*, 2015; Kovács *et al.*, 2014; Yano and Fidel, 2011;). On Day 3, mice were given a 2^{nd} estrogen injection (to maintain pseudoestrus phase) as well as one of the treatments described in Table 3 (repeated on day 4 and day 5 as well). On day 6, all mice were euthanized (24 h after the last treatment) and the vaginal tract were lavaged and excised for further analyses. The vaginal tissues were trimmed at the base of the opening and the cervix for histopathological analysis (Liao *et al.*, 2017; Yano and Fidel, 2011; Zhang *et al.*, 2013;).

.

Table 3:Summary of treatment groups included in the Intervention study

Groups	Treatment	No. of animals	Endpoint	Rationale for use
Group 1	Naive	n=7	Day 6	This group served as a negative control for the whole study since unlike humans' mouse does not harbor yeast in their vagina.
Group 2	3rd day infected	n=6	Day 3	This group was infected with S1 strain and sacrificed on day 3 to demonstrate that intravaginal infection has been achieved.
Group 3	6th day infected (control) (Estrogenized and infected)	n=8	Day 6	This group was infected with yeast but did not receive any treatment and hence shows the difference amongst treatment groups.
Group 4	Blank without tea tree oil (20 µl) DMA, Captex 300 EP/NF, Kolliphor ELP	n=6	Day 6	This group served as a vehicle group to Group 6 and 7 to determine whether these ingredients have any effect of their own
Group 5	Blank + TTO (27 µl) DMA, Captex 300 EP/NF, Kolliphor ELP and tea tree oil	n=9	Day 6	This group served as a vehicle group to Group 6 and 7 to determine whether TTO has any antifungal effect of its own.
Group 6	Ebselen (5 mg/kg) 0.10 mg in 27 µl (DMA, Captex 300 EP/NF, Kolliphor ELP & tea tree oil)	n=7	Day 6	This dose has shown a desired effect in our previous lab work in a mouse model of chemical induced injury.

Group 7	Ebselen (12.5 mg/kg) 0.25 mg in 27 µl (DMA, Captex 300 EP/NF, Kolliphor ELP and tea tree oil)	n=8	Day 6	This dose has shown a desired effect in our previous lab work in a mouse model of chemical induced injury.
Group 8	Vehicle (27 µl) DMA (20 µl) + 1 % HPMC (190 µl)	n=7	Day 6	This group served as vehicle group to Group 9.
Group 9	EB Suspension (12.5 mg/kg) 0.25 mg EB in 27 µl DMA +1% HPMC solution	n=7	Day 6	This group demonstrated the difference amongst conventional and nanoemulsion EB (Groups 6 & 7).
Group 10	MICO 2% cream 30 µl	n=7	Day 6	Miconazole served as a positive control and is one of the standard intravaginal drugs of treatment for VVC.
Group 11	FLU (25 mg/kg) in 200 µl Kolliphor EL	n=7	Day 6	FLU was administered by oral gavage and served as a positive control. It is a standard oral drug treatment for VVC.

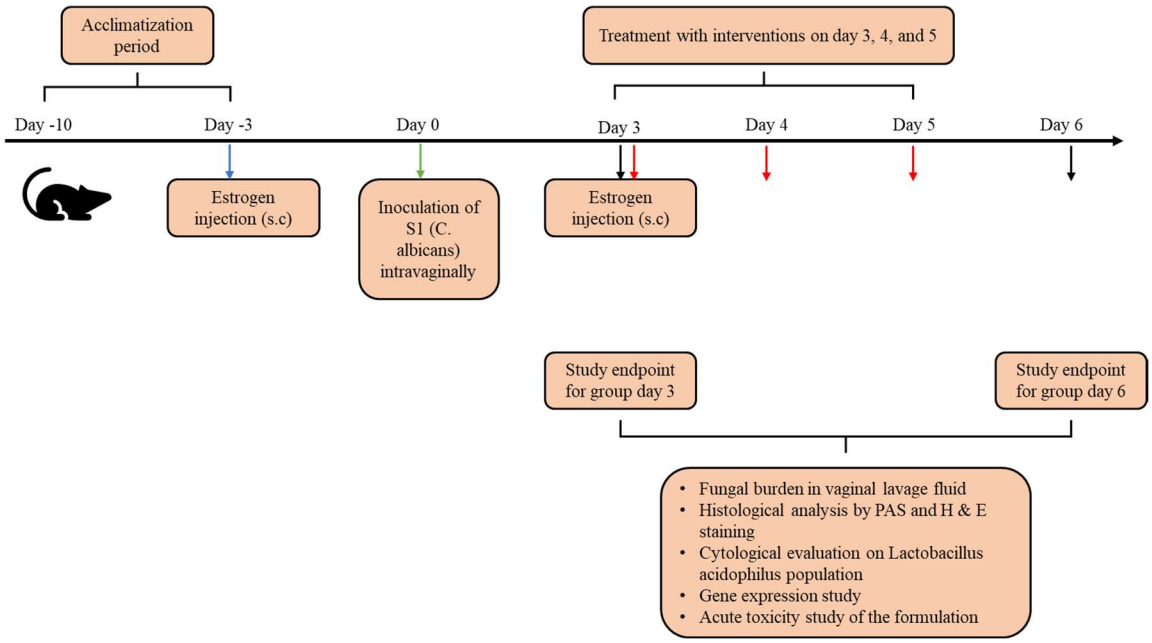

Figure 5: Schematic representation of experimental setup and timeline for the *in vivo* intervention study for construction of mouse VVC model. Day -10 to -3 indicates acclimatization, day -3 indicates subcutaneous s.c. estrogen injection, day 0 indicates intravaginal yeast inoculation, day 3 indicates second s.c estrogen injection and day 3 and 6 indicates study endpoints for the respective groups

c) Vaginal lavage and fungal burden: After euthanization, vaginal lavage for each animal were collected using 100 µl of sterile PBS with gentle aspiration and agitation with a pipette tip for the group (day 3 infected mice) and on day 6 as endpoints. Aliquots from recovered lavage fluids were removed to determine fungal burden. The supernatants of the remaining fluids were centrifuged at 2000 g and stored at -80°C until use. To assess vaginal fungal burden, serial dilutions of the vaginal lavage fluid were cultured on YPD agar plates supplemented with ampicillin. CFU levels were enumerated after incubation for 48 h at 30°C, and results were expressed as CFU/100 µl of lavage fluid.

d) Paraffin Embedding: The excised vaginal tissues were longitudinally excised into halves and one half was used for dehydration and fixation process and so were preserved

in formalin, while the other half of the vaginal tissues were preserved in RNAlater. The tissues were dehydrated using increasing concentrations of 30% (1 h), 60% (1 h), and left in 70% ethanol overnight. The tissues were then dehydrated in 95 % and 100% ethanol for three changes, each for 30 min. The samples were then processed three times in xylene with changes after 1 h, followed by processing with 1:1 mixture of xylene and paraffin in an oven at 54 - 58°C for 1 h. In the end, the samples were suspended in paraffin for three changes of 1 h each in the oven 54- 58°C and embedded in the paraffin cassettes and kept in the refrigerator (4°C) for at least 24 h before use (Tumu *et al.*, 2020).

e) Tissue Sectioning: Tissue sections of 5 µm thickness were sectioned using a standard rotary microtome, placed in a water bath at 40°C with a pinch of 5% gelatin. Sections were lifted from the water bath onto 4-5 slides/sample and dried overnight. The next day, slides with visible tissue sections were selected for staining with H & E and other analysis (Tumu *et al.*, 2020)

f) Hematoxylin and Eosin (H & E) staining: The slides with intact tissue sections were selected and arranged in a slide holder. The tissues were then deparaffinized by placing them in xylene, then rehydrated with a series of alcohol concentrations (Tumu *et al.*, 2020). The hematoxylin (a deep blue-purple dye) stains nuclei in sections whereas Eosin (an acidic pink dye) stains proteins including cytoplasm and extracellular matrix. Following are the steps carried out for H & E (Figure 6).

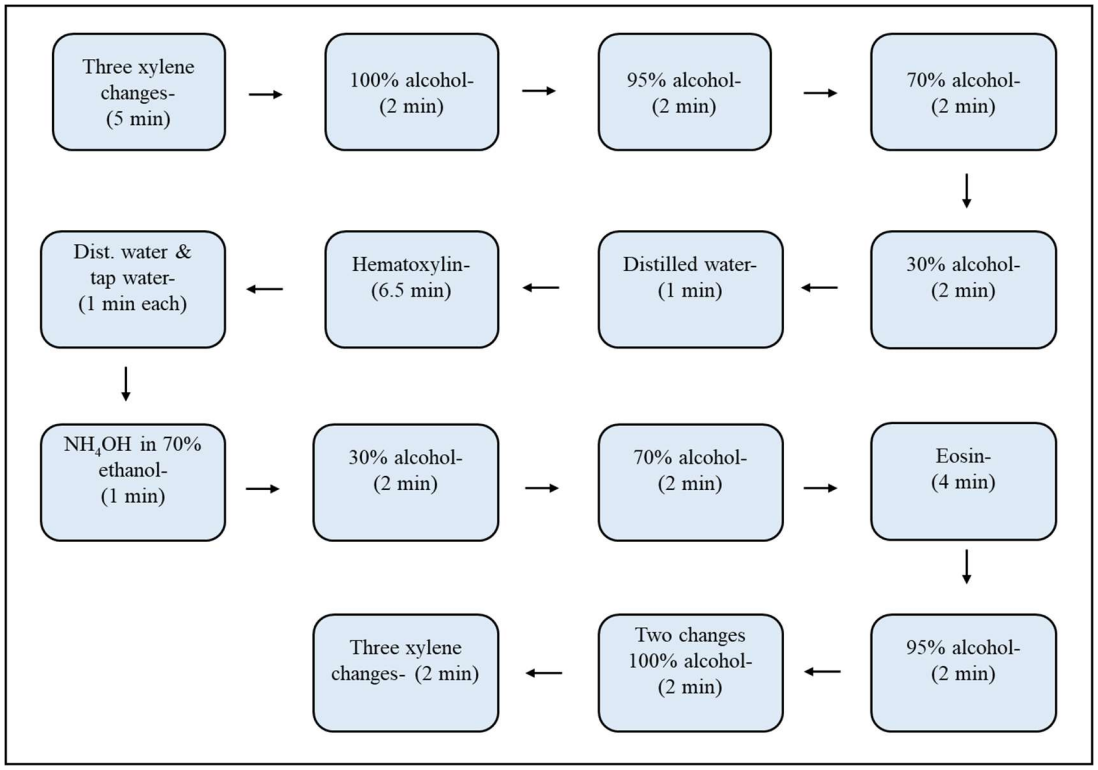

Figure 6: Flowchart depicting each step in H & E staining technique

g) Immunohistochemistry: The paraffin embedded vaginal tissues following hydration were incubated overnight with antigen retrieval solution. Briefly, tissues were treated with primary antibody myeloperoxidase (MPO) (1:1000; Cat # ab208670; Abcam) in normal goat serum for 2 h at room temperature. MPO is a peroxidase enzyme and acts as a marker for activated neutrophils. After quenching with 0.3% hydrogen peroxide, the slides were washed with TBS and incubated with biotinylated secondary antibody followed by ABC reagent, and finally developed with DAB substrate solution. The tissues were counterstained with methyl green (1% w/w) followed by dehydration and mounted with cover slips to observe at 400× magnification by light microscopy.

The polymorphonuclear leukocytes (PMNs) in the vaginal tissue were counted in 5 nonadjacent fields at 200× and 400× by light microscopy and averaged (n=2). The PMN

counts from 5 fields of view (FOV) for the treatment groups (naive, 6th day infected, MICO, Blank + TTO, EB-SNEP (12.5 mg/kg), and EB-suspension) were enumerated and plotted on a graph.

12. Acute toxicity study of EBN formulation

This study was carried out to determine the toxicity of EBN formulation, if any, on the healthy mouse vaginal tissues. It should be noted that these mice were 15-week-old and weighed 23-24 g due to coronavirus pandemic. A total of 14 mice were divided into four groups: [EB-SNEP (12.5 mg/kg), n=4; Blank + TTO, n=4; naive estrogenized mice, n=3; and naive unestrogenized, n=3. Note that none of the mice were infected with yeast throughout the study period of 9 days. Animal protocol was similar to the intervention study except for the infection on day 0 (Figure 5), except that there was no infection on day 0. Animals were euthanized on day 6 and vaginal tissues were collected and preserved in formalin for tissue processing followed by histological staining with H & E as described above in the intervention study.

13. Statistical analysis of data

Unless otherwise indicated, all experiments were carried out in triplicate and their results are reported as the geometric mean ± the standard error of the mean (S.E.M.) from at least three representative experiments. GraphPad Prism 8.4.0 (GraphPad Software Inc., San Diego, CA) was utilized to perform one-way ANOVA followed by the Kruskal-Wallis test (with Dunn's post-test for multiple comparisons). Statistical differences were significant at $p<0.05$.

CHAPTER III

IN VITRO RESULTS

1. *In vitro* assessment of antifungal activity of EB and its analogs against *C. albicans* (S1 and S2 strains)

1.1.Minimum Inhibitory Concentration (MIC) of EB and its forty analogs against FLU-sensitive (S1) and FLU-resistant (S2) strains of *C. albicans*

In view of the current interest in organoselenium inhibitors of the plasma membrane H^+ -ATPase (Pma1p), (Chan *et al.*, 2007; Orie *et al.*, 2017) we evaluated the antifungal activity of forty novel EB analogs in S1 (FLU sensitive) and S2 (FLU resistant) strains. The lowest concentration of test agent that inhibited the growth (MIC values) of S1 & S2 strains after a specified incubation period of 24 or 48 h was determined by visual inspection. The forty EB analogs were categorized into 4 groups based on their R1 group (Groups I-IV), where each group comprised of 10 compounds with varying R2 groups (see Methods section). Unless otherwise stated, stock solutions of the test compounds were prepared at a final concentration of 100 mM.

1.1.1 Group I (Compounds with R1= 5-CH_3):

Visual assessment of turbidity was carried out for the S1 and S2 strains incubated with the Group I series (G1- G10 test compounds) at 24 and 48 h. Due to solubility limitations, test compounds G5, G8, and G9 could only be tested at 25 μM, 50 μM, and 3.3 μM, respectively, and, except for G5 in S1 only, were not active at these concentrations. The MIC values of test compounds against S1 strain at 24 h exhibited the following trend in order of decreasing potency: G4 > G2, G5> G3 > G1, G6, G7, G10 whereas, at 48 h, the potency decreased in the following order: G4 > G2, G3 > G1, G6, G7, G10. In the S2 strain,

the potency decreased in the following order: G4 > G2, G3 > G6 > G1, G7 > G10 after 24 h and G2, G3, G4 > G6 > G7 > G1, G10 after 48 h. The FLU sensitive strain and FLU resistant strain displayed a MIC of >100 μM. The parent compound, EB exhibited antifungal activity against S1 strain ($MIC_{24h\ \&\ 48h}$= 25 μM; ~6.85 μg/ml) and against S2 strain ($MIC_{24h\ \&\ 48h}$= 33.3 μM; ~9.13 μg/ml). Comparing EB to its analogs, EB was more potent than G2 and G3 (MIC_{48h} against S1= 50 μM), however, compounds G2, G3, and G4 (MIC_{48h}= 25 μM) were more active against S2 strain than EB. In summary, the most consistent compound of the group I was G4 [MIC_{48h} value against S1 and S2= 25 μM (6.7 μg/ml)]. These data are summarized in Table 4.

1.1.2 Group II (Compounds with R1= 5-Cl):

The Group II compounds were comprised of another ten EB analogs (G11 – G20) and were tested for growth inhibition activity against S1 and S2 strains as described above. Due to solubility limitations, test compounds G15, G16, G17, G18, and G19 could only be tested at 37.5 μM, 25 μM, 37.5 μM, 25 μM and 2.1 μM, respectively, and, with the exceptions of G15 and G16 in S1 strain only, were not active at these concentrations. Comparison of the antifungal activity of the test compounds against S1 strain at 24 h and 48 h displayed the following trend in order of decreasing potency: G20 > G13 > G15 > G12, G14, G16 and G20 > G13 > G12, G14, respectively. The MIC values of the test compounds against S2 strain at 24 h and 48 h exhibited a similar trend in order of decreasing potency: G20 > G12, G13 > G14. As mentioned before, the MIC for EB against S1 strain was ($MIC_{24h\ \&\ 48h}$= 25 μM; ~ 6.85 μg/ml) and against S2 strain ($MIC_{24h\ \&\ 48h}$= 33.3 μM; ~9.13 μg/ml), whereas, FLU showed >100 μM for both the strains. In comparison to MIC values of EB, FLU and the test compounds, G20 [equivalent MIC_{48h} against S1 and

S2 strains= 3.125 μM (1.2 μg/ml)] followed by G13 [MIC_{48h} value against S1 strain= 12.5 μM (3.4 μg/ml) and S2 strain= 25 μM (6.8 μg/ml)], were most potent against both strains within this group. These data are summarized in Table 5.

1.1.3 Group III (Compounds with R1= 5-NO_2):

The Group III included G21- G30 compounds and were tested for growth inhibition activity against S1 and S2 strains as described above. Due to solubility limitations, test compounds G22, G24, G27, G28, and G29 could only be tested at 50 μM, 50 μM, 50 μM, 3.5 μM and 3.8 μM, respectively, and were not active at these concentrations. The MIC values of test compounds against S1 and S2 strains at 24 h and 48 h both exhibited the similar trend in order of decreasing potency: G30 > G23 > G21. Comparing to the EB analogs in this series, EB showed antifungal activity against S1 strain ($MIC_{24h\ \&\ 48h}$= 25 μM; ~6.85 μg/ml) and against S2 strain ($MIC_{24h\ \&\ 48h}$= 33.3 μM; ~9.13 μg/ml), whereas, FLU showed >100 μM for both the strains. From the data summarized in Table 6, the most potent compound within this series is G30 [MIC_{48h} value against S1- 6.25 μM (2.5 μg/ml) and S2- 20.83 μM (8.5 μg/ml)].

1.1.4 Group IV (Compounds with R1= 5-CH_3SO_2):

Growth inhibition assays were carried out for the Group IV series of test compounds (G31- G40). Due to solubility limitations, test compounds G31, G35, and G39 could only be tested at 50 μM, 50 μM, 3.9 μM, respectively, and, with the exception of G31 in S1 strain, were not active at these concentrations. The MIC values of test compounds against S1 strain at 24 h exhibited the following trend in order of decreasing potency: G31 > G32, G33, G36 > G38 > G34, G37, and G40; whereas, at 48 h the potency decreased in the

following order: G31 > G32, G33, G36 > G34, G37, G38, and G40. In the S2 strain, the potency decreased in the following order: G31 > G36, G37 > G32, G33, G34, G38, and G40 after 24 h and G36 > G32, G33, G34, G37, G38, and G40 after 48 h, respectively. The MIC values of EB against S1 strain was ($MIC_{24h\ \&\ 48h}$= 25 μM; ~6.85 μg/ml) and against S2 strain ($MIC_{24h\ \&\ 48h}$= 33.3 μM; ~9.13 μg/ml), whereas, FLU showed >100 for both the strains. None of the test compounds within this group were as potent as EB. From the data summarized in Table 7, G31 [MIC_{48h} value against S1- 33.3 μM and S2 strain- >50 μM] was the most active in this series.

1.1.5 Summary of the MIC values

To summarize, test compounds G4, G13, G20, G23, and G30 were more potent than EB based on their MIC values. The Group II series showed the most active compounds followed by Group III, Group I, and Group IV. Table 8 summarizes the potent compounds from each series of EB analogs.

1.2.Half maximal inhibitory concentration (IC_{50} values) of EB and its analogs against FLU-sensitive (S1) & FLU- resistant (S2) strains of *C. albicans*

The IC_{50} values for EB and its analogs were determined by measuring the turbidity of treated samples from each well spectrophotometrically at A_{600nm} following the MIC evaluations at 48 h. For each test compound, the average of the triplicate measurements was plotted as a function of the respective drug concentration. The IC_{50} values for the four groups of test compounds against both S1 and S2 strains are described in Table 9 (Group I), Table 10 (Group II), Table 11 (Group III) and Table 12 (Group IV). Table 13 summarizes the potent compounds from all four series of analogs.

1.2.1. Group I (G1-G10): The IC_{50} values was determined for the S1 and S2 strains incubated with the compounds of Group I series at 48 h. Due to solubility limitations, test compounds G5, G8, and G9, these compounds could only be tested at concentration of 25 μM, 50 μM, and 3.3 μM and were not active at these test concentrations. The IC_{50} values of group I test compounds against S1 and S2 strains showed the following trend in order of decreasing potency: FLU > EB > G4, G2 > G3 > G1, G6, G7, and G10 while in the S2 strain**,** the potency decreased in the following order: G4 > G2, G3, EB > G6, G7 > G1, G10, and FLU. EB showed an IC_{50} value against S1 and S2 strains of 15.0 and 16.5 μM, respectively. The standard antifungal drug FLU showed an IC_{50} against S1 strain of 3.64 μM, whereas S2 strain proved to be resistant to FLU (IC_{50} >100 μM). Test compounds G2 and G4 showed IC_{50} values similar as EB against the S1 strain (16.8 and 16.1 μM), respectively, however, test compound G4 (IC_{50}= 13.6 μM) was slightly more active against S2 strain than EB. Moreover, the Log P did not have an impact on the IC_{50} of the test compounds. To summarize the data in Table 9, test compound G4 exhibited similar antifungal activity as EB against S1 strain and was ~1.2-fold more active than EB against S2 strain.

1.2.2. Group II (G11-G20): The IC_{50} values was determined for the S1 and S2 strains incubated with the compounds of Group II series at 48 h. Due to solubility limitations, test compounds G15, G16, G17, G18, and G19 could only be tested at 37.5 μM, 25 μM, 37.5 μM, 25 μM and 2.1 μM, respectively, and were not active at these test concentrations. The IC_{50} of test compounds against S1 strain at 48 h exhibited the following trend in order of decreasing potency: G20 >> FLU > G13 > G14 > EB > G12 > G11 whereas in the S2 strain, the potency decreased in the following order: G20 >> G12 > G13 > EB > G14 >

G11 > FLU. EB showed an IC_{50} value against S1 and S2 strains of 15.0 and 16.5 μM, respectively. Test compound G13 showed better antifungal activity (IC_{50}= 8.1 μM) against S1 strain and an IC_{50}= 15.7 μM against S2 strain. The most potent test compound in this group was G20 against both S1 and S2 strains (IC_{50}= 0.5 and 1.8 μM, respectively). Note that the log P value did not correlate with the IC_{50} values of the test compounds. In conclusion, G20 exhibited ~30 and ~9-fold stronger antifungal activity than EB against S1 and S2 strains, respectively. The average IC_{50} values of the test compounds in this series are described in Table 10.

1.2.3. Group III (G21-G30): The IC_{50} values was determined for the S1 and S2 strains incubated with the compounds of Group III series at 48 h. Due to solubility limitations, test compounds G22, G24, G27, G28, and G29 could only be tested at 50 μM, 50 μM, 50 μM, 3.5 μM, 3.8 μM, respectively, and were not active at these working concentrations. The IC_{50} of test compounds against S1 strain at 48 h exhibited the following trend in order of decreasing potency: FLU > G30 > G23 > EB > G21 > G25 and G26, while in the S2 strain, the potency decreased in the following order: G30 > EB > G23 > G21 > G25, G26, and FLU. The IC_{50} value of EB against S1 and S2 strains were 15.0 and 16.5 μM, respectively. Test compound G21 showed ~1.9- and 3.3- fold less activity compared to EB against S1 and S2 strains. Compound G23 was more active against S1 (IC_{50}= 8.2 μM) than S2 strain (IC50= 17.3 μM). The most potent compound in this group was G30 with IC_{50} values against S1 and S2 strains (4.1 and 3.4 μM, respectively). Furthermore, based on the IC_{50} values, the log P did not have an impact on the antifungal activity. To recapitulate, G30 showed ~ 3.6- and 4.8- fold stronger antifungal activity compared to EB against S1 and S2 strains, respectively. The IC_{50} values are listed in Table 11.

1.2.4. Group IV (G31-G40): The IC_{50} values were determined for the S1 and S2 strains incubated with the compounds of Group IV series at 48 h. Due to solubility limitations, test compounds G31, G35, and G39 could only be tested at 50 μM, 50 μM, 3.9 μM, respectively, and, with the exception of G31 in S1 strain only, were not active at these working concentrations. The IC_{50} of test compounds against S1 strain at 48 h exhibited the following trend in order of decreasing potency: FLU > G31 > EB > G36 > G32 > G33 > G37 > G34, G38 and G40, while in the S2 strain, the potency decreased in the following order: G36 > EB > G37 > G34 > G32, G33, G38, G40, and FLU. Test compound G31 exhibited an IC_{50} of 9.1 μM and was ~1.6- fold more active than EB; however, in S2 strain, G31 showed growth in the highest concentration tested (IC_{50} > 50 μM). Test compounds G32 and G33 showed antifungal activity against S1 strain (IC50= 17.8 and 31.5 μM, respectively); however, these compounds failed to inhibit S2 growth at all test concentrations (IC_{50} > 100 μM). Test compounds G38 and G40 exhibited IC_{50} > 100 μM and were deemed to be inactive. EB showed an IC_{50} value against S1 and S2 strains of 15.0 and 16.5 μM, respectively, whereas FLU showed an IC_{50} against S1 strain of 3.64 μM, and S2 strain proved to be resistant to FLU (IC_{50} >100 μM). Moreover, the log P did not show an impact on the antifungal activity of the test compounds. To summarize the IC_{50} values for the test compounds in this series, G31 showed stronger antifungal activity than EB in S1 strain, while G36 proved to be more active than EB against S2 strain. The IC_{50} values for the Group IV series in both strains are listed in Table 12.

1.2.5. Summary for IC_{50} values against S1 and S2 strains of *C. albicans*

To conclude, based on the IC_{50} values, G20 was the most potent test compound followed by G30, G13 and G4 against S1 and S2 strains of *C. albicans*. Table 13 summarizes the potent compounds from each series of EB analogs. Group II and Group III compounds appeared to be better antifungals than Group I and Group IV.

1.3.Determination of MIC by colorimetric assay for EB and its analogs along with EB nanoformulation

Resazurin assay is a simple and rapid viability assay to determine the viability of the living cells. After incubation period of ~2-4 h with resazurin dye, wells with pink-violet or pink color indicated fungal viability with chemical reaction of oxidation-reduction of resazurin into resorufin, therefore the last blue well (left to right) is designated as the MIC. (Vasconcelos *et al.*, 2014).

To confirm the growth inhibitory effect of EB analogs in the living yeast cells, we determined the minimum inhibitory concentration (MIC) for the active test compounds from Groups I-IV and fluconazole against S1 and S2 strains using a colorimetric assay with resazurin dye in 96-well microplates. From left to right, compounds were added in the range (100-0.78 µM) in the microplate except for G20 due to low MIC it was added in the range (25-0.39 µM). Each plate had yeast only and DMSO wells as controls.

1.3.1. Compound G4: The plates were treated with G4 and EB starting from 100 µM – 0.78 µM against both S1and S2 strains. The test compound G4 exhibited MIC value of 25 µM in both S1 and S2 strains (Figure 7A and 7B). On the other hand, EB showed a MIC

of 50 μM in the S1 strain and 25 μM in the S2 strain. DMSO and the control (yeast cells only) showed growth in all the wells.

1.3.2. Compound G13: The plates were treated with G13 starting from 100 μM – 0.78 μM against S1and S2 strains. The test compound G13 exhibited MIC value of 12.5 μM in the S1 strain (Figure 8A) and 25 μM in the S2 strain (Figure 8B). On the other hand, EB showed a MIC of 25 μM against both S1 and S2 strains. DMSO and the control (yeast cells only) showed growth in all the wells.

1.3.3. Compound G20: The plates were treated with G20 starting from 25 μM – 0.39 μM against S1and S2 strains. The test compound G20 exhibited MIC value of 3.125 μM in both S1 and S2 strains (Figure 9A and 9B). DMSO showed growth in all the wells. The test compound G20 was also tested with DMA against S1 strain to compare the effect of the vehicle for cytotoxicity, if any (Figure 9C). The plated with G20 in DMA as vehicle exhibited similar MIC value of 3.125 μM and no cytotoxicity as DMSO.

1.3.4. Compound G30: The plates were treated with G30 starting from 100 μM – 0.78 μM against S1and S2 strains. Compound G30 was active in S1 strain (Figure 10 A) with MIC of 6.25 μM, whereas, less active in S2 strain (Figure 10 B) with MIC of 25 μM. On the other hand, EB showed a MIC of 50 μM in the S1 strain and 25 μM in the S2 strain. DMSO and the control (yeast cells only) showed growth in all the wells.

1.3.5. FLU: The plates were treated with FLU and EB starting from 100 μM – 0.78 μM against both S1 (Figure 11A) and S2 strains (Figure 11B). FLU-treated wells reduced the dye to pink color at all concentrations (MIC >100 μM) confirming that it is a fungistatic agent. The MIC of EB-treated wells against S1 and S2 strains were 50 μM and 25 μM, respectively. DMSO and the control (yeast cells only) showed growth in all the wells.

1.3.6. Summary: Of all the EB analogs tested from Groups I- IV, G20 and G30 proved to be the most potent against both S1 and S2 strains (Table 14). These results are more or less similar with the data obtained from broth microdilution method (Table 8).

1.3.7. Comparison of Resazurin data to broth microdilution method: Table 15 summarizes and compares the data obtained from broth microdilution assay and resazurin assay. Thus, resazurin assay is a simple and rapid viability assay which provides similar results as broth microdilution assay.

2. The yeast proton pump (Pma1p) as a viable target for EB and its analogs

2.1. Effect of EB and selected analogs on medium acidification against S1 and S2 strains of *C. albicans*

The yeast proton pump Pma1p is critical to fungal survival as it plays an essential role in regulating intracellular pH and uptake of nutrients. It has been earlier proven that EB (30 μM) can inhibit the medium acidification by S2 strain (Orie *et al.*, 2017). To test this, a modified version of the medium acidification assay described by (Perlin *et al*., 1988) was performed. The most active test compounds from Groups I-IV (G-4, G-13, G-20 and, G-30) were selected based on the MIC and IC_{50} values to evaluate the inhibitory effect at an increasing concentration (1, 3, 10, and 30 μM) on acidification of growth medium by S1 or S2 strains. The inhibitory activity of these compounds was compared to that of EB, which is a documented inhibitor of medium acidification (Chan *et al.*, 2007) and FLU, which does not possess activity against this plasma membrane pump. The concentration of test compounds required to inhibit medium acidification by 50% (IC_{50MA}) was then determined from a plot of the change in pH at 10 and 30 min versus the concentration of

test compound, and compared with the results for untreated cells, which were assigned the value of 100%.

As anticipated, EB suppressed the medium acidification by S1 and S2 cells in a concentration-dependent manner (Figure 12) with significant inhibition seen at 10 μM and total blockage of proton extrusion at concentrations of 30 μM. The IC_{50MA} at 30 mins of EB in this assay was found to be 4.7 and 4.4 μM in S1 and S2 cells, respectively (Table 16). Next, G4 (Figure 13) and G13 (Figure 14) showed a similar inhibitory effect as EB in a time- and concentration-dependent manner at 30 mins (IC_{50MA}= 3.6 μM for both compounds in S1 and 5.6 μM and 5.2 μM, respectively, in S2 strain). The IC_{50MA} at 30 min for G20 for S1 and S2 strain was 6.0 μM and 3.9 μM, while for G30 IC_{50MA} was 5.0 μM and 4.5 μM. The IC_{50MA} at 10 min for G20 (Figure 15) and G30 (Figure 16) could not be determined in S1 strain (>30 μM) due to the erratic pattern of the graph, however IC_{50MA} for S2 strain was 3.9 and 4.5 μM, respectively. We assume that this late inhibitory effect on medium acidification may be due to the bulky nature of the substituents of the test compounds G20 and G30. As expected, treatment with the FLU had no effect on medium acidification in both strains (>30 μM); thereby serving as a negative control (Figure 17, Table 16).

To summarize, the most active EB analogs from the Groups I- IV (G4, G13, G20 and G30) inhibited the H+-ATPase pump at similar concentrations as EB in a time- and concentration dependent manner. It is worthy to note that although the compounds differed in MIC compared to EB, the effects on medium acidification by these compounds were similar to EB.

3. Scanning Electron Microcopy

To investigate the effect of EB, compound G30, and FLU on the architecture of yeast cells, scanning electron microscopy was performed (Chan *et al.*, 2007). To this end, untreated control yeast cells (Figure 18 A and Figure 20A) were found to be ovoid in shape and exhibited smooth appearance and bud scars. On the other hand, cells treated with EB (Figure 18B and 20B) and G30 (30 μM) (Figure 19A and 21A) appeared rough, crinkled, and showed deformed phenotype. The images at lower magnification of EB and G30 clearly displayed fewer cells compared to control (untreated yeast cells S1 and S2) indicating the antifungal potency of EB and G30. FLU- treated S1 cells (Figure 19B) showed crinkled surface phenotype as EB. However, FLU-treated S2 cells (Figure 21B) showed smooth phenotype as control cells indicating that S2 cells are resistant to FLU treatment.

To recapitulate, the SEM images display noticeable surface phenotype of S1 and S2 when treated with G30 which substantiates that this EB analog, indeed, possesses antifungal activity.

Table 4: Growth Inhibitory effects of Group I test compounds (G1-G10), EB, and FLU against S1 and S2 strains of *C. albicans*

Compound	**S1 strain**		**S2 strain**	
	Average MICs µM (24 h)	Average MICs µM (48 h)	Average MICs µM (24 h)	Average MICs µM (48 h)
G1	>100	>100	100	>100
G2	25	50	25	25
G3	50	50	25	25
G4	12.5	25	12.5	25
G5	25	>25	>25	>25
G6	>100	>100	83.3	83.3
G7	>100	>100	100	100
G8	>50	>50	>50	>50
G9	>3.3	>3.3	>3.3	>3.3
G10	>100	>100	>100	>100
EB	25	25	33.3	33.3
FLU	>100	>100	>100	>100

*MIC is the lowest concentration of an antimicrobial drug that inhibits the visible growth of a microorganism after a specified incubation period.

*Unless otherwise indicated, all the MIC values represent the average of 3 experiments performed in triplicate.

Table 5:Growth Inhibitory effects of Group II test compounds (G11-G20), EB, and FLU against S1 and S2 strains of C. albicans

Compound	**S1 strain**		**S2 strain**	
	Average MICs μM (24 h)	Average MICs μM (48 h)	Average MICs μM (24 h)	Average MICs μM (48 h)
G11	100	100	100	>100
G12	25	25	25	25
G13	12.5	12.5	25	25
G14	25	25	50	50
G15	18.75	>37.5	>37.5	>37.5
G16	25	>25	>25	>25
G17	>37.5	>37.5	>37.5	>37.5
G18	>25	>25	>25	>25
G19	>2.1	>2.1	>2.1	>2.1
G20	3.125	3.125	3.125	3.125
EB	25	25	33.3	33.3
FLU	>100	>100	>100	>100

*MIC is the lowest concentration of an antimicrobial drug that inhibits the visible growth of a microorganism after a specified incubation period.

*Unless otherwise indicated, all the MIC values represent the average of 3 experiments performed in triplicate.

Table 6:Growth Inhibitory effects of Group III test compounds (G21-G30), EB, and FLU against S1 and S2 strains of C. albicans

Compound	**S1 strain**		**S2 strain**	
	Average MICs μM (24 h)	Average MICs μM (48 h)	Average MICs μM (24 h)	Average MICs μM (48 h)
G21	50	50	100	>100
G22	>50	>50	>50	>50
G23	25	25	25	25
G24	>50	>50	>50	>50
G25	>100	>100	>100	>100
G26	>100	>100	>100	>100
G27	>50	>50	>50	>50
G28	>3.5	>3.5	>3.5	>3.5
G29	>3.8	>3.8	>3.8	>3.8
G30	6.25	6.25	12.5	20.83
EB	25	25	33.3	33.3
FLU	>100	>100	>100	>100

*MIC is the lowest concentration of an antimicrobial drug that inhibits the visible growth of a microorganism after a specified incubation period.

*Unless otherwise indicated, all the MIC values represent the average of 3 experiments performed in triplicate.

Table 7:Growth Inhibitory effects of Group IV test compounds (G31-G40), EB, and FLU against S1 and S2 strains of C. albicans

Compound	**S1 strain**		**S2 strain**	
	Average MICs μM (24 h)	Average MICs μM (48 h)	Average MICs μM (24 h)	Average MICs μM (48 h)
G31	25	33.3	50	>50
G32	50	50	>100	>100
G33	50	50	>100	>100
G34	>100	>100	>100	>100
G35	>50	>50	>50	>50
G36	50	50	100	100
G37	>100	>100	100	>100
G38	100	>100	>100	>100
G39	>3.9	>3.9	>3.9	>3.9
G40	>100	>100	>100	>100
EB	25	25	33.3	33.3
FLU	>100	>100	>100	>100

*MIC is the lowest concentration of an antimicrobial drug that inhibits the visible growth of a microorganism after a specified incubation period.

*Unless otherwise indicated, all the MIC values represent the average of 3 experiments performed in triplicate.

Table 8:Table summarizing the most active EB compounds from Group I- IV against both S1 and S2 strains of *C. albicans*[1]

Groups	**Compounds**	**S1 strain**	**S2 strain**
		Average MICs (48 h) µM	Average MICs (48 h) µM
Group I	G4	25	25
Group II	G13	12.5	25
Group II	G20	3.125	3.125
Group III	G23	25	25
Group III	G30	6.25	20.8
Group IV	G31	33.3	>50
-	EB	25	33.3
-	FLU	>100	>100

[1]This table was compiled from data found in Table 4-7

Table 9: IC_{50} values for Group I test compounds (G1-G10), EB, and FLU against S1 and S2 strain of *C. albicans*

Compound	**Log P**	**S1 strain**	**S2 strain**
		Average IC_{50} ± SEM (μM)	Average IC_{50} ± SEM (μM)
G1	2.0	>100	>100
G2	2.07	16.8 ± 0.0	16.1 ± 0.1
G3	1.10	33.4 ± 0.5	16.2 ± 0.3
G4	3.25	16.1 ± 0.4	13.6 ± 0.4
G5	3.97	>25	>25
G6	3.34	>100	36.9 ± 3.0
G7	4.02	>100	37.9 ± 2.8
G8	2.86	>50	>50
G9	3.71	>3.3	>3.3
G10	5.46	>100	>100
EB	2.65	15.0 ± 0.3	16.5 ± 0.0
FLU	-0.12	3.64	>100

*IC_{50} is defined as the drug concentration that inhibits microbial growth by 50% as compared to untreated cells.

*Unless otherwise indicated, all IC_{50} values represent the average of 3 experiments performed in triplicate ± the S.E.M.

Table 10: IC_{50} values for Group II test compounds (G11-G20), EB, and FLU against S1 and S2 strain of *C. albicans*

Compound	**Log P**	**S1 strain**	**S2 strain**
		Average IC_{50} ± SEM (μM)	Average IC_{50} ± SEM (μM)
G11	2.23	69.5 ± 1.6	65.6 ± 0.2
G12	2.29	16.7 ± 0.2	14.7 ± 0.1
G13	1.32	8.1 ± 0.0	15.7 ± 0.2
G14	3.48	9.2 ± 0.8	32.9 ± 0.2
G15	4.20	>37.5	>37.5
G16	3.57	>25	>25
G17	4.25	>37.5	>37.5
G18	3.09	>25	>25
G19	3.94	>2.1	>2.1
G20	5.69	0.54 ± 0.0	1.89 ± 0.1
EB	2.65	15.0 ± 0.3	16.5 ± 0.0
FLU	-0.12	3.64	>100

*IC_{50} is defined as the drug concentration that inhibits microbial growth by 50% as compared to untreated cells.

*Unless otherwise indicated, all IC_{50} values represent the average of 3 experiments performed in triplicate ± the S.E.M.

Table 11: IC_{50} values for Group III test compounds (G21-G30), EB, and FLU against S1 and S2 strain of *C. albicans*

Compound	**Log P**	**S1 strain**	**S2 strain**
		Average IC_{50} ± SEM (μM)	Average IC_{50} ± SEM (μM)
G21	1.51	28.0 ± 3.4	55.8 ± 0.2
G22	1.58	>50	>50
G23	2.31	8.2 ± 0.1	17.3 ± 0.3
G24	2.76	>50	>50
G25	3.48	>100	>100
G26	2.85	>100	>100
G27	3.53	>50	>50
G28	2.37	>3.5	>3.5
G29	3.22	>3.8	>3.8
G30	4.97	4.1 ± 0.0	3.4 ± 0.2
EB	2.65	15.0 ± 0.3	16.5 ± 0.0
FLU	-0.12	3.64	>100

*IC_{50} is defined as the drug concentration that inhibits microbial growth by 50% as compared to untreated cells.
*Unless otherwise indicated, all IC_{50} values represent the average of 3 experiments performed in triplicate ± the S.E.M.

Table 12: IC_{50} values for Group IV test compounds (G31-G40), EB, and FLU against S1 and S2 strain of *C. albicans*

Compound	**Log P**	**S1 strain**	**S2 strain**
		Average IC_{50} ± SEM (μM)	Average IC_{50} ± SEM (μM)
G31	0.72	9.1 ± 0.4	>50
G32	0.78	17.8 ± 0.4	>100
G33	1.52	31.5 ± 0.1	>100
G34	1.97	>100	72.7 ± 0.9
G35	2.69	>50	>50
G36	2.06	16.2 ± 2.2	15.1 ± 0.4
G37	2.74	37.2 ± 1.9	32.3 ± 1.6
G38	1.58	>100	>100
G39	2.43	>3.9	>3.9
G40	4.18	>100	>100
EB	2.65	15.0 ± 0.3	16.5 ± 0.0
FLU	-0.12	3.64	>100

*IC_{50} is defined as the drug concentration that can inhibit microbial growth by 50% as compared to untreated cells.
*Unless otherwise indicated, all IC_{50} values represent the average of 3 experiments performed in triplicate ± the S.E.M.

Table 13: Table summarizing IC_{50} values for Group I- IV test compounds, EB, and FLU against S1 and S2 strain of *C. albicans*[1]

Groups	Compounds	S1 strain	S2 strain
		Average MICs (48 h) µM	**Average MICs (48 h) µM**
Group I	G2	16.8 ± 0.0	16.1 ± 0.1
Group I	G4	16.1 ± 0.4	13.6 ± 0.4
Group II	G13	8.1 ± 0.0	15.7 ± 0.2
Group II	G14	9.2 ± 0.8	32.9 ± 0.2
Group II	G20	1.5 ± 0.0	1.89 ± 0.1
Group III	G23	8.2 ± 0.1	17.3 ± 0.3
Group III	G30	4.1 ± 0.0	3.4 ± 0.2
Group IV	G31	9.1 ± 0.4	>50
Group IV	G36	16.2 ± 2.2	15.1 ± 0.4
-	EB	15.0 ± 0.3	16.5 ± 0.0
-	FLU	3.64	>100

[1]This table was compiled from data found in Table 9-12

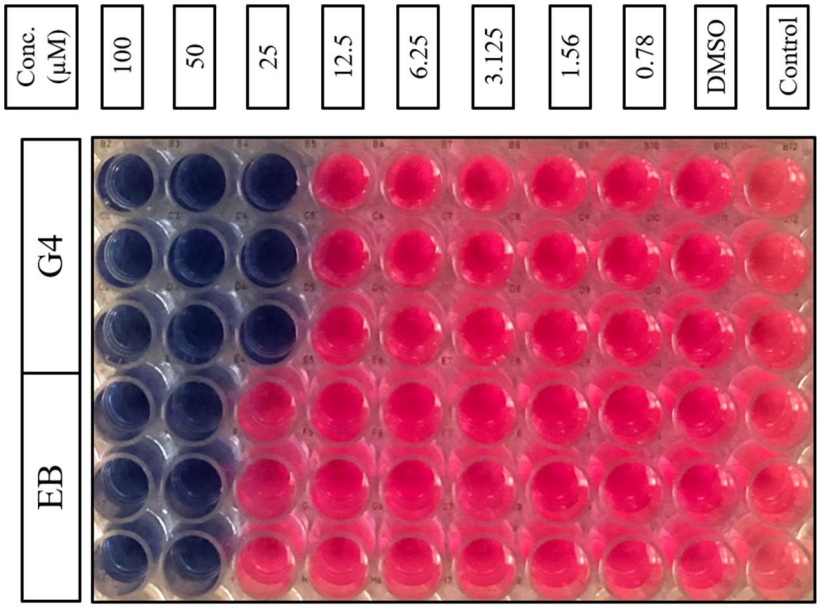

Figure 7A

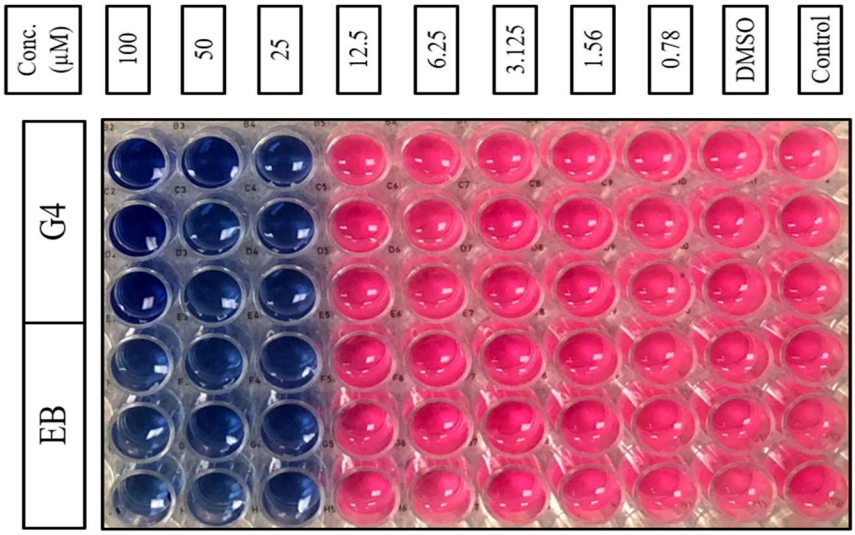

Figure 7B

Figure 7: Representative image of resazurin assay for G4 (MIC= 25 μM) and EB (MIC= 50 μM) against S1 strain (Figure 7A), whereas G4 exhibits an equivalent MIC as EB (25 μM) against S2 strain (Figure 7B). Each plate represents experiments done in triplicate.

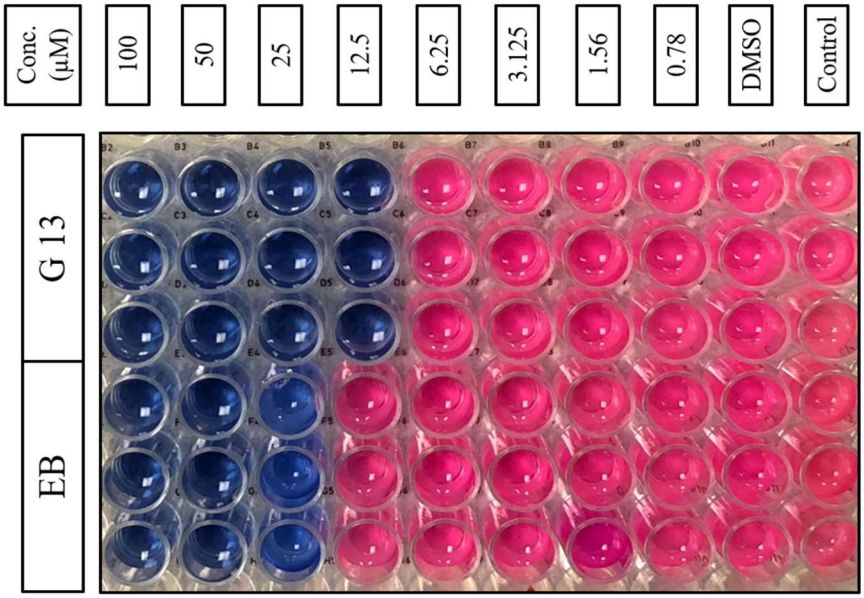

Figure 8A

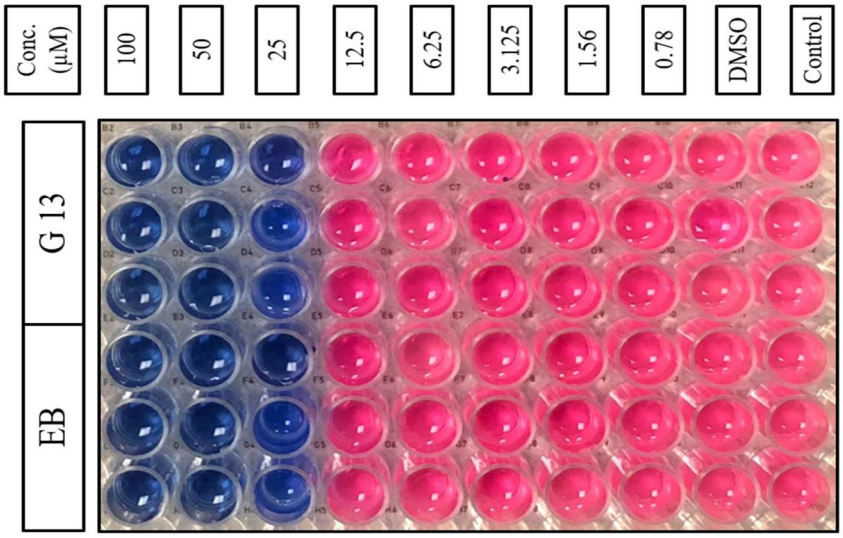

Figure 8B

Figure 8: Representative image of resazurin assay for G13 (MIC= 12.5 µM) and EB (MIC= 25 µM) against S1 strain (Figure 8A), whereas G13 exhibits an equivalent MIC as EB (25 µM) against S2 strain (Figure 8B). Each plate represents experiments done in triplicate.

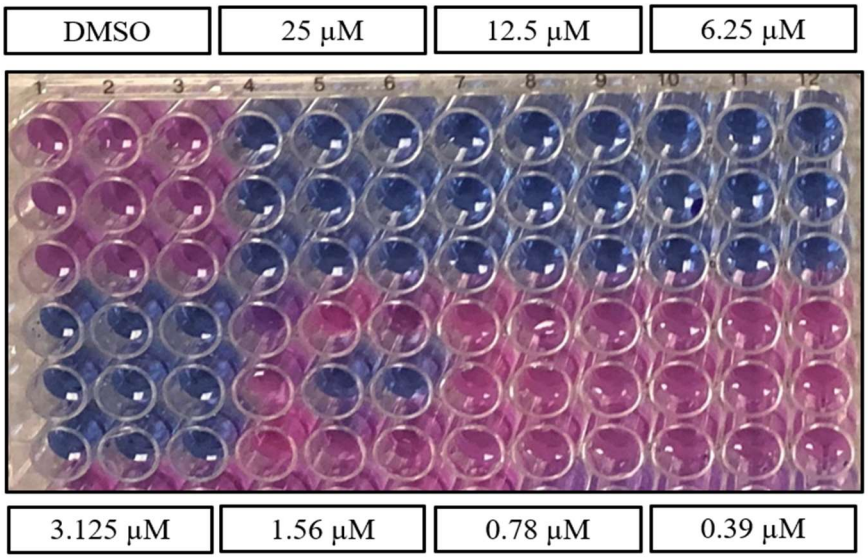

Figure 9A

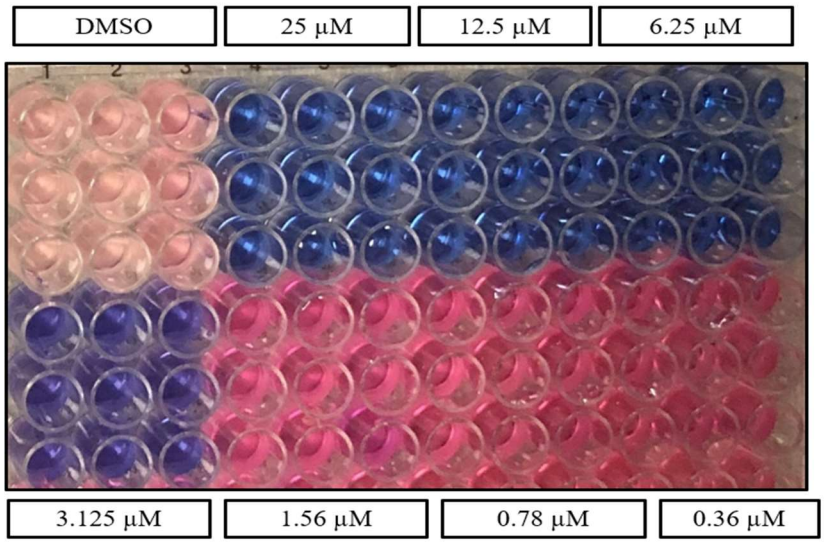

Figure 9B

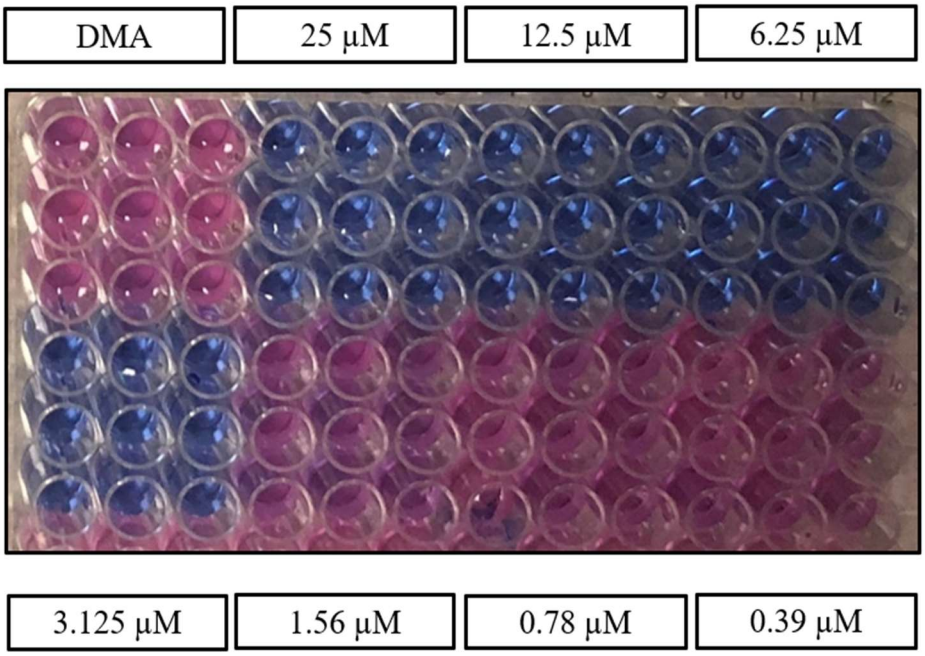

Figure 9C

Figure 9: Representative image of resazurin assay for G20 with an equivalent MIC= 3.125 µM in S1 strain (Figure 9A) and in S2 strain (Figure 9B). Figure 9C indicates a similar MIC for G20 (3.125 µM) when DMA was used as vehicle. Each plate represents experiments done in triplicate.

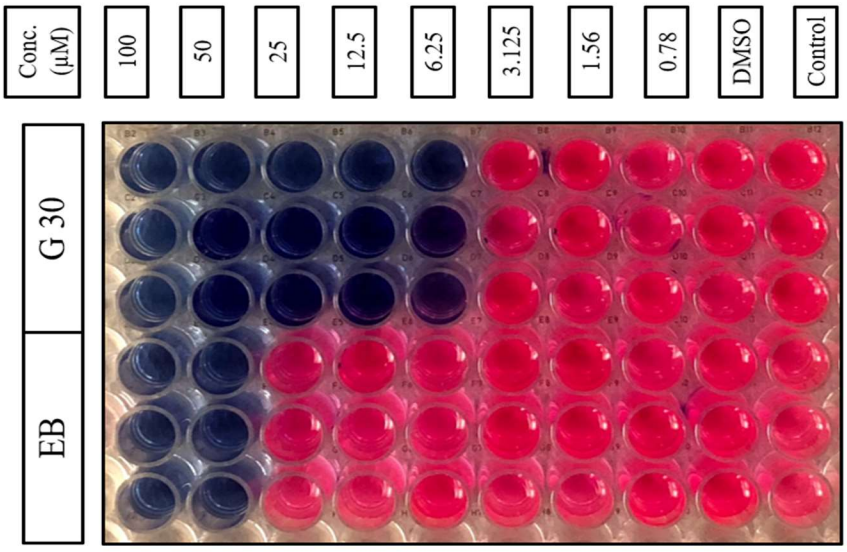

Figure 10A

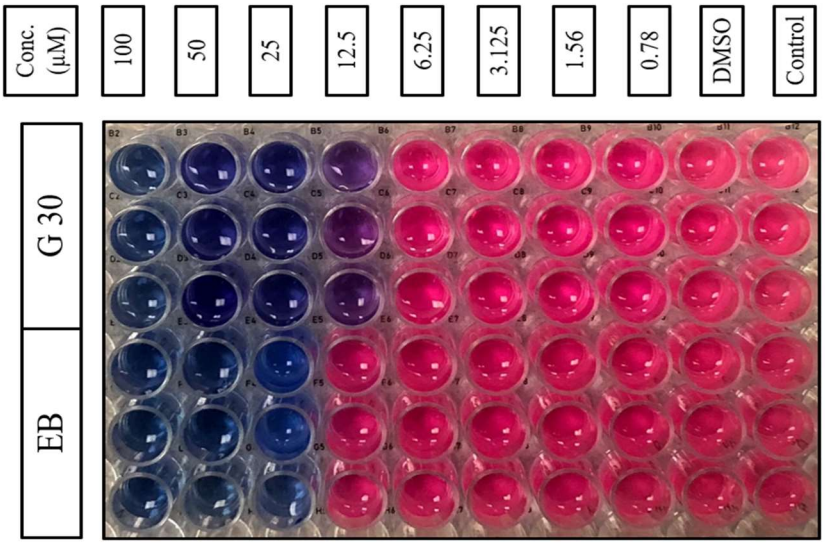

Figure 10B

Figure 10: Representative image of resazurin assay for G30 (MIC= 6.25 µM) and EB (MIC= 50 µM) against S1 strain (Figure 10A), whereas G30 exhibits a similar MIC as EB (MIC= 25 µM) against S2 strain (Figure 10B). Each plate represents experiments done in triplicate.

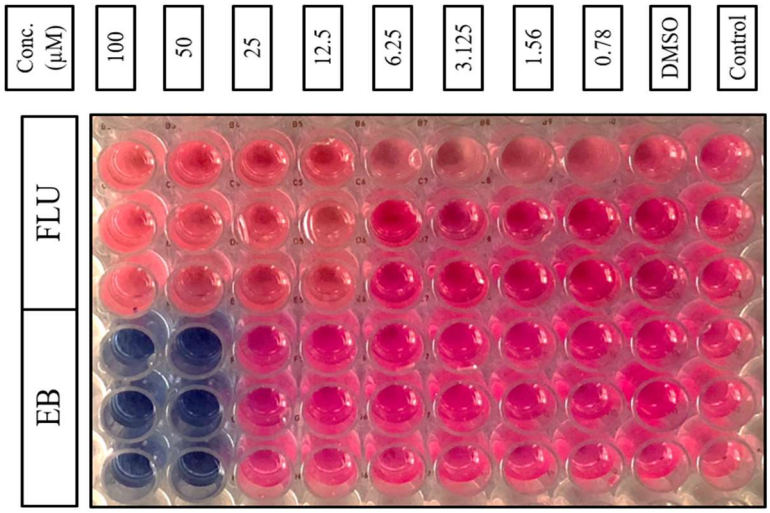

Figure 11A

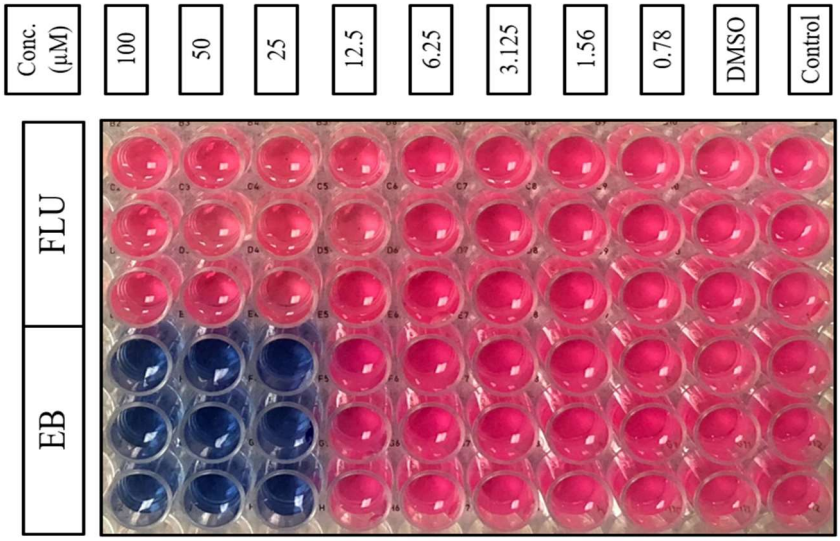

Figure 11B

Figure 11: Representative image of resazurin assay for FLU with MIC >100 μM and EB (MIC= 50 μM) against S1 strain (Figure 11A), whereas FLU exhibits MIC >100 μM and EB with MIC= 25 μM) against S2 strain (Figure 11B). Each plate represents experiments done in triplicate.

Table 14: Table summarizing resazurin assay data against S1 and S2 strains of *C. albicans*[1]

Compound	**S1 strain**	**S2 strain**
	MIC from resazurin assay (µM)	**MIC from resazurin assay (µM)**
G4	25	25
G13	12.5	25
G20	3.125	3.125
G30	6.25	25
EB	50	25
FLU	>100	>100

[1] This data was compiled from figures 7-11

Table 15: Summary of broth microdilution method and resazurin assay against S1 and S2 strains of *C. albicans*[1]

Compound	S1 strain	S2 strain	S1 strain	S2 strain
	MIC_{48h} from broth microdilution (µM)	**MIC_{48h} from broth microdilution (µM)**	**MIC from Resazurin assay (µM)**	**MIC from Resazurin assay (µM)**
G4	25	25	25	25
G13	12.5	25	12.5	25
G20	3.125	3.125	3.125	3.125
G30	6.25	20.8	6.25	25
EB	25	33.3	50	25
FLU	>100	>100	>100	>100

[1] This data was compiled from Tables 8 and 14

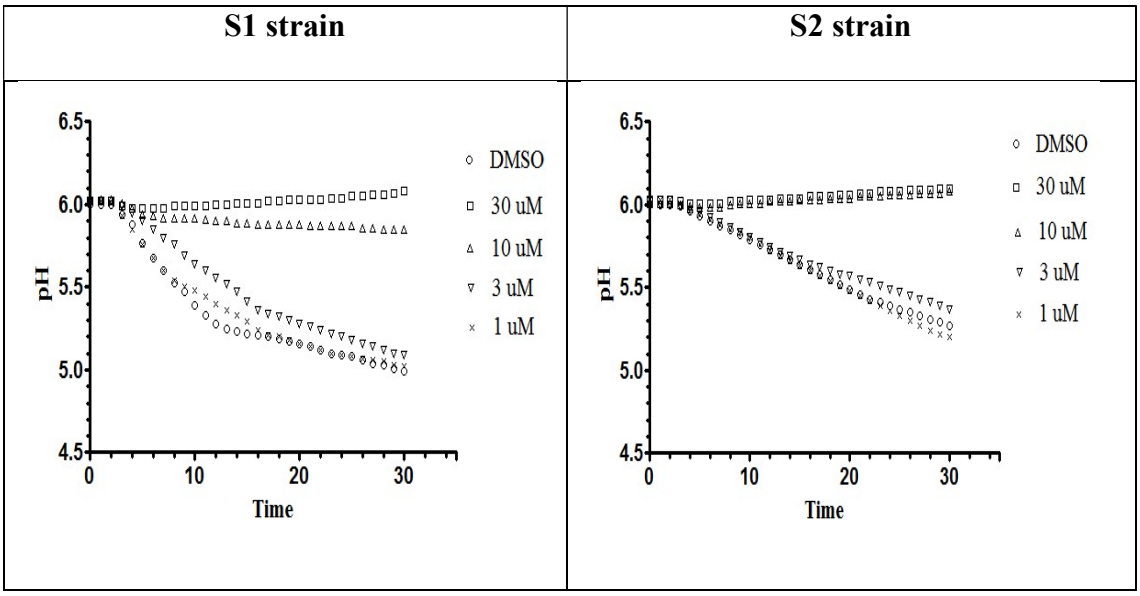

Figure 12:Effect of EB on medium acidification exhibited by yeast strains S1 (left panel) and S2 (right panel). Each graph is representative of one of three experiments.

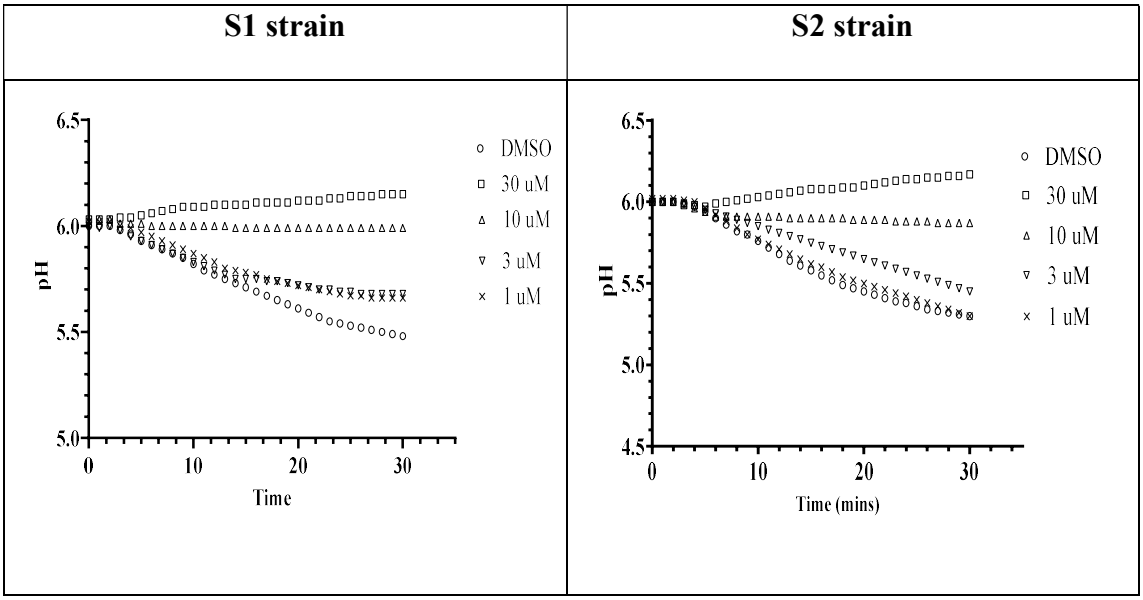

Figure 13: Effect of G4 on medium acidification exhibited by yeast strains S1 (left panel) and S2 (right panel). Each graph is representative of one of three experiments.

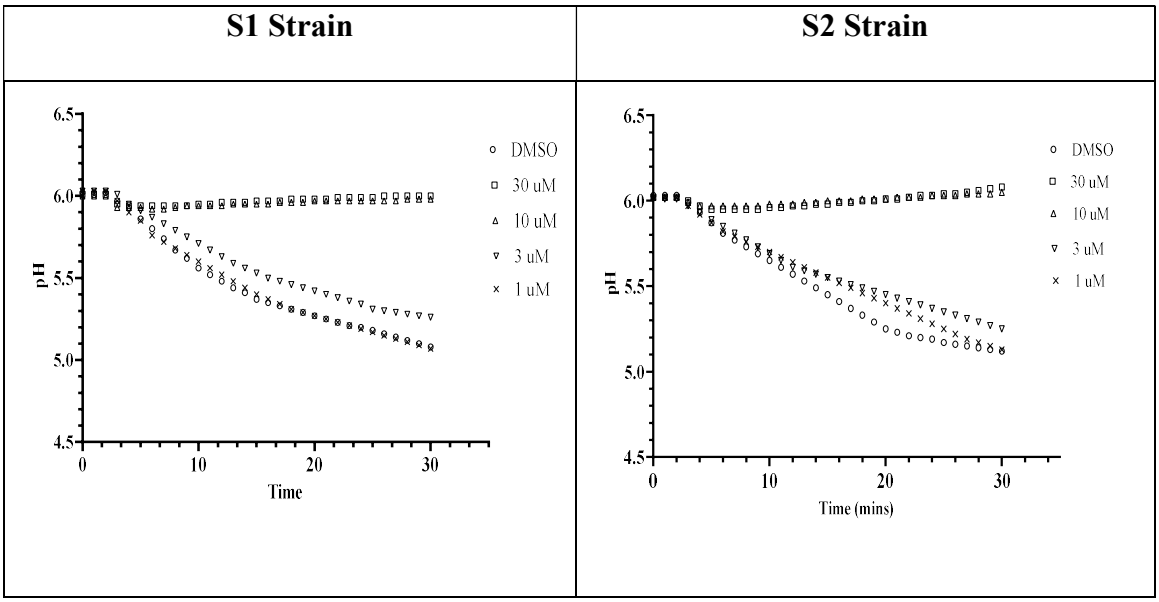

Figure 14: Effect of G13 on medium acidification exhibited by yeast strains S1 (left panel) and S2 (right panel). Each graph is representative of one of three experiments.

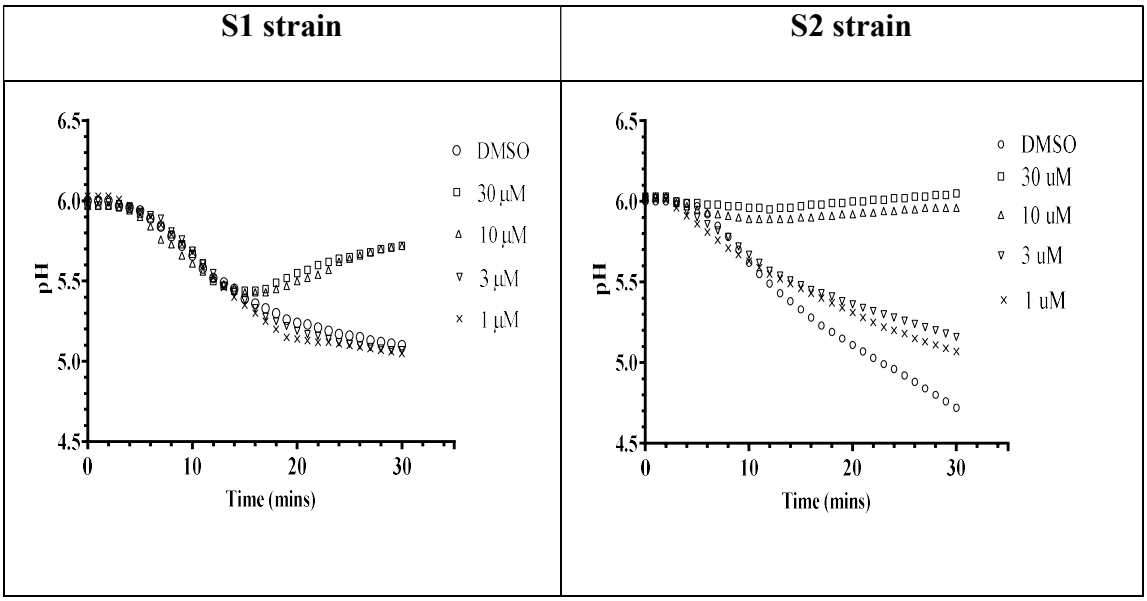

Figure 15: Effect of G20 on medium acidification exhibited by yeast strains S1 (left panel) and S2 (right panel). Each graph is representative of one of three experiments.

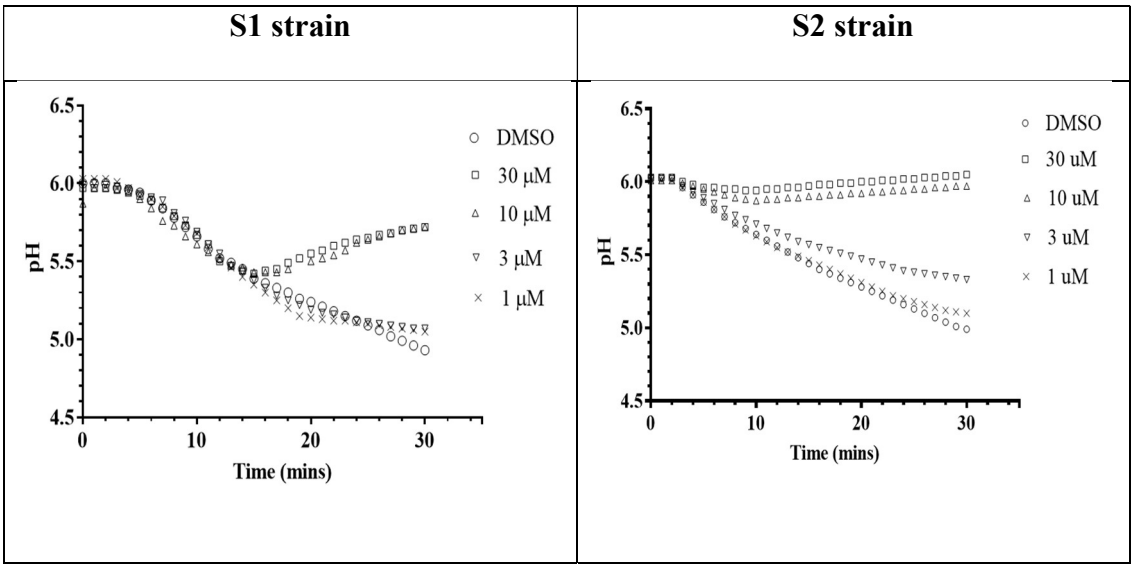

Figure 16: Effect of G30 on medium acidification exhibited by yeast strains S1 (left panel) and S2 (right panel). Each graph is representative of one of three experiments.

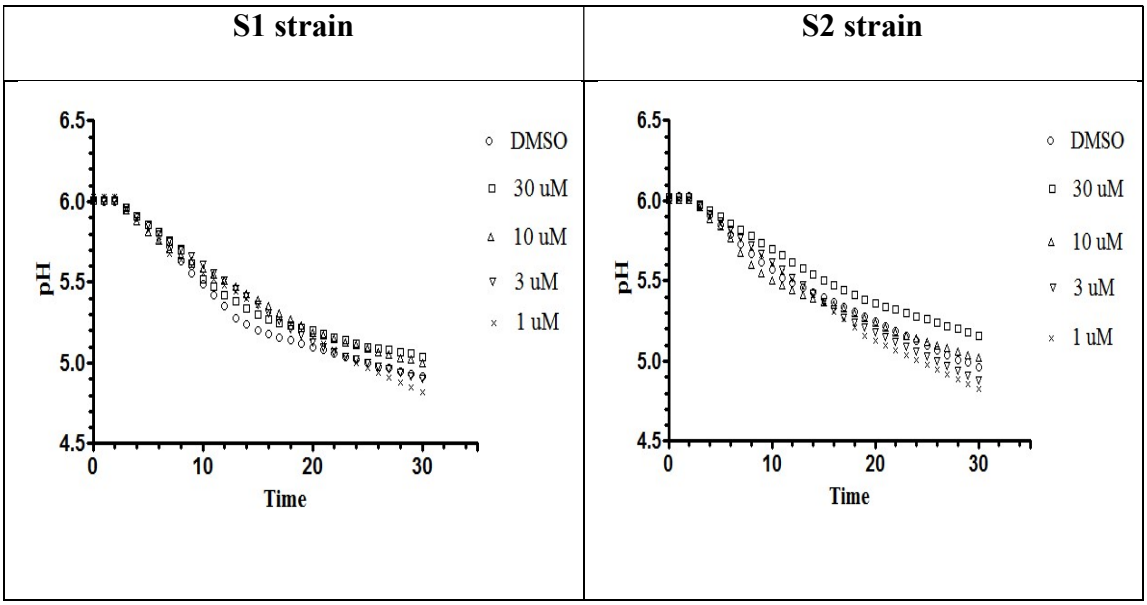

Figure 17: Effect of FLU on medium acidification exhibited by yeast strains S1 (left panel) and S2 (right panel). Each graph is representative of one of three experiments.

Table 16: Growth and Pma1p inhibition by FLU, EB and its analogs in S1 and S2 strains of *C. albicans*

Compound	**S1 strain**		**S2 strain**	
	Average IC_{50MA} at 10 min (µM)	**Average IC_{50MA} at 30 min (µM)**	**Average IC_{50MA} at 10 min (µM)**	**Average IC_{50MA} at 30 min (µM)**
G4	5.5 ± 0.4	3.6 ± 0.2	5.7 ± 0.8	5.6 ± 0.2
G13	3.8 ± 0.8	3.6 ± 1.3	5.9 ± 0.4	5.2 ± 0.3
G20	>30	6.0 ± 0.8	7.2 ± 0.6	3.9 ± 0.9
G30	>30	5.0 ± 0.7	8.1 ± 0.9	4.5 ± 0.3
EB	4.8 ± 0.6	4.7 ± 0.6	5.5 ± 0.1	4.4 ± 0.5
FLU	>30	>30	>30	>30

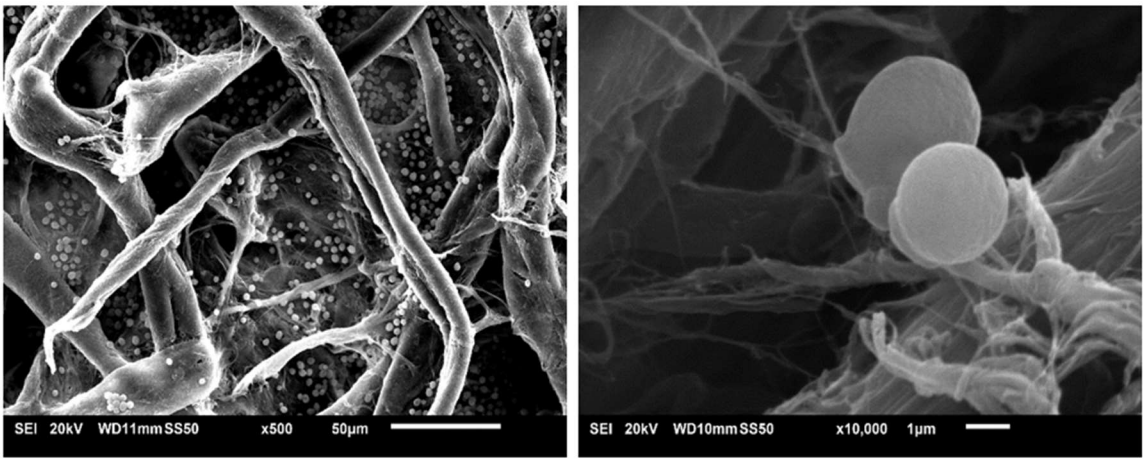

Figure 18A: Control yeast cells (S1 strain)

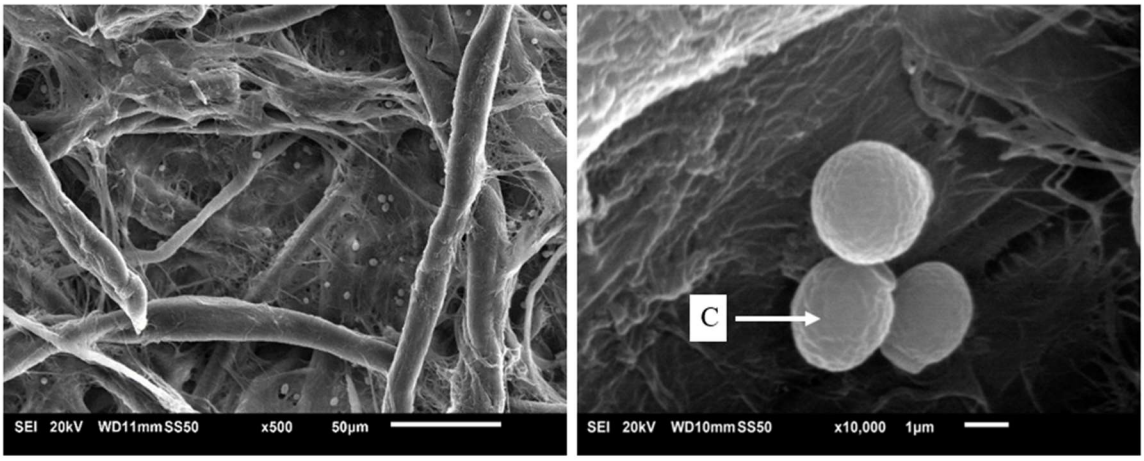

Figure 18B: S1 cells treated with EB (30 µM)

Figure 18:Representative scanning electron micrographs showing surface phenotype of S1 *C. albicans* grown in the absence or presence of EB (30 µM). Figure 18A shows abundant yeast cells at 500x and at 10,000x exhibits smooth phenotype of control yeast cells. Figure 18B represents yeast cells treated with EB (30µM). At 500x, few yeast cells can be seen, whereas at 10,000x, the image shows rough, crinkled (c) phenotype.

Figure 19A: S1 cells treated with G-30 (30 µM)

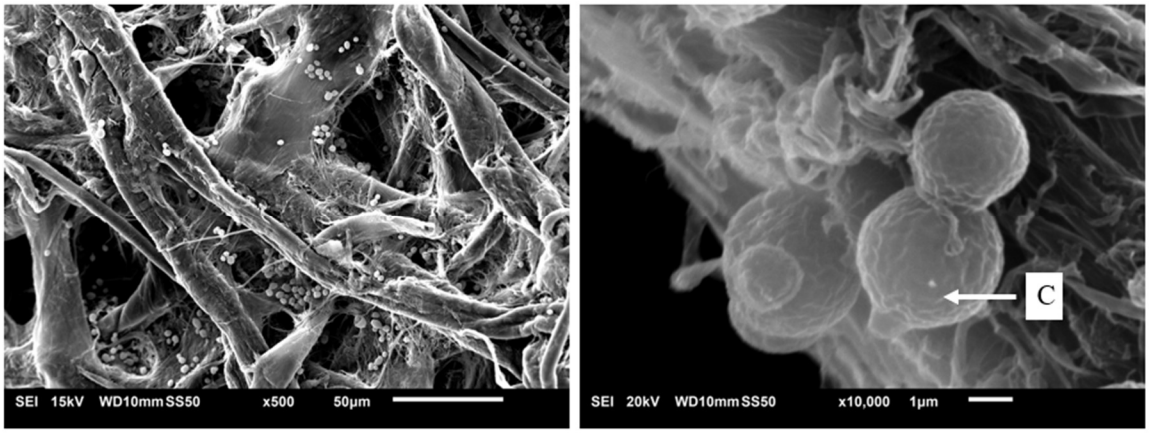

Figure 19B: S1 cells treated with FLU (30 µM)

Figure 19: Representative scanning electron micrographs showing surface phenotype of S1 *C. albicans* grown in the absence or presence of G-30 (30 µM) or FLU (30 µM). Figure 19A displays the yeast cells treated with G30 (30µM) and exhibits scantier cells at 500x. At 10,000x, the image exhibits rough, crinkled (c), and deformed phenotype. Figure 19B represents yeast cells treated with FLU (30µM) and displays fewer cells compared to control yeast cells at 500x. At 10,000x, the cells showed crinkled (c) and a rough surface.

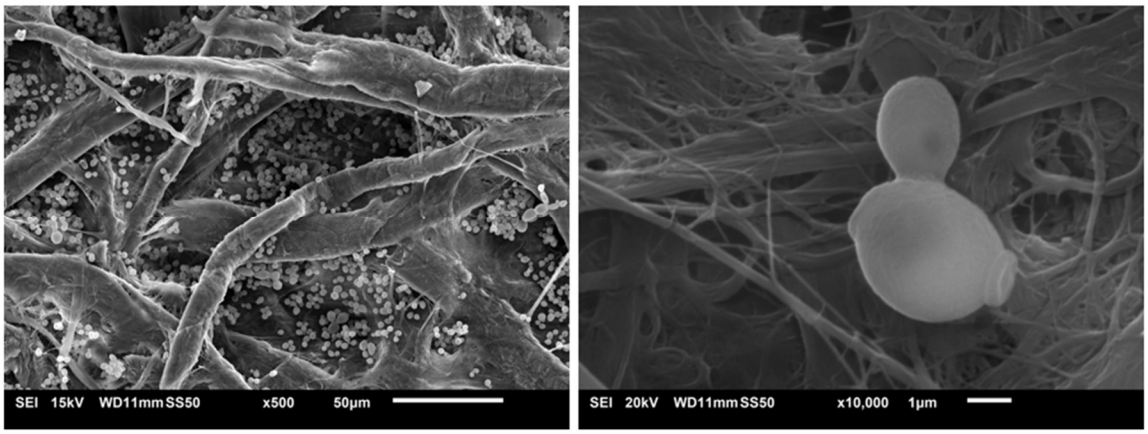

Figure 20A: Control yeast cells (S2 strain)

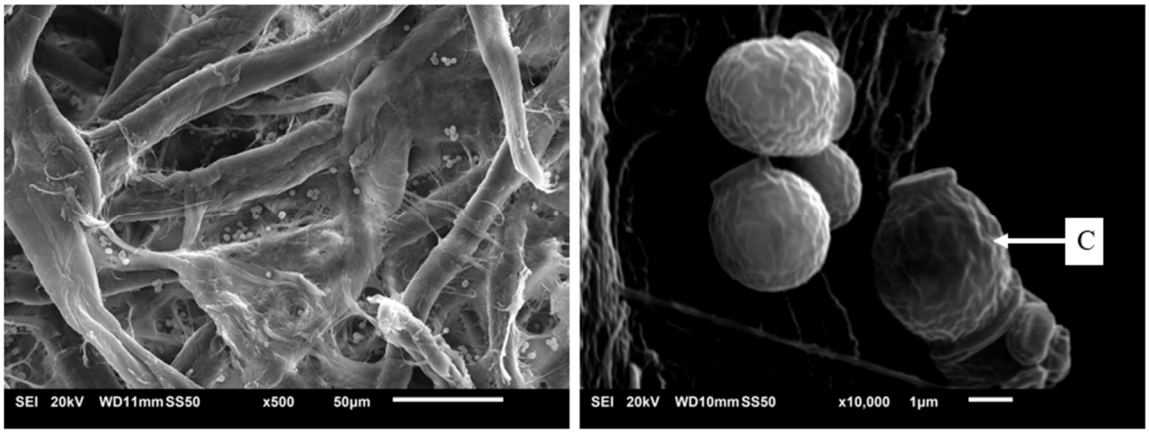

Figure 20B: S2 cells treated with EB (30 µM)

Figure 20: Representative scanning electron micrographs showing surface phenotype of S2 *C. albicans* grown in the absence or presence of EB (30 µM). Figure 20A shows abundant yeast cells at 500x and at 10,000x exhibits smooth phenotype of control yeast cells. Figure 20B represents yeast cells treated with EB (30µM). At 500x, few yeast cells can be seen, whereas at x10,000, the image shows rough, crinkled (C), and deformed phenotype.

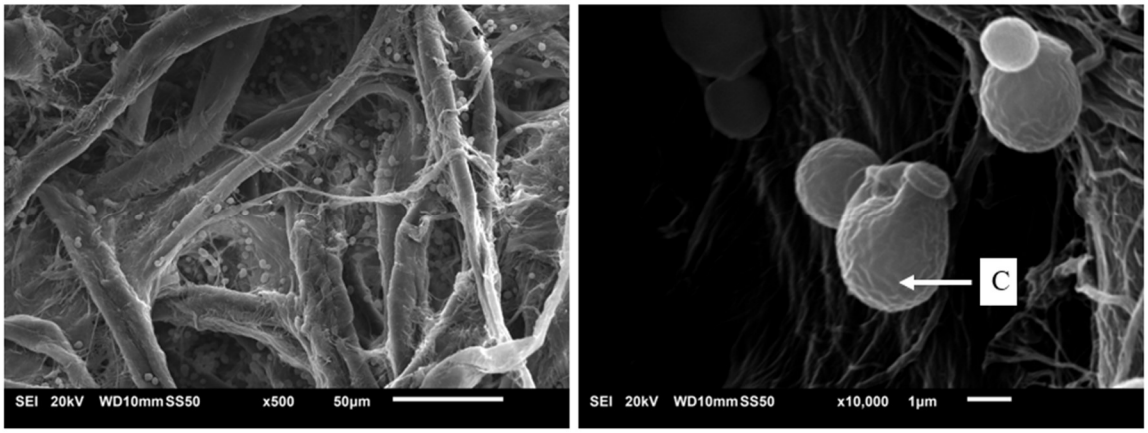

Figure 21A: S2 cells treated with G30 (30 µM)

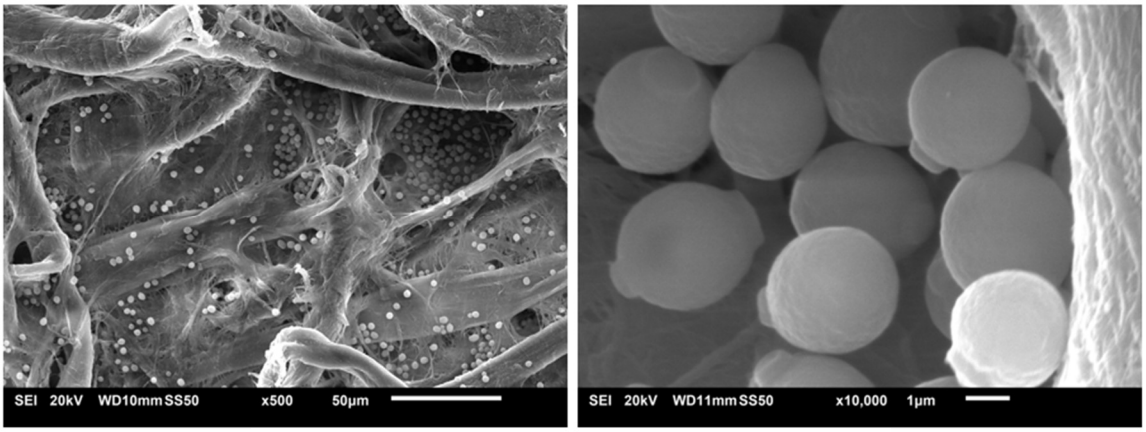

Figure 21B: S2 cells treated with FLU (30µM)

Figure 21:Representative scanning electron micrographs showing surface phenotype of S2 *C. albicans* grown in the absence or presence of G-30 (30 µM) or FLU (30 µM). Figure 21A displays the yeast cells treated with G30 (30µM) and exhibits scantier cells at 500x. At 10,000x, the image exhibits rough, crinkled (arrow pointed on surface), and deformed phenotype. Figure 21B represents yeast cells treated with FLU and no phenotype difference was observed compared to control yeast cells.

IN VIVO RESULTS

1. A pilot study to implement a mouse model of Vulvovaginal candidiasis (VVC)

The VVC model established by Dr. Fidel and colleagues (2011) was modified and used in this study to assess the antifungal activity of EB and its active analogs *in vivo*. The purpose of the pilot animal study was to achieve a robust mouse model of VVC using two yeast test strains (10231, a standard lab strain and S1, a clinical isolate).

Candida albicans vaginal infections were initiated as previously described by (Yano and Fidel, 2011). Briefly, mice were estrogenized (0.02 mg/kg) followed 72 h later by a vaginal inoculation with viable 10231 or S1 strain blastoconidia in a volume of 20 µl of YPD. To this end, 18 mice were estrogenized and later infected with n=9 for each strain (10231 or S1). Estrogen treatments were given weekly thereafter. An additional three mice per test strain were inoculated with yeast but not exposed to estrogen and these mice served as the controls for this study bringing the total to 24 mice in all. On day 3, 6 and 9 post-inoculation, three mice from each group & strain were euthanized and the vaginas were lavaged and then excised for further analyses. The endpoints included evaluating the tissue fungal burden at a specified time points (day 3, 6, and 9), recording daily body weights and histopathological studies.

1.1 Assessment of vaginal infection in mouse model of VVC with 10231 strain

To establish a mouse model of VVC with a lab strain (10231), BALB/c mice were estrogenized and vaginally inoculated 72 h later with an inoculum of ~5.5 x 10^6 viable 10231 strain blastoconidia in a 20 µl of YPD. On days 3, 6, and 9 post-inoculation, the mice were sacrificed, and the vaginal fungal burden quantified.

1.1.1 Analysis of vaginal fungal burden in mouse inoculated with 10231 strain

For assessment of the *Candida* colonization, quantification of CFUs is suitable for the VVC model as *Candida* blastoconidia and pseudohyphae normally do not penetrate beyond the superficial layer of vaginal epithelium (Zhang *et al.*, 2013). The vaginal lavage fluid was serially diluted (1: 10) and plated on YPD agar plates supplemented with ampicillin. The colony-forming units (CFU) were enumerated 48 h after incubation at 30°C. As shown in Figure 22, consistent infection was achieved in all estrogenized mice tested by day 6 (~10^4 CFU/100 µl), however the fungal burden dropped drastically by day 9. To recapitulate, vaginal infection increased from day 3 and was established by day 6 with *Candida*; however, intravaginal inoculation of 10231 did not show a robust model of VVC as the infection rate significantly reduced by day 9.

1.1.2 Histological analysis of vaginal tissue

The H & E stained tissues did not show any presence of pseudohyphae or blastoconidia adhered to the cornified epithelial layer (Figure 23, Panel A). Compared with the non-estrogenized infected mice, vaginal tissues from infected animals showed the presence of polymorphonuclear leukocytes (PMNs) in the submucosal layer on day 6 (Figure 23, Panel B). The Periodic acid Schiff (PAS) stained tissues also did not demonstrate any presence of fungal growth (Figure 24).

1.2 Assessment of vaginal infection in mouse model of VVC with S1 strain

To establish a mouse model of VVC using clinical yeast isolate S1, BALB/c mice were estrogenized and vaginally inoculated 72 h later with an inoculum of ~5.5 x 10^5 viable S1 strain blastoconidia in a 20 µl of YPD. On days 3, 6, and 9 post-inoculation, the mice were sacrificed, and the vaginal fungal burden quantified.

1.2.1 Analysis of vaginal fungal burden in mouse inoculated with S1 strain

For assessment of the *Candida* colonization, quantification of CFUs is suitable for the VVC model as *Candida* blastoconidia and pseudohyphae normally do not penetrate beyond the superficial layer of vaginal epithelium. The vaginal lavage fluid was serially diluted (1: 10) and plated on YPD agar plates supplemented with ampicillin. The colony-forming units (CFU) were enumerated 48 h after incubation at 30°C. As shown in (Figure 25), a consistent infection was achieved in all estrogenized mice tested by day 3 (~1 x 10^5 CFU/100 µl). The *Candida* infection persisted throughout the study period up through day 9. Using an estrogen-dependent murine model of vaginal candidiasis, we have demonstrated that mice given a vaginal inoculation of *C. albicans* in the absence of estrogen failed to maintain an infection. The fungal burden eventually dropped by day 9 in non-estrogenized mice. To recapitulate, vaginal infection was established on day 3 and increased by day 6 with *Candida* persisting up through day 9 in estrogenized infected mice. The S1 strain showed maintenance of yeast colonization throughout 9 days of the study after intravaginal inoculation of yeast thereby resulting in a robust mouse model of VVC.

1.2.2 Histopathological study

The H & E stained vaginal tissues of estrogenized infected mice from day 6 showed profound presence of PMNs, predominantly neutrophil infiltration in the submucosal layer when compared to non-estrogenized mice. In addition, the tissues from this group showed slight edematous cells compared to the non-estrogenized infected mice. There were no micro-abscesses in either of the groups (Figure 26). Compared to PAS stained tissue of non-estrogenized mice, with no *C. albicans* in the vaginal cavity, vaginal samples from estrogenized and infected animals contained vast numbers of filamentous pseudohyphae

and blastoconidia adhering to the cornified epithelial layer and in the vaginal lumen (Figure 27). The results from histopathological analysis is well in agreement with the day 9 lavage fluid CFUs (10^0/100 µl) and (10^5/100 µl) for non-estrogenized and estrogenized infected mice, respectively.

1.2.3 Other observations

Another visible signs that can be considered indicative of candidiasis infection was the presence of vaginal discharge during the study period (Figure 28). Swollen uterine horns indicative of estrogen treatment (pseudoestrus phase) were observed in estrogenized mice (Figure 29).

1.3 Summary of the *in vivo* pilot study:

We implemented the murine VVC model which is useful for investigating the antifungal efficacy of novel compounds as well as understanding their fungal pathogenicity and host defenses. In the current study, we tested two *C. albicans* strains (10231 and S1), where the mice were divided into two groups: group I (non-estrogenized inoculated mice) and group II (estrogenized inoculated mice). In group I, mice were intravaginally inoculated with the either strains 10231 (5.5 x 10^6 CFU) or S1 strain (5.5 x 10^5 CFU) without estrogen whereas, group II mice were estrogenized and intravaginally inoculated with either strains. The S1 strain successfully demonstrated a robust VVC model in mouse with indicators such as CFU, and histological analysis of vaginal tissues as compared to 10231 strain. Other observations such as mouse vaginal discharge and swollen uterine horns were the indications of a successful VVC infection model. In conclusion, we have demonstrated several important features and representative results of the experimental model of vaginal candidiasis with S1 strain of *C. albicans*.

2. An intervention study to evaluate the antifungal activity of EB and its analogs against S1 strain in the mouse model of VVC

The brick dust characteristic of EB i.e. poor aqueous solubility causes the compound to precipitate in presence of water. Based on the results from *in vitro* studies, EB and its analogs were taken a step further by developing a formulation with the aid of nanotechnology (Vartak *et al.*, 2020b). Apart from EB, the preconcentrate comprised of DMA as co-solvent, Captex as oil, and Kolliphor® ELP as surfactant. Also, 30% TTO was incorporated into the preconcentrate as oil because of its dual function, i.e., TTO possesses antifungal properties and acts as a stabilizer for the preconcentrate. Altogether, these components helped in the development of preconcentrate of EB along with TTO (EB-SNEP) which prevailed over the shortcomings of EB. This preconcentrate when administered intravaginally resulted in EB nanoemulsion (EBN) providing a local antifungal effect without any precipitation. Following are a few preformulation studies to optimize the EB nanoformulation followed by the *in vitro* and *in vivo* study to assess the antifungal activity.

2.1 Preformulation studies to optimize EB nanoformulation

2.1.1 Optimization and characterization of EB-SNEP

EB is a poorly soluble, brick dust molecule and hence the approach of SNEDDS was adopted to develop a formulation with improved aqueous solubility and stability. As per the previous reports by (Vartak *et al.*, 2020b), DMA was chosen as an ideal co-solvent for EB due to its high solubilizing capacity for hydrophobic molecules. The medium chain triglycerides (MCT; Captex 300®) and Kolliphor® ELP were used as an oil and surfactant

in an optimized concentration of 5:7, respectively, to increase the self-emulsifying capacity and solubility of EB.

As shown in Figure 30A, a ternary phase diagram was constructed to optimize the concentration of each component in the nanoemulsion. The light blue region enclosed within triangle represents the clear nanoemulsion region. Within this region, all the excipient ratios showed a particle size of < 100 nm with no phase separation. A decrease in particle size from 0 to 10% DMA was observed which than increased with increasing DMA concentration. Tea tree oil from 0 to 40% showed proportional increase in particle size. However, EB stability was prolonged with increasing TTO concentration from 0-30% which drastically decreased at higher concentrations.

EB-SNEP up to 30% TTO produced a blue tinge after dispersion in water, indicating the formation of a stable nanoemulsion (Figure 30B). The blue tinge represents a stable nanoemulsion because when light of different wavelengths is incident on a particle with a diameter less than the wavelength of visible light, the resultant intensity of the scattered light is ¼ of the wavelength. Since the violet-blue wavelengths are scattered more than red wavelengths of light, the dispersion of particles with < 100 nm diameter will have a blue hue (Giusto *et al.*, 2019).

Optimum TTO concentration was further confirmed by performing precipitation study. The precipitation rate of EB from EB preconcentrates loaded with varying test concentrations of TTO were assessed by dispersing in SVF. As shown in Figure 31A, compared to EB in DMA alone, EB-SNEP significantly increased the overall stability of formulation. With increasing TTO concentration, the precipitation rate of EB substantially reduced. At 4 h, EB-SNEP with 30% TTO showed 3-fold higher drug retention compared

to EB-SNEP alone, whereas EB in DMA completely precipitated by 4 h. Therefore, to recapitulate, the optimized SNEDDS contained EB (0.95 % w/v), DMA (9.5 % v/v), Captex® 300 (25.79 % v/v) and Kolliphor® ELP (37.91 v/v), and TTO (28.57 % v/v).

Intensity readings of the optimized formulation (EBN) acquired from dynamic light scattering techniques (Figure 31B) showed a mean particle size of 47.29 ± 1.52 nm with a low polydispersity index of 0.064 indicating a monomodal distribution of nanoparticles.

2.2 EBN shows improved antifungal profile against *Candida* spp. *in vitro*

To validate the antifungal efficacy of EBN formulation, a broth microdilution assay was performed in S1, S2, and *C. glabrata* strains followed by a colorimetric assay to confirm the viability of the cells. After 48 h of incubation with the respective treatments (EB in DMA only, EBN, Blank, FLU and MICO), the plates were then incubated up to 2 h with resazurin dye. Wells with pink-violet or pink color indicated fungal activity with chemical reaction of oxidation-reduction of resazurin into resorufin, therefore the last blue well (left to right) is designated as the MIC. Based on resazurin data, EBN showed fungicidal effect in the *Candida* strains with MIC = 25 μM (6.8 μg/ml) for S1 and S2 strains and 12.5 μM (3.4 μg/ml) for *C. glabrata* when compared to the reference standard treatment, FLU [MIC = >100 μM (>30.6 μg/ml)]. EBN also proved to be 4-fold more potent than MICO in both S1, S2, and *C. glabrata* strains (Table 17). The excipients did not contribute to additional antifungal efficacy of EBN formulation as Blank formulation showed no inhibitory effect in fungal growth at nanoparticle concentrations equivalent to EBN. The controls (yeast cells only and the blank formulation) showed pink color throughout the wells, whereas RPMI only (without cells) showed blue color in all the wells

(Figure 32). Overall, EBN formulation showed improved antifungal efficacy against both *C. albicans* and *C. glabrata* when compared to the EB in DMA, FLU, and MICO.

2.3 *In vitro* toxicity testing of EBN formulation

Cytotoxicity of EBN formulation on HeLa cell line was evaluated by LDH assay. Both formulations (EBN with and without TTO) demonstrated no toxic effect on HeLa cells after 3 h at concentrations as high as 100 μM of EB (Figure 33).

To determine the toxicity of EBN formulation on *Lactobacillus* spp. *in vitro*, bacterial suspension was treated with EBN, Blank, Blank + TTO and ampicillin (positive control) for 24 h. After incubation, addition of resazurin dye showed pink color in all the wells treated with formulation except for the blue color in the wells with media only or ampicillin. In other words, this colorimetric assay demonstrates that EBN formulation or any of its components causes no toxicity to *Lactobacillus* at the highest concentration tested (100 μM) (Figure 34).

Collectively, the optimized EBN formulation showed enhanced stability profile compared to EB in DMA only, with no *in vitro* cytotoxicity.

2.4 *In vivo* studies of EB nanoemulsion

2.4.1 Analysis of vaginal fungal burden with different treatments in mouse model of VVC

Assessment of vaginal fungal burden proved to be a reliable method for assessing the intensity of *Candida* infection in murine model of VVC. The intervention study was carried out with S1 strain based on the results from the pilot study. Animals were randomized and coded into treatment groups and the study was carried out in a wave

fashion with 7 animals picked randomly each time. As mentioned in Methods section, mice received the treatment on day 3, 4, and 5 and the animals were euthanized on day 6.

To investigate the VVC infection, vaginal lavage fluid was collected immediately after the animal euthanization, on day 3 or day 6. After 48 h, CFUs were enumerated and counted manually for determining the vaginal fungal burden (Figure 35). Animals in the naive group showed no infection compared to the 6^{th} day group (control) which showed on average, 6.32 x 10^5 CFU/100 µl of vaginal lavage fluid. The Blank group (without TTO) showed slightly higher fungal burden compared to the control group. However, Blank + TTO group showed a 11.4-fold reduction in the CFU/100 µl compared to the control group indicating that TTO possesses a minimal antifungal activity of its own. Mice that received an intravaginal administration of EB-SNEP (5mg/kg) showed only 2.6-fold reduction when compared to the control group. Notably, the number of *C. albicans* cells recovered from the vaginal lavage fluid was significantly reduced by a 780-fold in mice that had received EB-SNEP (12.5 mg/kg) compared to the control. The treatment group EB suspension (12.5 mg/kg) showed a 4.7-fold reduction in CFU/100 µl, whereas the Blank-suspension showed negligible reduction (~ 1.1-fold) compared to the control group. The positive control used for the study, MICO and FLU showed a 15.8-fold and 23.6-fold reduction, respectively in vaginal fungal burden compared to the control. Comparison of the antifungal activity of the various treatments displayed the following trend in order of decreasing efficacy: EB-SNEP (12.5 mg/kg) > MICO > FLU > EB suspension (12.5 mg/kg) > Blank + TTO. Taken together, EB-SNEP (12.5 mg/kg) represented the most effective formulation for VVC infection *in vivo*. Body weights were measured throughout the study period and no signs of toxicity were seen (Figure 36).

To abridge the results obtained from assessing the vaginal lavage fluid, EB-SNEP (12.5 mg/kg) outperformed the standard antifungal drug FLU and the conventional product (2% Miconazole nitrate cream). It is worth mentioning that EBN remarkably reduced the *Candida* infection unlike the EB-suspension and therefore can be extensively studied for clinical trials.

2.4.2 Histopathological analysis of mice vaginal tissues

For the intervention study, H & E analysis was carried out to investigate the infiltration of PMNs, if any, and to look for signs of toxicity such as epithelial hyperplasia and/ or edema. Vaginal tissues of mice were excised longitudinally, fixed in formalin and stained with H & E stain. As seen in Figure 37A, the naive group showed neither epithelial hyperplasia nor an excess presence of PMNs (Figure 37B). The 3rd day infected group showed increased hyperplasia and infiltration of PMNs (Figure 37, Panel C and D). Similarly, the 6th day infected (control) group showed significant hyperplasia (more than 3 layers of epithelium) (Figure 37E) as well as PMNs throughout the tissue (Figure 37F). Blank without TTO group showed no epithelial hyperplasia (Figure 38A) and less PMNs (Figure 38B) as compared to the control group. Animals that were treated with Blank + TTO showed slight edema in the epithelial layers (Figure 38C) and a few PMNs in the submucosal area (Figure 38D)compared to the control. Vaginal administration of EB-SNEP (5 mg/kg) and (12.5 mg/kg) did not result in a visible change in the histology (Figure 39A and C) and showed a fewer PMNs (Figure 39B and D), respectively, compared to the control group (see Figure 37, Panels E and F). In the vehicle for EB suspension group, epithelial hyperplasia (Figure 40A) was evident with a mild infiltration of PMNs in the submucosal layer (Figure 40B), while the EB suspension (12.5 mg/kg) group showed less

epithelial hyperplasia (Figure 40C) and a fewer PMNs (Figure 40D) compared to the vehicle and control group. The treatment group MICO and FLU showed no remarkable changes in histology (Figure 41A and C) and less PMNs throughout the tissue (Figure 41B and D) compared to the control group.

2.5 Immunohistochemical analysis

IHC for MPO confirmed the results obtained from H & E stained tissues. The naive tissues showed slight expression of MPO (brown spots) (Figure 42, Panel A), however control (infected, untreated) (Figure 42, Panel B) showed higher levels of MPO expression thereby confirming the inflammatory response during VVC infection. Blank + TTO (Figure 42, Panel D) and EB-suspension groups (Figure 42, Panel F) showed an increase in expression of MPO compared to the naive group, however MICO group (Panel C) showed similar PMN expression to the naive tissue. Tissues sections from EB-SNEP (12.5 mg/kg) (Panel E) showed significant reduction in PMN infiltration compared to the control (infected, untreated group) (Figure 42, Panel B). The number of MPO+ cells in 5 fields of view for each section was then counted and the average was plotted on a graph (Figure 43).

To summarize, EB-SNEP (12.5 mg/kg) showed a dramatically improved antifungal efficacy compared to EB suspension and MICO and no histopathological signs of toxicity.

3. Acute toxicity study of EBN formulation

An H & E study of vaginal tissues obtained from non-infected mice was carried out to better understand the toxicity of the formulations used on the female reproductive tract. H & E stained tissues from mice treated intravaginally with EB-SNEP (12.5 mg/kg) showed (Figure 44, Panel A) more or less similar number of epithelial layers compared to naïve

groups with (Figure 44, Panel C) and without estrogen treatment (Figure 44, Panel D). Both the EB-SNEP (12.5 mg/kg) group and the Blank + TTO group (Figure 44, Panel B) showed slight edematous cells in the epithelial layer. However, the keratin layer was intact for both the groups. No effects of estrogen were seen on the epithelial layer in the naive + estrogenized group (Figure 44, Panel C) compared to the naïve and non-estrogenized group (Figure 44, Panel D).

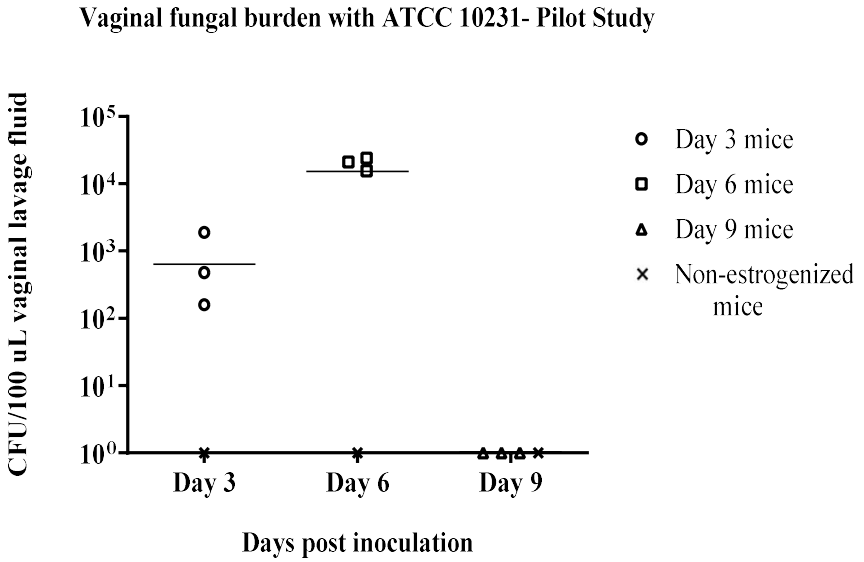

Figure 22: Quantification of vaginal fungal burden in estrogen-treated and non-estrogenized infected mice with 10231 strain. CFU/100 µl of lavage fluid from inoculated mice were assessed on indicated time points (day 3, 6, and 9). Each point represents an individual mouse, and the horizontal bar indicates the geometric means. The experiments included n=3 estrogenized and infected mice and n=1 non-estrogenized and infected mouse for each time point. Note that the infection was initially robust on days 3 and 6 but cleared by day 9. Note also that non-estrogenized mice do not show vaginal fungal burden.

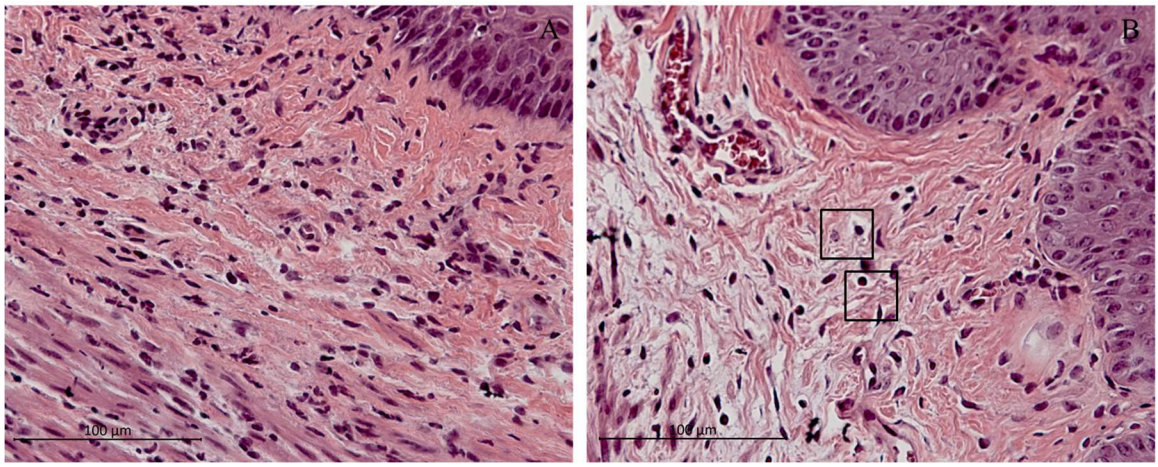

Figure 23: Representative light micrographs of H and E stained 10231 infected mouse vaginal tissue. Each section of paraffin-embedded tissues was stained with H and E stain and then observed under microscope. (A) Non-estrogenized and infected mouse vaginal tissue and (B) Estrogenized and infected mouse vaginal tissue (PMNs highlighted). Images are shown at 400x magnification. Scale bars on the micrographs represent a length of 100 µm.

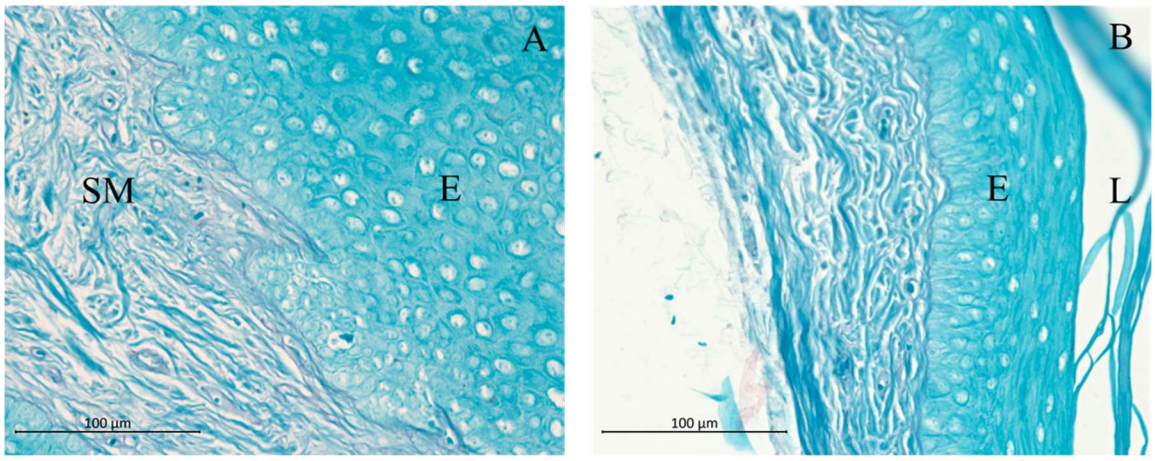

Figure 24: Representative light micrographs of PAS stained 10231 infected mouse vaginal tissue. Each section of paraffin-embedded tissues was stained with PAS stain and then observed under light microscope. Mouse vaginal tissue from day 6 showed no hyphal growth or blastoconidia in both the groups: non-estrogenized and infected (A) and estrogenized and infected (B). Images are shown at 400x magnification. Scale bars on the micrographs represent a length of 100 µm.

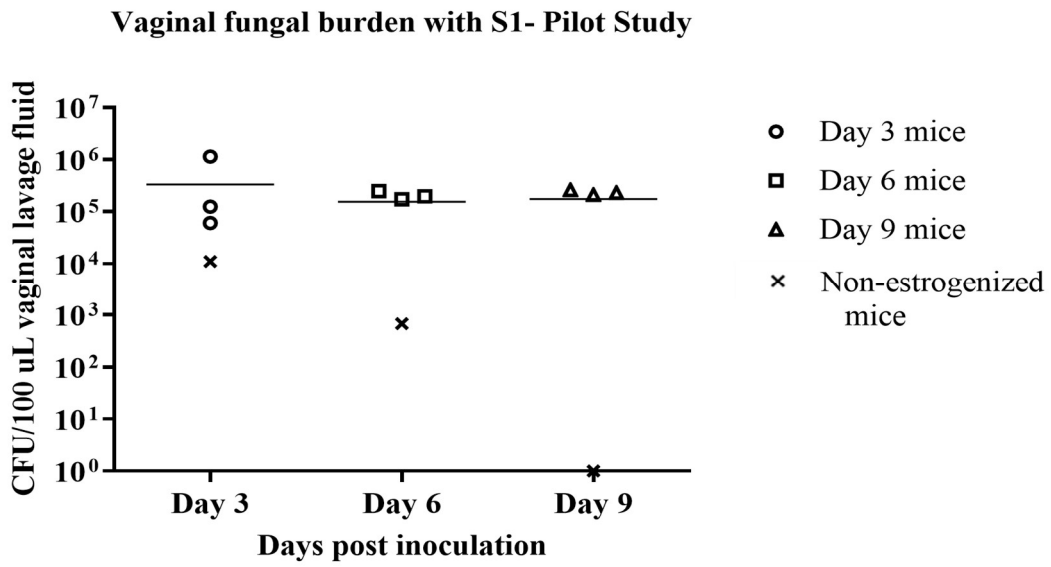

Figure 25: Quantification of vaginal fungal burden in estrogen-treated and non-estrogenized infected mice with S1 strain. CFU/100 µl of lavage fluid from inoculated mice were assessed on indicated time points (day 3, 6, and 9). Each point represents an individual mouse, and the horizontal bar indicates the geometric means. The experiments included n=3 estrogenized and infected mice and n=1 for non-estrogenized and infected mouse for each time point. Note that the infection was maintained throughout the 9-day study in estrogenized mice, but not in non-estrogenized mice.

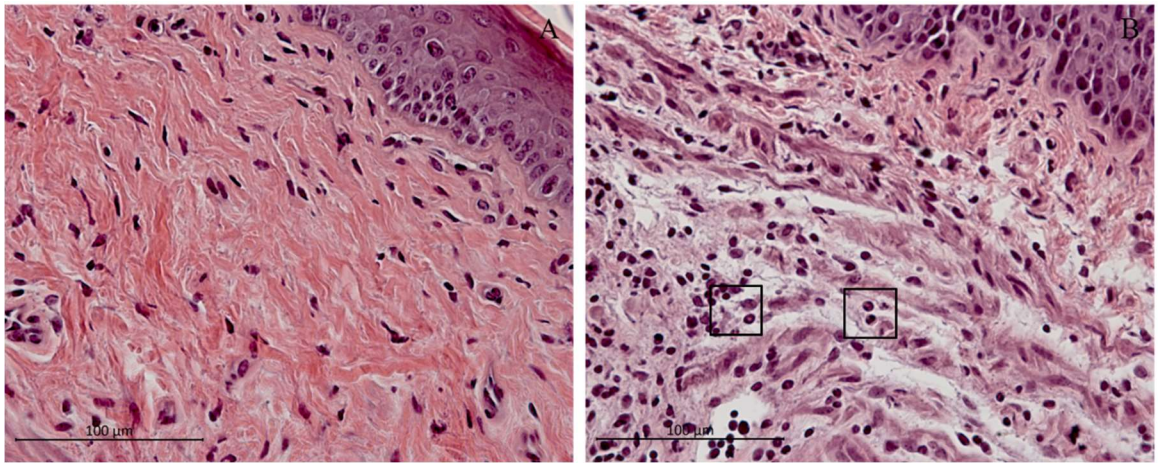

Figure 26:Representative light micrographs of H & E stained S1 infected mouse vaginal tissue. (A) Non-estrogenized mouse tissue with less PMNs. (B) Estrogenized mouse vaginal tissue with significant infiltration of neutrophil (purple bodies) in the submucosal layer. Images are shown at 400x magnification. Scale bars on the micrographs represent a length of 100 µm.

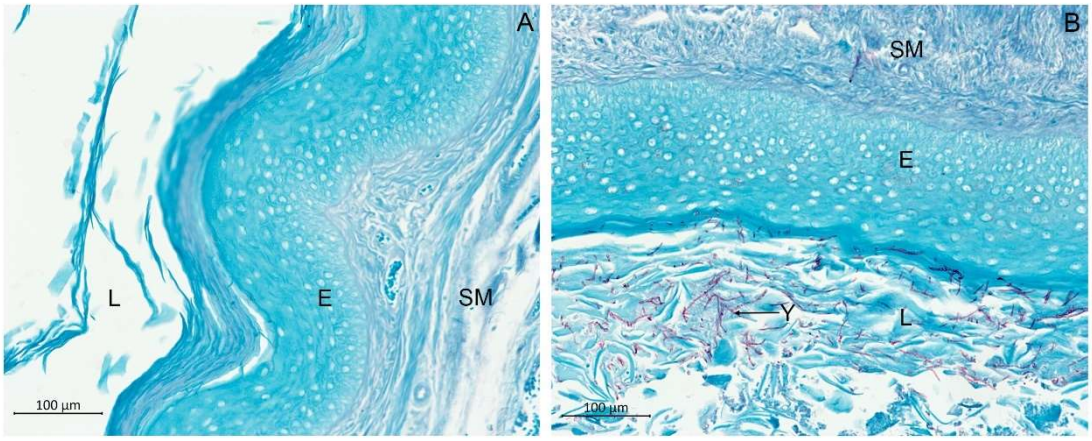

Figure 27: Representative light micrographs of PAS stained S1 infected mouse vaginal tissue. Each section of paraffin-embedded tissues was stained with PAS and then observed under microscope. (A) Unestrogenized mouse vaginal tissue (day 6) with no *C. albicans* cells in lumen (L) followed by epithelial layer (E) and submucosa (SM). (B) Estrogenized and infected mouse vaginal tissue from day 6 with large amounts of filamentous pseudohyphae and blastoconidia (Y) in the vaginal lumen adhered to the cornified epithelial layer.

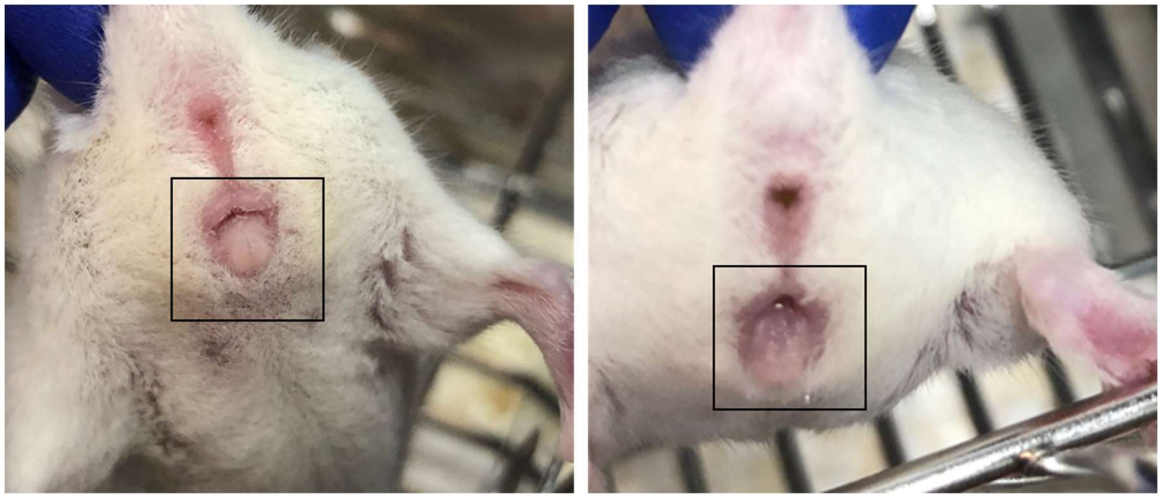

Figure 28: Images of signs of *Candida* infection in mouse. Non-estrogenized and infected mouse (left panel) showed no vaginal discharge while estrogenized infected mice (right panel) showed vaginal discharge during the study period.

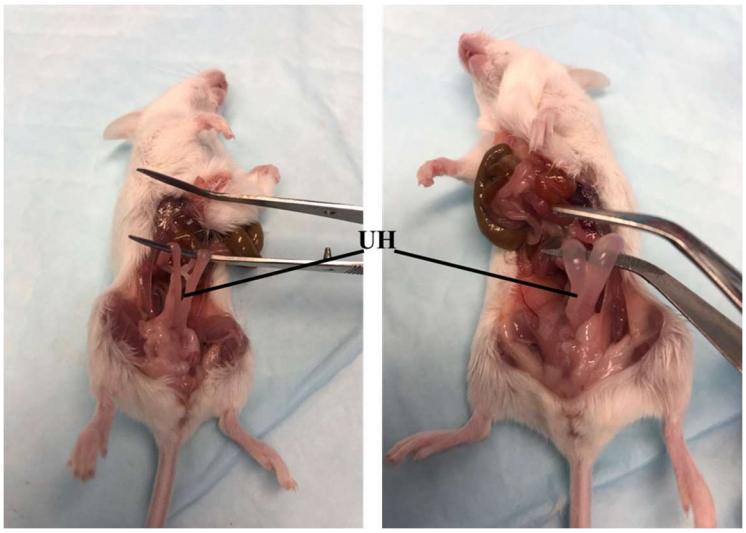

Figure 29: Images of clinical signs of *Candida* infection in mouse. Non-estrogenized and infected mouse with no change in uterine horns (left image). Estrogenized and infected mouse showed swollen uterine horns (UH) during infection (right image).

A

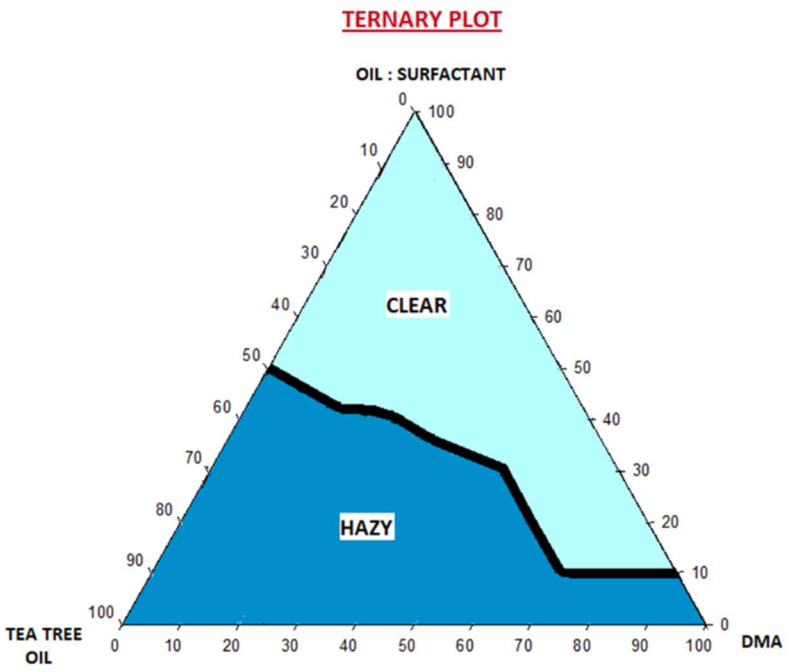

B

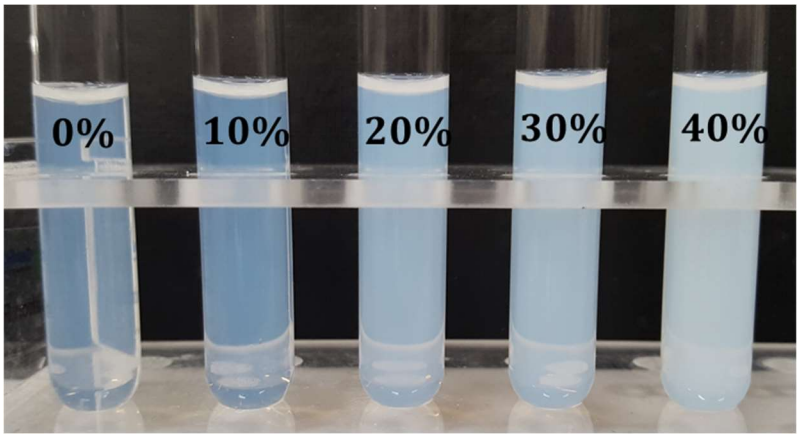

Figure 30: The optimized proportion of Captex 300 EP/NF, Kolliphor® ELP, dimethylacetamide, and tea tree oil in the preparation of EB-SNEP. (A) A ternary phase diagram of a self-nanoemulsifying system with a large clear region. (B) A stable nanoemulsion was confirmed up to 30 % TTO concentration by the presence of a blue tinge after dispensing the EB-SNEP in water.

A

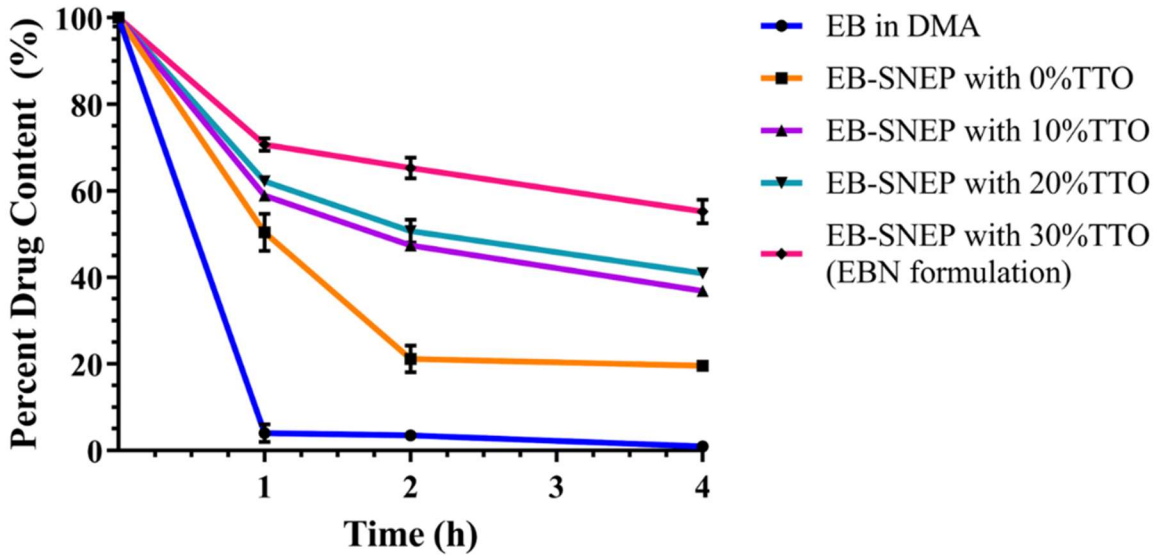

B

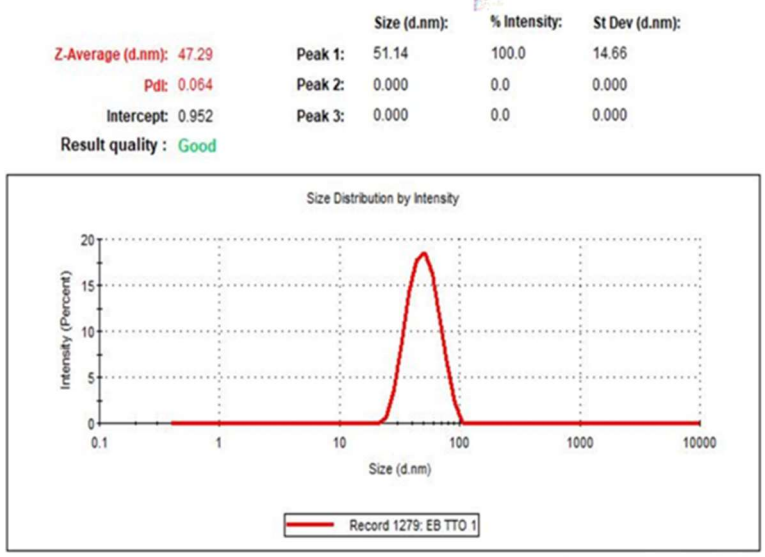

Figure 31: Optimization of TTO concentration in EBN formulation. (A) Precipitation study of EB at different concentrations of TTO. (B) Average particle size of optimized EBN formulation.

Table 17:MIC determination of EBN formulation in *Candida* spp. using resazurin assay[*, †]

Test compounds	S1 strain	S2 strain	*C. glabrata*
	Average MICs (48 h) µM	**Average MICs (48 h) µM**	**Average MICs (48 h) µM**
EBN formulation	25	25	12.5
Blank formulation[‡]	> 4 mg/ml	> 4 mg/ml	> 4 mg/ml
MICO	100	100	50

[*]MIC is the lowest concentration of an antimicrobial drug that exhibits no change in resazurin blue dye after a specified incubation period.

†Unless otherwise indicated, all the MIC values represent the average of 3 experiments performed in triplicate.

‡The highest working concentration of TTO tested was 4 mg/ml

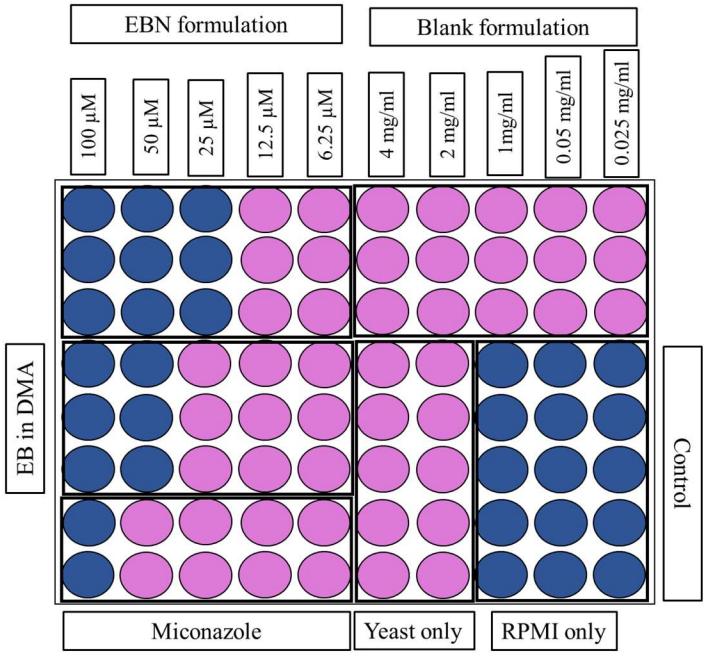

Figure 32:MIC determination using cell viability assay in S1 strain of *C. albicans*. This is a graphical depiction of the actual data.

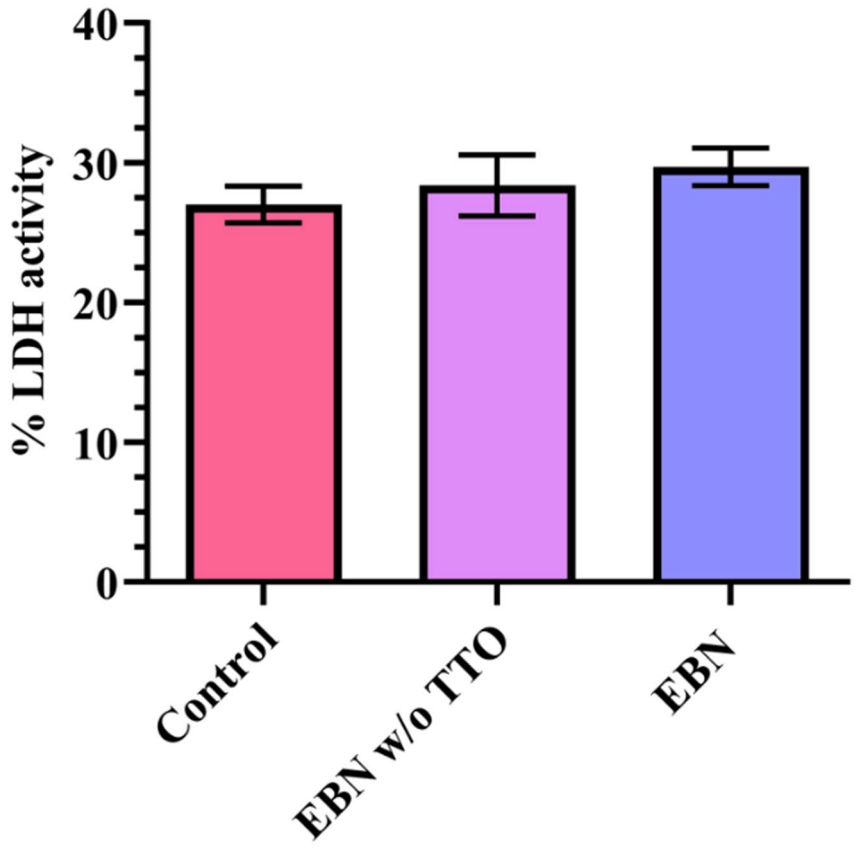

Figure 33: Cytotoxicity evaluation of EBN formulation. Percentage of LDH released from HeLa cells following 3 h exposure to EBN with and without TTO. The EBN formulation (with and without TTO) showed similar % LDH activity as control cells.

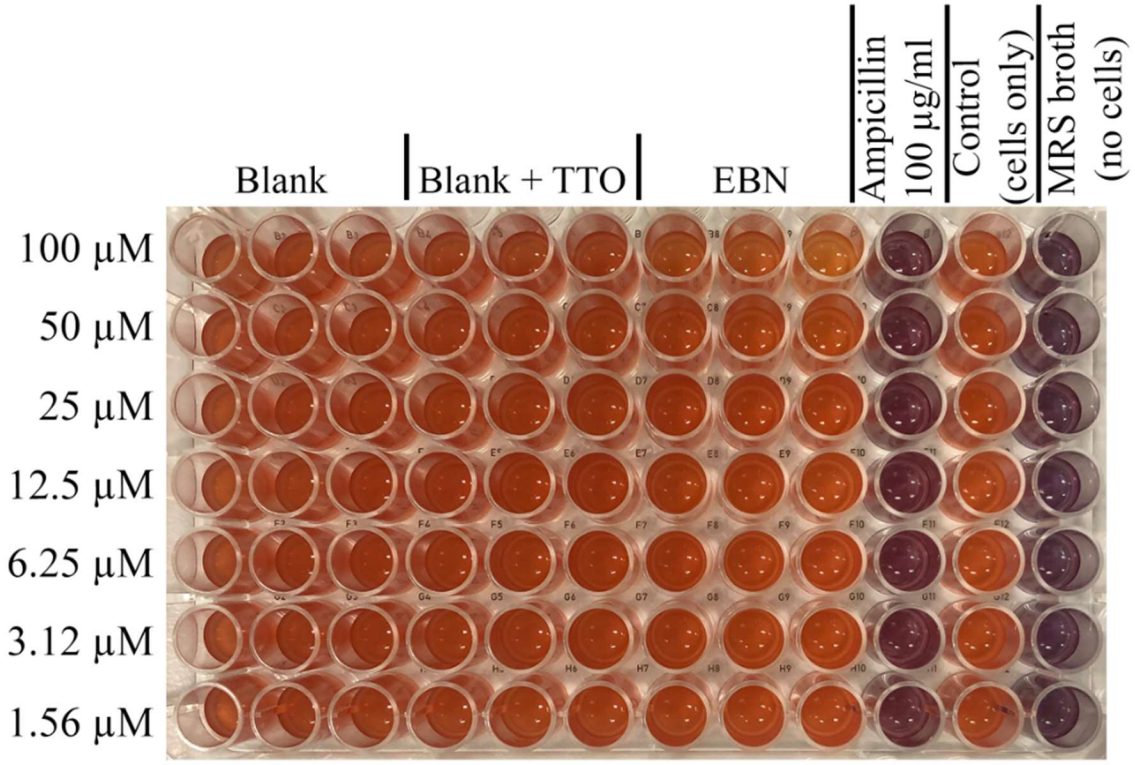

Figure 34: Cytotoxicity evaluation of EBN formulation on Lactobacillus spp. using resazurin assay. Formulations were tested at 1.56 – 100 µM, while the positive control, ampicillin stock was prepared at 100 µg/ml. Negative controls included control (cells only) and MRS broth (no cells).

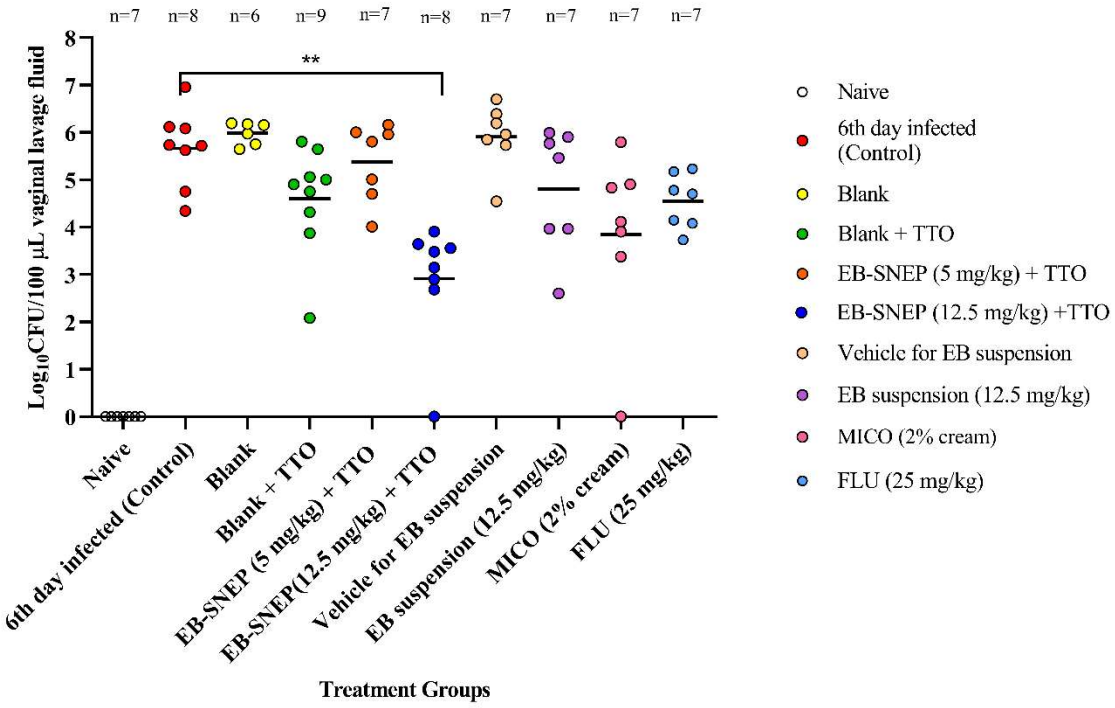

Figure 35: Efficacy of EB-SNEP (12.5 mg/kg) in the mouse model of VVC. On days 3, 4 and 5, mice with VVC received respective treatments via the intravaginal route once per day. Data shown are the CFUs obtained from each animal from the respective groups. The fungal burden of murine VVC was calculated on a scale of log10 (CFU/100 µL) in the vaginal lavage. MICO and FLU served as a positive control group for treatment. Points on the curve represent individual mice, horizontal lines represent the geometric mean of each group.

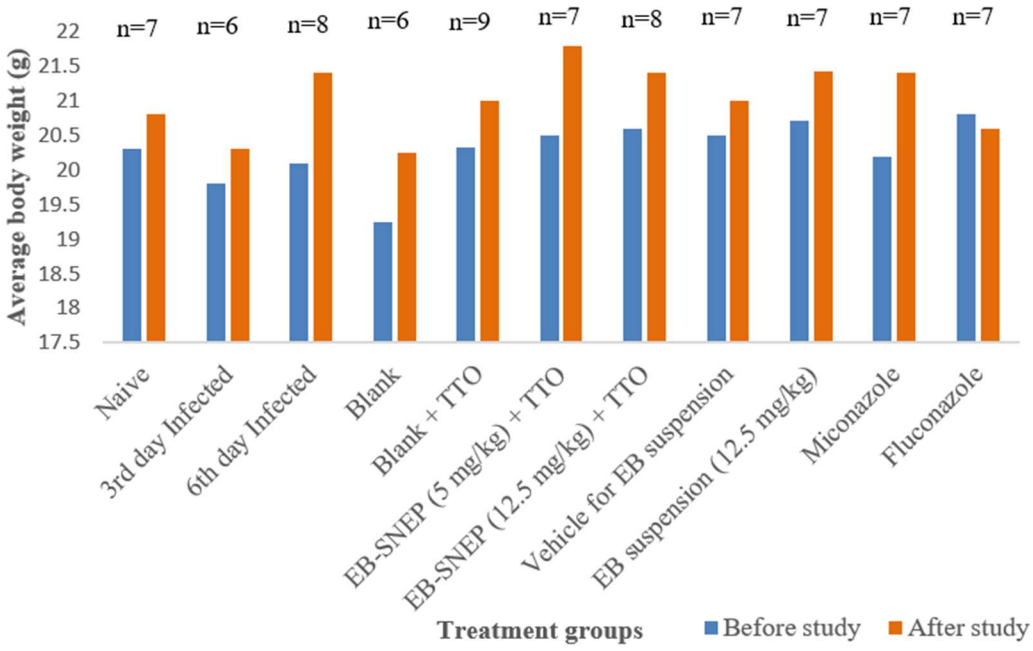

Figure 36: Figure depicting change in average body weight before the study and after the treatment. No significant change in body weight was observed during the study period. Bars represent the mean value for each treatment group. N numbers are indicated above the bars.

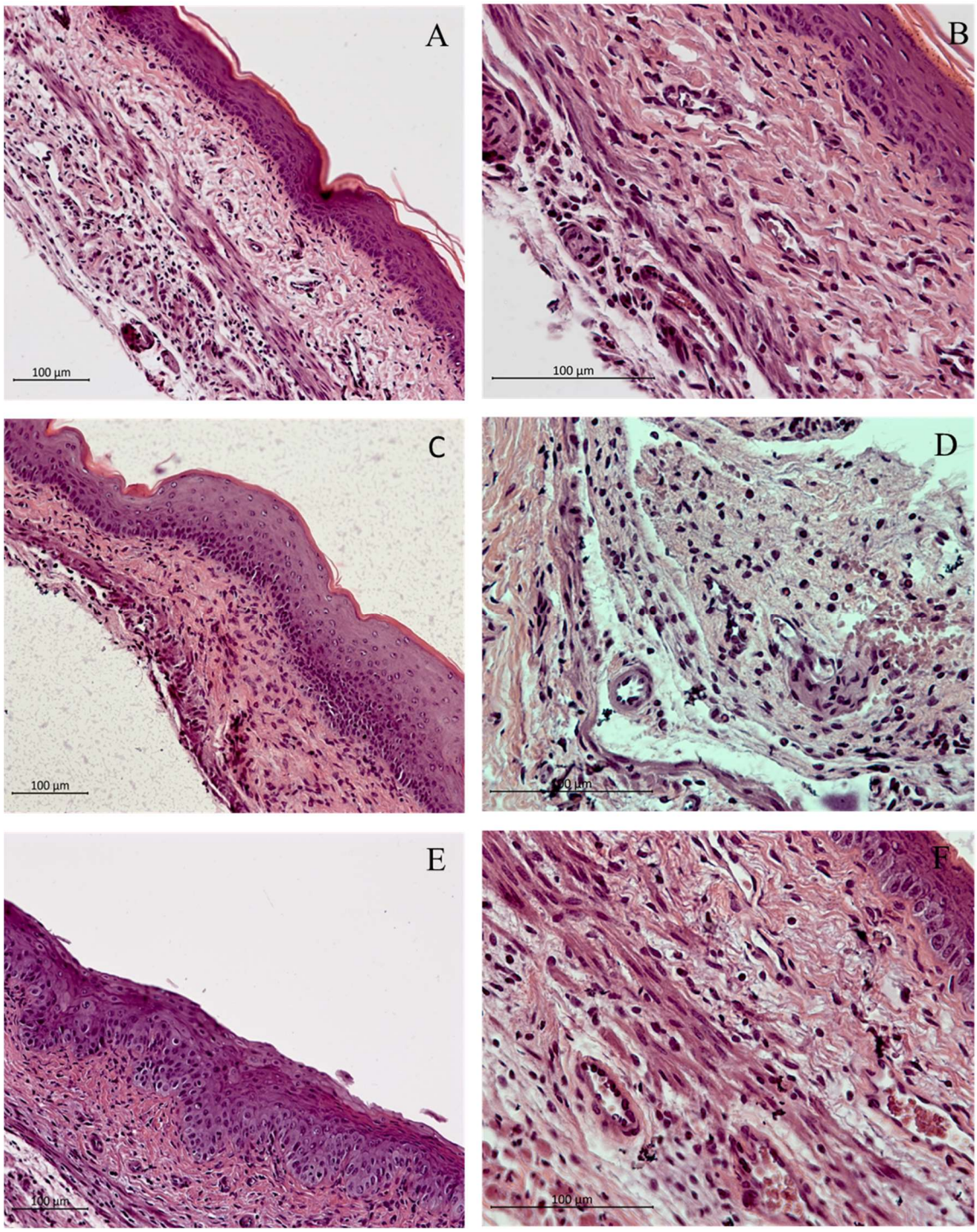

Figure 37: Representative light micrographs of H & E stained mouse vaginal tissues. (A) and (B) Naive group with healthy mouse vaginal tissue; (C) and (D) 3rd day infected group showing PMN infiltration in the epithelial layer; (E) and (F) 6th day infected group (control) showed epithelial hyperplasia. Magnification used was 200x and 400x. Bars on the micrograph represent a length of 100 µm.

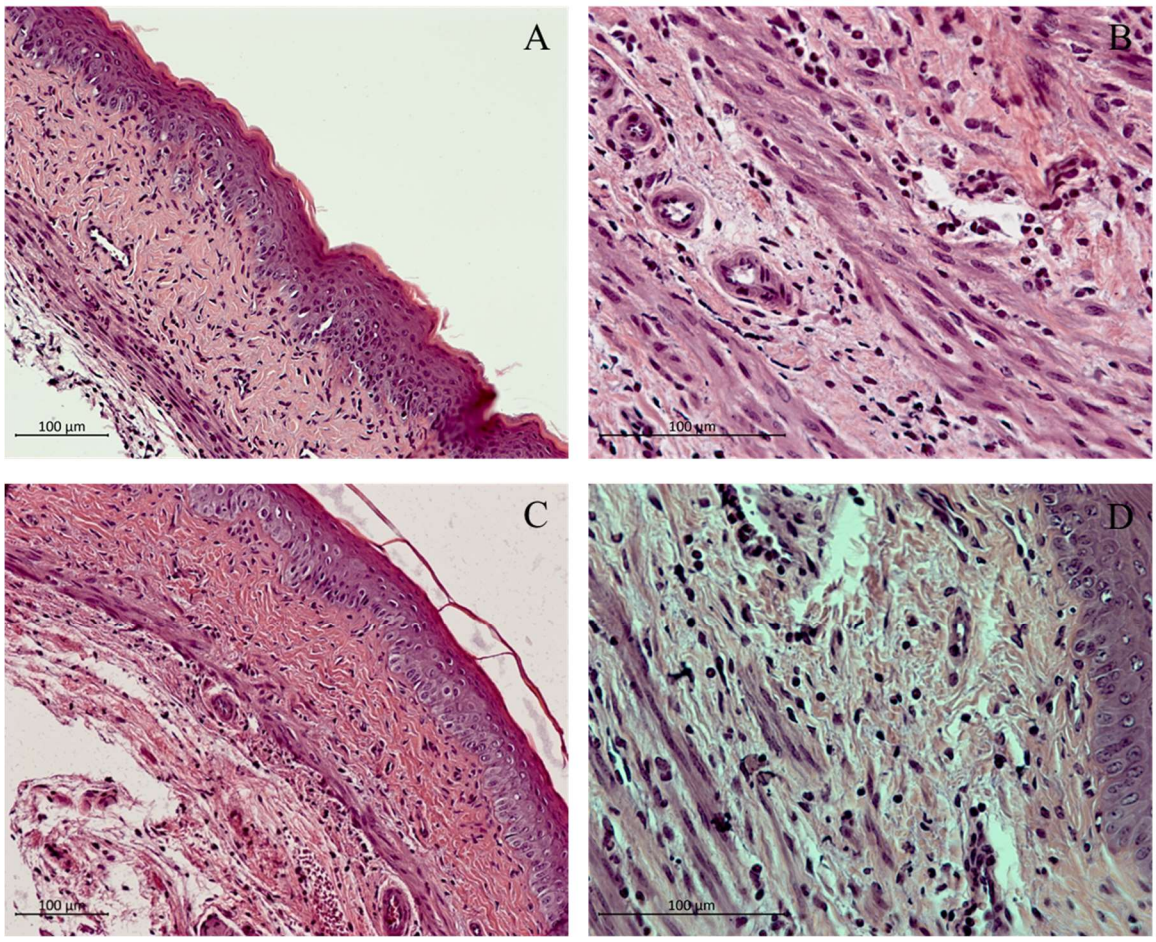

Figure 38: Representative light micrographs of H & E stained mouse vaginal tissues treated with (A) and (B) Blank group without TTO; (C) and (D) Blank + TTO group Magnification used was 200x and 400x; Bars on the micrograph represent a length of 100 µm.

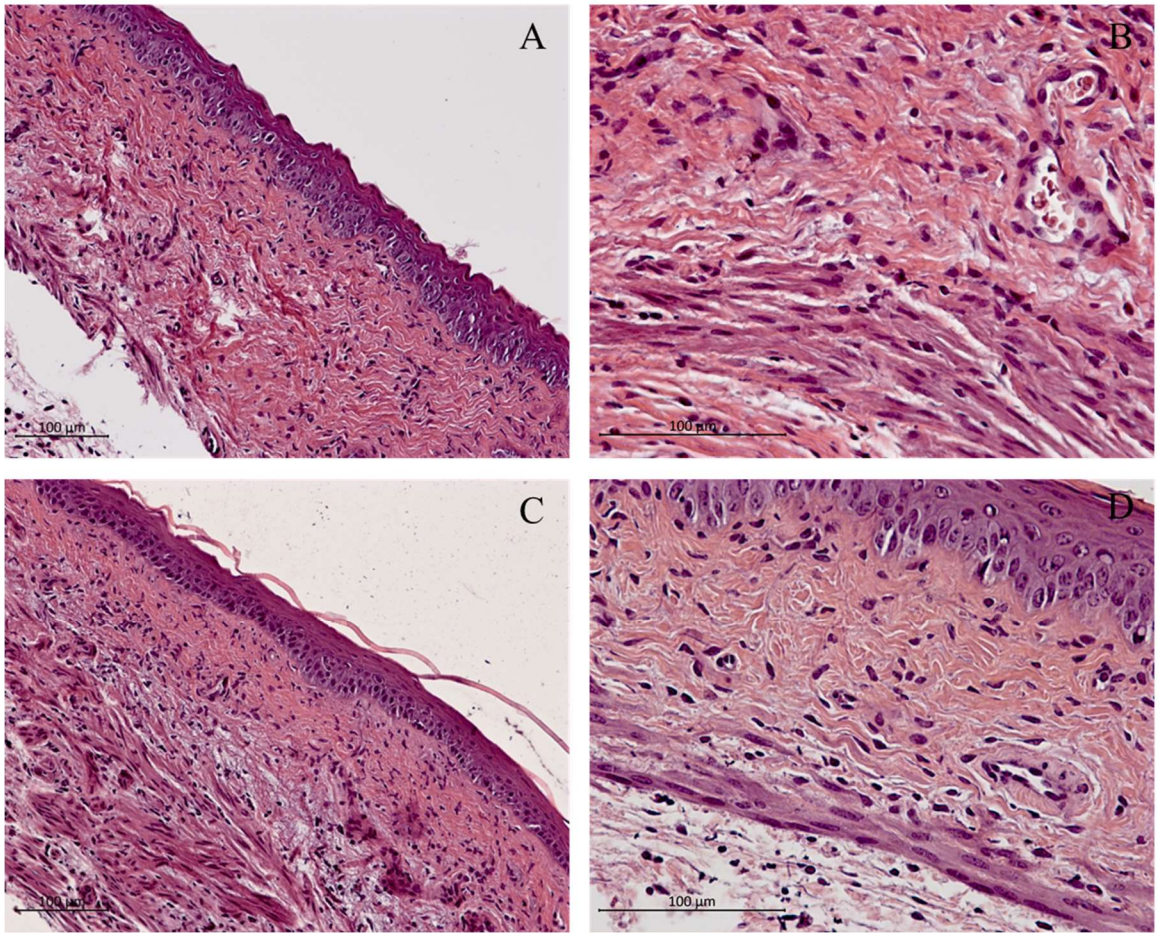

Figure 39: Representative light micrographs of H & E stained mouse vaginal tissues treated with (A) and (B) EB-SNEP (5 mg/kg); (C) and (D) EB-SNEP (12.5 mg/kg). Magnification used was 200x and 400x; Bars on the micrograph represent a length of 100 µm.

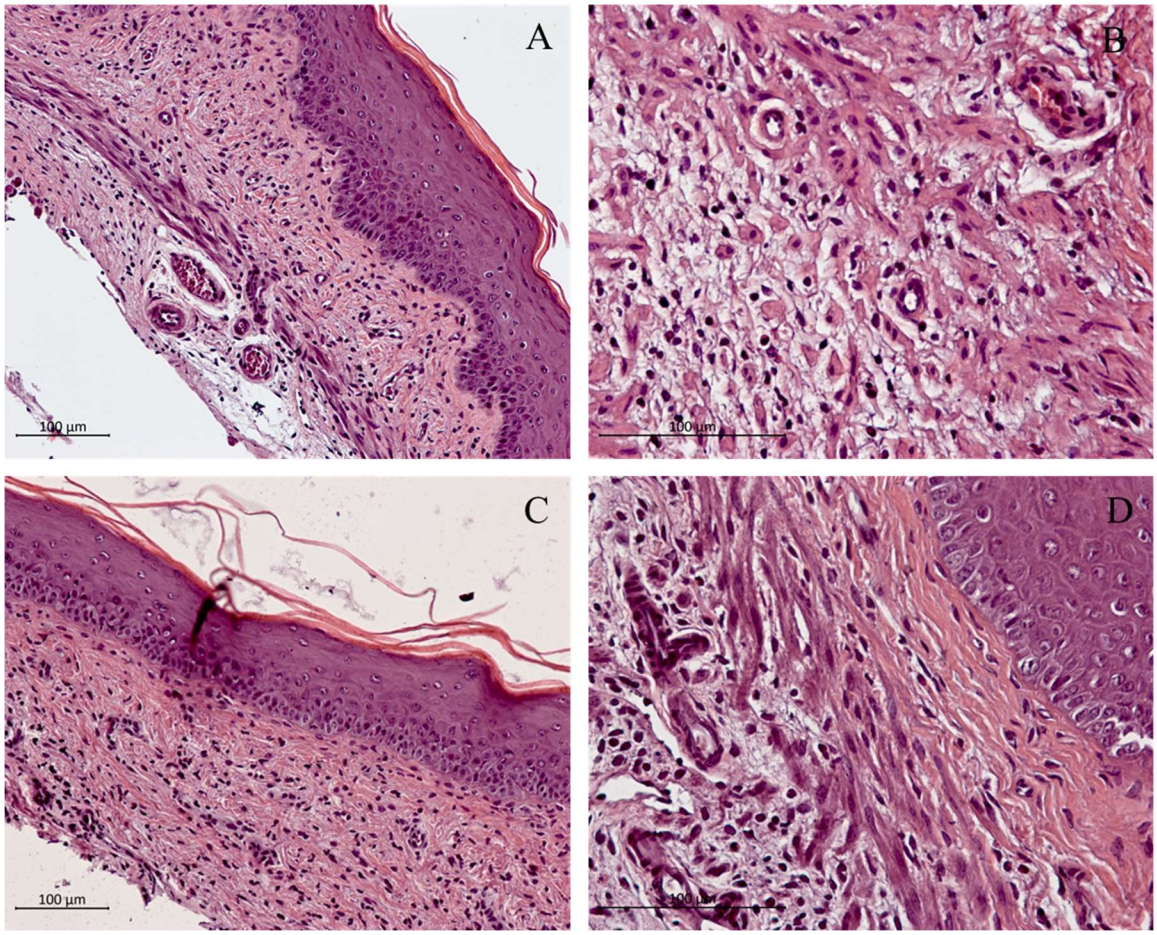

Figure 40:Representative light micrographs of H & E stained mouse vaginal tissues treated with (A) and (B) Vehicle for EB suspension; (C) and (D) EB suspension (12.5 mg/kg). Magnification used was 200x and 400x; Bars on the micrograph represent a length of 100 µm.

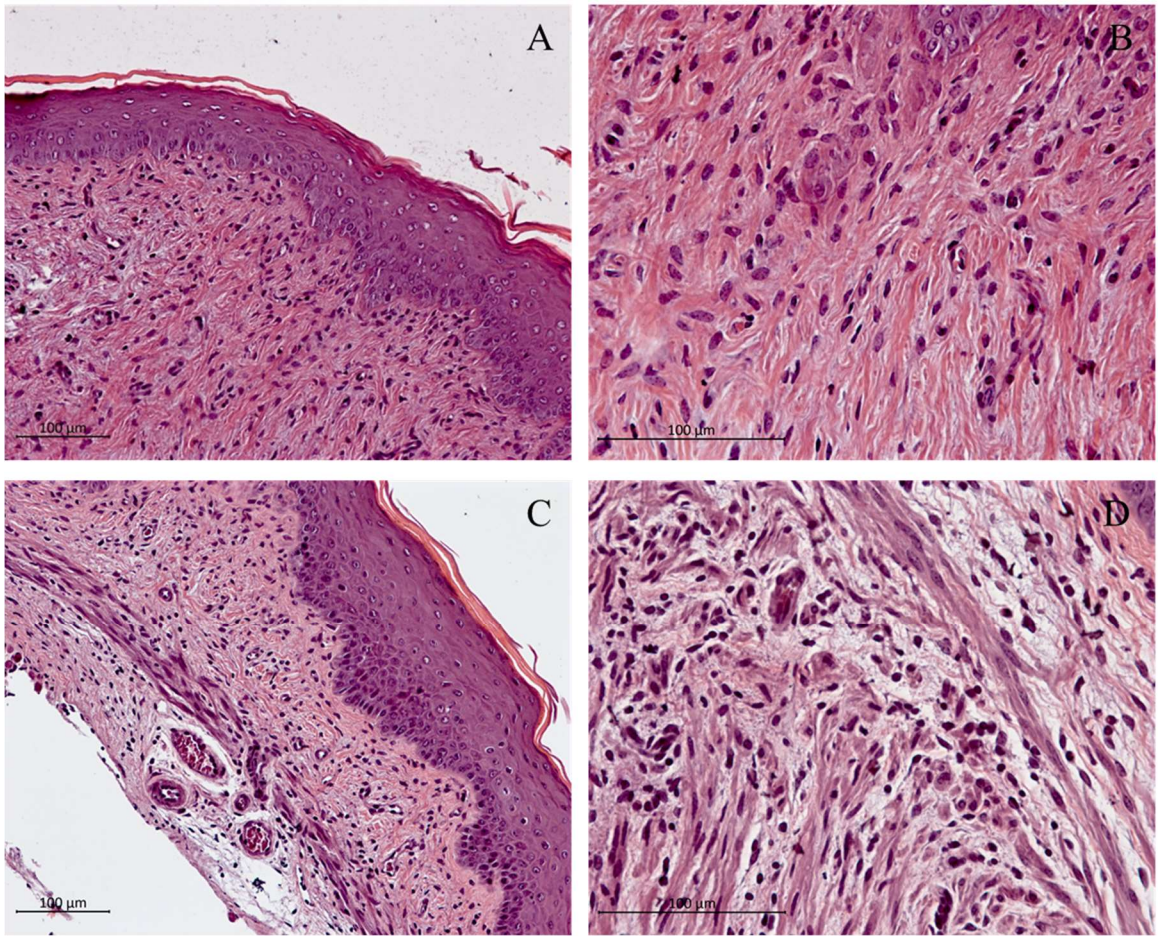

Figure 41: Representative light micrographs of H & E stained mouse vaginal tissues treated with (A) and (B) Miconazole 2% cream; (C) and (D) Fluconazole (25 mg/kg). Magnification used was 200x and 400x; Bars on the micrograph represent a length of 100 µm.

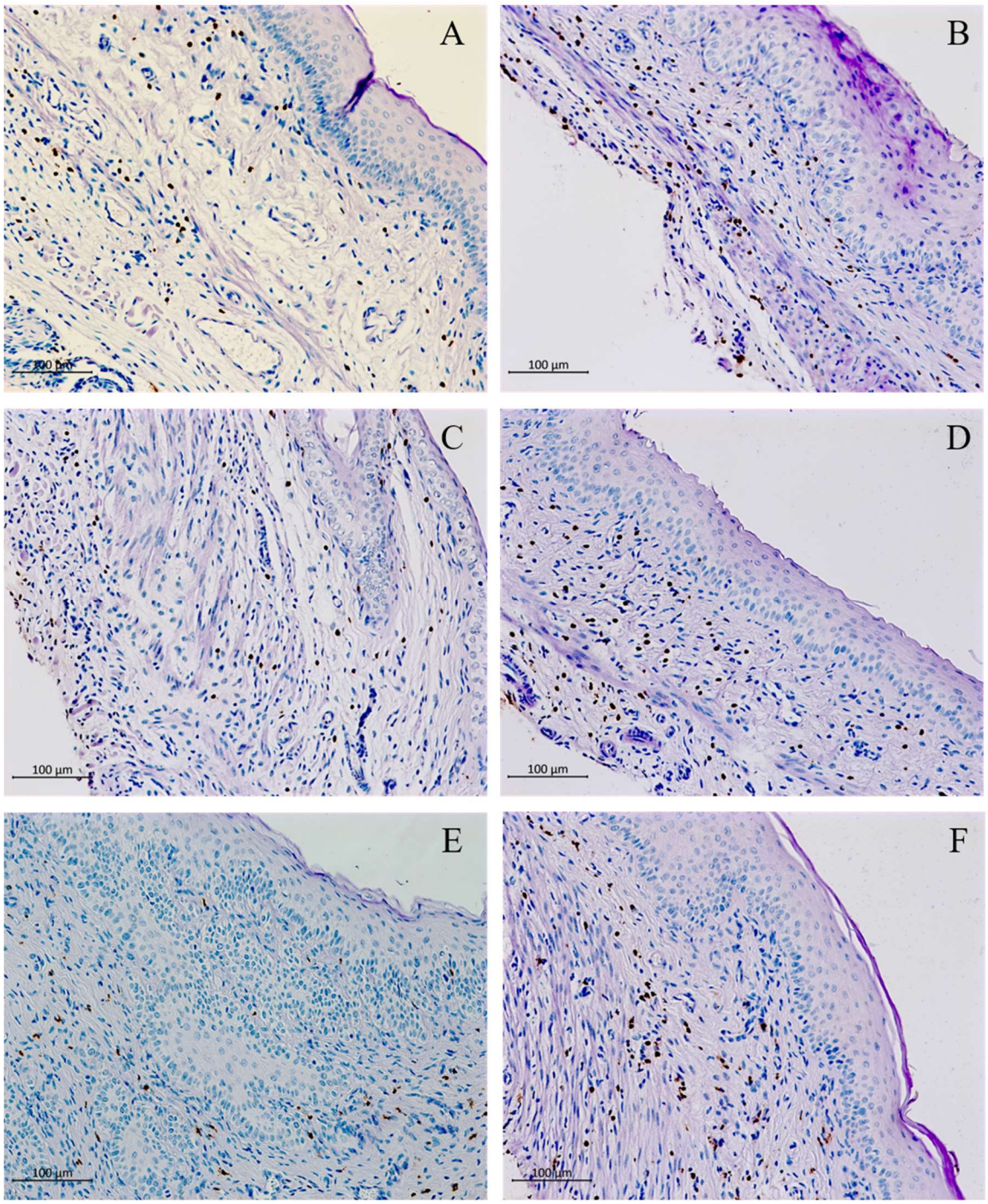

Figure 42:Representative light micrographs of IHC staining for MPO of the mouse vaginal tissue sections following VVC infection. (A) Naive group with healthy mouse vaginal tissue; (B) 6th day infected group (control); (C) Miconazole group; (D) Blank + TTO group; (E) EB-SNEP (12.5 mg/kg), and (F) EB suspension (12.5 mg/kg). Magnification used was 200x; Bars on the micrograph represent a length of 100 µm.

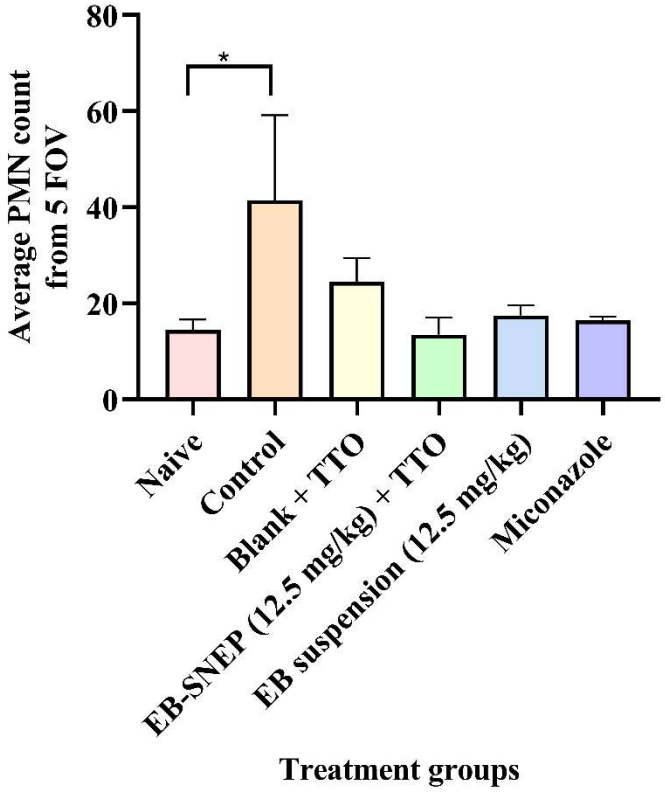

Figure 43: Average PMN counts from 2 experiments using IHC staining for MPO. High PMN counts were observed in the control group followed by the Blank + TTO group and EB suspension. EB-SNEP + TTO ($p<0.05$, Dunnett's multiple comparison test) showed less PMN counts compared to MICO and Naive group. Each bar represents the average of 2 tissues per treatment and vertical lines represent the standard deviation.

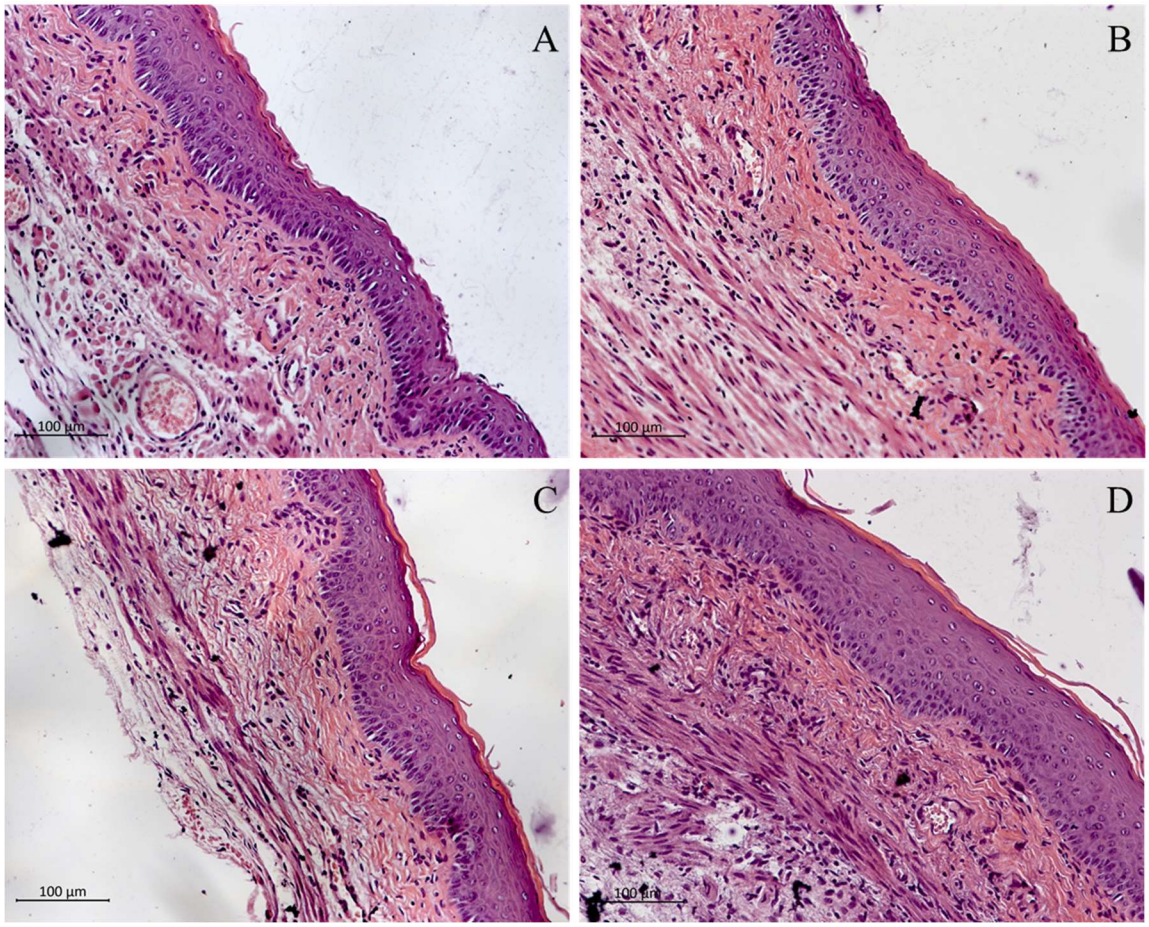

Figure 44: Representative light micrographs of H & E stained mouse vaginal tissues treated with (A) EB suspension (12.5 mg/kg); (B) Blank + TTO; (C) Naive and estrogenized group and (D) Naïve and non-estrogenized group. Magnification used was 200x; Bars on the micrograph represent a length of 100 µm.

CHAPTER IV

DISCUSSION

Of all the fungal infections, infections by *Candida* spp. are by far the most common and debilitating ailments, especially in patients with the immunocompromised system. VVC, caused by *C. albicans* is an acute inflammatory infection experienced quite often by women during their reproductive years. Although VVC is not a severe and life-threatening infection, it has a strong negative impact on both social and work life of women. The impact of this infection on a woman's emotional and psychological front is marked, making some feel embarrassed and stigmatized in some societies (Chapple, 2001; Irving *et al.*, 1998). Despite the easy availability of azoles as standard antifungal treatment, their limited efficacy, rising resistance, and fungistatic nature contribute to the relapse and morbidity of fungal infections. Furthermore, the small antifungal library reveals the difficulty in finding targets since fungi are eukaryotes and share several similarities to mammalian cells which increases the likelihood of off-target toxicity. Moreover, the pace of successful entry of novel antifungal drugs in the market is too slow to keep up with the increase in resistant and more virulent strains which necessitates urgent attention to investigate and construct a repertoire of potent antifungal agents.

Ebselen (EB) has been long studied for its antifungal and anti-inflammatory properties in our laboratory. Numerous studies from our lab and other researchers have demonstrated EB to possess antifungal activity against various fungal pathogens such as *Candida*, *Cryptococcus*, etc. (Billack *et al.*, 2009; Soteropoulos *et al.*, 2000). Interestingly, pioneering research works on this multifunctional drug has coined out a novel fungi target,

the yeast plasma membrane H^+-ATPase pump as being responsible for its antifungal activity *in vitro* (Billack *et al.*, 2010; Chan *et al.*, 2007; Soteropoulos *et al.*, 2000). Keeping in mind EB as a prime example of the extensively repurposed multifaceted drug, we hypothesized EB to be a potent antifungal treatment for VVC.

This Ph.D. project was planned and executed with a view to address the drug resistance issue and identify novel treatments for VVC with the help of the following hypotheses:

- EB possesses antifungal activity against *C. glabrata,* a strain associated with VVC as well as *C. albicans* S1 (FLU-sensitive) and S2 (FLU- resistant) strains.
- Novel organoselenium compounds possess antifungal activity against S1 and S2 strains.
- EB-SNEP exhibits antifungal activity for VVC *in vivo*.
- EB-SNEP is safe in in vitro cells and in vivo mouse model of VVC.

In vitro antifungal activity of EB

In vitro studies with EB against *Candida* spp. (S1 and S2 strains) were carried out as a reference point to study EB analogs (Orie *et al.*, 2017). S1 and S2 strains are clinical isolates from the oral thrush of an immunocompromised patient (Franz *et al.*, 1999b; Morschhäuser, 2002). We also tested EB against *C. glabrata,* as it ranks the second most causative strain in VVC (Fidel *et al.*, 1999).

In vitro susceptibility tests were carried out with EB against S1, S2 and *C. glabrata* to determine the MIC at 24 and 48 h. The results were in line with the previously established studies for EB (Billack *et al.*, 2009; Orie *et al.*, 2017) and were demonstrated

using turbidity assays and a colorimetric assay. Previous studies from our laboratory have shown that EB exhibits antifungal activity by inhibiting the yeast plasma membrane H^+-ATPase (Pma1p) (Billack *et al.*, 2010; Chan *et al.*, 2007). Our medium acidification assay results with EB demonstrates a concentration-dependent decrease in pH levels indicating that EB, indeed attacks the fungal S1 and S2 plasma membrane H^+- ATPase pump.

In vitro antifungal susceptibility test of forty EB analogs

In order to identify new structures in the group of organoselenium derivatives with improved antifungal activity, forty EB analogs were tested against S1 and S2 strains. These forty EB analogs were divided into a set of four groups (I-IV) with each group comprising of 10 compounds with similar R1 group and different R2 groups. After taking in to account the MIC and IC_{50} results, the lead compounds with similar or better antifungal activity to EB were selected for further study.

Consequently, there is a continued interest in exploring the structure-activity relationship (SAR) of antifungal drugs as a way to build and modulate the antifungal library targeting the emerging resistant strains. To elaborate on the SAR with the forty EB analogs, we can say that selected compounds belonging to the group II and III showed overall superior antifungal activity than EB. The significant enhancement of the activity against *Candida* strains was particularly observed for the compounds G20 and G30. We speculate that the strong antifungal activity was attributed due to the electron- withdrawing R1 group (Cl and NO_2) at the 5' position as well as the bulky substituent R2 group (diphenylamine). It is to be noted that compounds (G10 and G40) lacking an electron- withdrawing R1 group but containing a diphenylamine R2 group did not show antifungal activity comparable to

EB. This leads us to the conclusion that together an electron-withdrawing and the diphenylamine group is required to elicit significant antifungal activity. Compounds G4 (R1= 5-CH_3, R2= t-Bu), G13 (R1= 5-Cl, R2= Pr), G23 (R1=5-NO_2, R2=Pr) and G31 (R1=5-CH_3SO_2, R2=H) showed more or less similar MICs as compared to EB in both the strains. A previous study has shown that higher lipophilic compounds allowed easier internalization into eukaryotic pathogens causing membrane perturbations (Malík *et al.*, 2012). In our study, the lead bulky compounds (G20 and G30) have a high log P (~5) indicating that lipophilicity may have played a key feature in their ability to act against yeast strains. Taken together, we postulate that the MIC and IC_{50} data of the lead compounds are structure dependent.

We carried out medium acidification assays on the selected EB analogs (G4, G13, G20, and G30) to determine if the EB analogs exhibit antifungal activity due to inhibition of the H^+-ATPase pump. To our surprise, EB analogs demonstrate more or less similar IC_{50} at 30 minutes which suggests that these EB analogs might exert an inhibitory action on other pumps or a separate target on the yeast cells. One such target could be thioredoxin reductase (TrxR) which has been evolutionarily conserved in all living organisms. This selenoenzyme is essential for several biological events such as RNA and DNA synthesis or for counteracting oxidative stress (Arnér and Holmgren, 2000). An *in vivo* study has shown that EB acts as a substrate of mammalian TrxR but a competitive inhibitor of bacterial TrxR (Zou *et al.*, 2017). Another study has reported that yeast *Cryptococcus neoformans* possesses a low-molecular-weight form of TrxR which shares little homology with that of mammalian host (Missall and Lodge, 2005). The different working mechanism

in mammalian TrxR and microbial TrxR provides specific toxicity to pathogens and makes EB a promising antimicrobial drug with high selectivity and safe profile (Ren *et al.*, 2018).

The scanning electron microscopy (SEM) images a specimen by scanning across its surface with a high-energy beam of electrons (De Nollin and Borgers, 1975). We carried the SEM imaging on both FLU-sensitive and resistant yeast cells incubated with EB, G30, or FLU for 12 h and the untreated yeast cells to obtain images at considerably enhanced resolution than light micrographs and gain an improved depth of field on the fungal surface. The ultrastructural differences readily visualized under SEM with EB, G30 treatment were major changes in the surface appearance from smooth to rough and crinkled, thus indicating outer cell wall damage. SEM studies revealed that like EB and G30 also affected the morphology of yeast making their surface look crinkled and rough unlike the smooth surface of control yeast cells. The SEM observations presented in this study clearly confirm the potent fungicidal action exerted by EB and its analogs. We consider these surface alterations most probably due to a change in cell permeability, causing osmotic imbalance and indentations on the cell surface as mentioned in other studies (De Nollin and Borgers, 1975) (Lara *et al.*, 2015).

In the future, we will investigate and build up the antifungal library within the class of organoselenium compounds by designing novel compounds with various electron-withdrawing groups at the R1 position and N-diphenyl or pyrimidine or imidazole ring at the R2 position. From our perspective, an organoselenium compound consisting of R1(electron-withdrawing group) and R2 diphenyl substituent would prove to be an ideal antifungal compound to be further investigated (Figure 45).

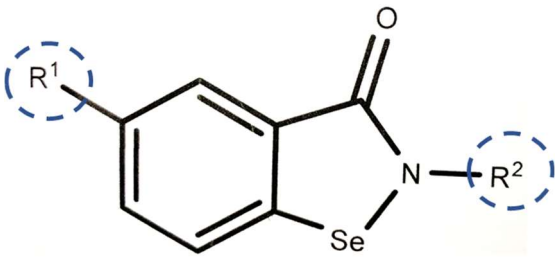

Figure 45: Chemical structure of an ideal organoselenium compound with R1 being electron withdrawing and R2 being bulky group.

Vulvovaginal candidiasis

Vulvovaginal candidiasis (VVC) has always been a common reason for women to visit a gynecologist or physician at least once during their reproductive age. It is estimated that ~ 1.4 million outpatient visits account for VVC in the United States (Benedict *et al.*, 2019). A healthy human vaginal microbiome has a unique and diverse environment with the inhabitation of probiotic *Lactobacillus* taxa and commensal fungi such as *C. albicans* (Martinez *et al.*, 2009; Superti and De Seta, 2020; Zangl *et al*., 2019). Under opportune conditions, the innocuous and highly adaptive yeast form (blastoconidia) switch to the pathogenic and invasive hyphal form (mycelium) which contributes to adherence to the VEC and mucosal invasion, thereby resulting in symptomatic VVC (Bradford and Ravel, 2016; Zangl *et al*., 2019). Currently available antifungal treatments, despite being highly effective, are unable to prevent recurrent VVC episodes resulting in boundless discomfort which entails the investigation of identifying novel compounds with intriguing targets and antifungal efficacy (Benedict *et al.*, 2019)

Development of EB- self nanoemulsifying preconcentrate (EB-SNEP)

Ebselen, an organoselenium compound has been sweepingly repurposed mainly due to its multidimensional properties. Noticeably, studies have also highlighted EB as a

promising drug against SARS-CoV-2 (Menéndez *et al.*, 2020). Moreover, pre-clinical and clinical studies have shown its safety profile and lack of immunogenicity which underscores the reason for drug repurposing (Nozawa *et al.*, 1996). Importantly, prior *in vitro* work in our laboratory has shown EB to be effective against FLU- resistant *Candida* spp. strains (Billack *et al.*, 2009; Orie *et al.*, 2017).

Considering the poor aqueous solubility of EB in organic solvents, novel strategies to deliver EB are necessary to achieve clinical relevance. A previous study from our lab demonstrated how to develop a locally active and stable EB nanoemulgel for topical antifungal activity (Vartak *et al*., 2020b). Another recent report demonstrated that EB can be repurposed as an antifungal agent in a nanosized system as appropriate and ideal for topical delivery for cutaneous candidiasis (Jaromin *et al.*, 2018). In the present work, we have built upon these studies and have taken nano-delivery of EB in a different direction compared to the prior work by developing SNEDDS incorporated with EB for intravaginal delivery. Furthermore, our work is the first to utilize a mouse model to investigate the potential of EBN as an antifungal treatment for VVC infection.

Since EB has a reputation of poor aqueous solubility, a EB self-nanoemulsifying preconcentrate (EB-SNEP) was prepared with a view to enhancing the drug delivery properties of nanoparticles. Nanoemulsion based formulation for vaginal drug delivery has several merits including ease of preparation, optical transparency, effective solubilization of hydrophobic drug, enhanced and controlled drug release locally, better permeability into the fungal cell due to nanosize, minimal leakage of the drug, and high stability of a range of pH (El-Hammadi and Arias, 2020). Taking advantage of the key attributes of nano-delivery technology and based on the preformulation studies, our EBN formulation was

developed using various excipients such as Captex 300, Kolliphor ELP, TTO, and DMA. As per the previous reports by (Vartak *et al*., 2020b), DMA was chosen as an ideal co-solvent for EB due to its high solubilizing capacity for hydrophobic molecules. All the *in vitro* studies were carried out in DMSO as a vehicle ensuring the safe concentration for fungal cells. However, this setup was not feasible moving forward in an *in vivo* setting since DMSO has been reported to cause skin irritation and erythema in some studies (Kollerup Madsen *et al.*, 2019). Besides, DMSO promotes the permeation of solutes by increasing membrane fluidity (Gurtovenko and Anwar, 2007). A way forward is adopting an accepted safer solvent such as DMA which has been extensively used in *in vivo* models considering its solubilizing capacity for hydrophobic molecules (Giusto *et al*., 2019) and no reported antifungal activity of its own. A wide range of studies in the cosmetics and pharmaceutics domain did not exhibit reproductive health toxicity and skin irritation (Giusto *et al*., 2019; Mirza *et al.*, 2013; Southwell *et al.*, 1997), thereby corroborating that these excipients are generally regarded as safe at the concentrations used here. Histopathological analysis in rabbits that received a gel-microemulsion formulation composed of Captex® 300 and Kolliphor® EL up to 10 consecutive days showed intact vaginal epithelium and no vaginal irritation (D'Cruz *et al.*, 2001). As shown in other studies (Giusto *et al*., 2019), we believe that maintaining the state of flux between the core of nanoparticle and in the vaginal tract would facilitate EBN formulation to release EB at a slow rate intravaginally. We also speculate that considering the hydrophobic components in the formulation, EB from EBN formulation would actively try to penetrate the fungal cell wall leading to minimalistic systemic exposure. Further studies will be required to confirm this hypothesis.

In the present work, a ternary phase diagram represented by an equilateral triangle was constructed to visualize the required amounts of oil phase (Captex® 300 EP/NF and TTO), surfactant phase (Kolliphor ELP), and co-solvent (DMA), as the starting point for the study to optimize the final formulation. However, constant drug precipitation was observed within 1 h indicative of an unstable system. Different approaches for increasing drug stability in such systems have been adopted which involve the use of co-surfactants, polymers, secondary oils, etc. Essential oils are comprised of phenolic moieties which are known to interact strongly with the fungal cell membrane thus increasing membrane permeability, leading to disruption of the original structure and cell lysis (Nazzaro *et al.*, 2017). Moreover, due to their lipophilic nature, they can help in solubilizing lipophilic drugs like EB and thus prolong the retentivity of nanoglobule integrity. Therefore, TTO was chosen as a secondary oil for this formulation. In view of the results from the ternary phase diagram, stable nanoemulsion with varying concentrations of TTO was investigated by drug precipitation study, particle size determination, and cytotoxicity assay. The optimized batch EBN with Kolliphor® ELP and MCT (5:7), TTO 30% gave a homogenous, bluish tinged solution with particle size within the nano range. Overall, these excipients enhanced the stability of EB in nanoformulation. Furthermore, based on the precipitation study, EBN with 30% TTO showed greater drug encapsulation within formed nanoglobules (~60%) indicating the role of 30% TTO in stabilizing the formulation and ensuring a controlled and prolonged release of EB.

Antifungal efficacy of EB-SNEP

Firstly, *in vitro* susceptibility tests were carried out with EB-SNEP against S1, S2, and *C. glabrata* to determine the performance of EB-SNEP to EB in DMA only. EB-SNEP

showed similar MIC as EB in DMA only, however, was more potent against *C. glabrata* strain at 24 and 48 h.

Animal studies have shown that VVC disrupts the vaginal epithelium causing inflammation and erythema (Qu *et al.*, 2019; Zhang *et al.*, 2018). Our *in vivo* study corroborates with the results shown by these groups of researchers. Our *in vitro* study demonstrates selective cytotoxicity of EBN towards fungal cells but not the mammalian and probiotic cells. We tested the cytotoxicity of our formulation on the HeLa cell line, an immortal cell line derived from the cervix which is in close proximity to the vaginal tract. In this study, EBN formulation displayed minimal *in vitro* cytotoxicity on these cells. Moreover, a healthy vagina is an abode to the predominant colonization of bacteria such as *Lactobacillus* spp. which contributes to protection against microbial pathogens (Cassone, 2015; Witkin and Linhares, 2017). In our research, EBN formulation at the highest *in vitro* concentration tested (100 μM) including the excipients did not actively kill these probiotic organisms suggesting that EBN formulation is safe for vaginal use. Therefore, we hypothesize that intravaginal use of EBN formulation would alleviate the use of probiotic supplements.

Resazurin is a redox indicator used for determining the viability of eukaryotic cells. MIC values based on turbidimetric assays unlike colorimetric assay are likely to subjective variation. Based on the antifungal data from a previous study (Vartak *et al*., 2020b), we believe that the colorimetric assay exhibits definitive color perception amongst the viable and dead cells. Commonly prescribed therapies like FLU and MICO showed light pink color at concentrations lower than MIC indicating an overall fungistatic effect in

comparison to EB which exhibited a potent fungicidal activity. This would help in curbing the fungal relapse and resistant species development.

Taking a step further, we implemented a mouse model of VVC (Yano and Fidel, 2011) in our lab to test the efficacy of EBN formulation as an alternative therapy to conventional antifungal agents. Interspecies differences in the vaginal environment between rodents and humans exist which is why there is a need to mimic the latter. The rationale behind the use of estrogen in the VVC model emerges from previous studies demonstrating the direct correlation of high estrogen levels with vaginal epithelium thickening and elevated glycogen content resulting in an increase in susceptibility to VVC infection as seen during pregnancy or menstrual cycle (Cassone, 2015; Fidel *et al.*, 2000; Fidel and Yano, 2011; Qu *et al.*, 2019). For this reason, mice were infected with yeast with the support of estrogen, a hormone that is requisite to maintain colonization by *C. albicans*. Our preliminary study for establishing mouse VVC model substantiated the maintenance of robust vaginal fungal burden with the use of estrogen by day 6. A copious number of hyphae were observed sticking to the vaginal epithelium in the control group (infected, untreated). Results from the intervention study with vaginal fungal burden indicated that the control group (infected, untreated) showed a high infection rate whereas EBN formulation remarkably reduced the fungal burden by 780-fold. This was further substantiated by the characteristic parameters of inflammation and damage to the vaginal mucosa such as vaginal epithelial hyperplasia, edema, and damage to the keratin layer. H & E stained vaginal tissues from the control group (infected, untreated) showed edematous and distressed VEC, whereas the tissue sections from EB-SNEP (12.5 mg/kg) resembled the naive group.

Another aspect of *in vivo* study that we observed was the infiltration of PMNs. PMNs have long been identified as the first line of defense against microbial pathogens, triggering other cytokines and proteases to arrive at the site of infection to fight off the invading pathogens. This ensuing cascade of inflammatory response proves to be distressing for vaginal mucosa. We have carried out IHC analysis using an MPO antibody (major protein in neutrophil granules) with a view to understanding the inflammatory response during VVC. In our research, H & E and IHC results indicate the abundant infiltration of PMNs in the control group (infected, untreated) which is in line with at least one previous report (Fidel *et al.*, 2004). In the case of treatment groups, EB-SNEP (12.5 mg/kg) and MICO showed similar levels of PMN infiltration as the naive group. These results substantiate the fact that EB possesses anti-inflammatory activity and is consistent with the previous reports (Cotgreave *et al.*, 1988). In addition, our H & E results portray that the control groups with elevated PMN levels showed epithelial sloughing and/or damage to the keratin layer. These results substantiate the fact that PMNs are responding to the infection in the mouse model of VVC. Others have reported that PMNs, while there, are not activated and exhibit a state of anergy and it is the accumulation of PMNs that induces symptomatic vaginitis (Yano *et al.*, 2018). More work will be required to determine the role of PMNs in VVC, but their presence was inhibited by EBN in our study.

From the toxicological aspect of EBN formulation, we tested EB-SNEP (12.5 mg/kg) and Blank + TTO in uninfected but estrogenized mice. The histological analysis demonstrated that neither formulation cause any perturbations to the vaginal epithelial layer

In summary, we have presented a proof-of-concept study of the *in vivo* potential of the EBN formulation in reducing fungal burden using the widely accepted mouse VVC model. Consolidating our data, we assert that the topical application of EB-SNEP (12.5 mg/kg) notably reduces the vaginal fungal burden and proved to be a feasible approach for treating the murine VVC. Our results also indicate neither the formulation nor any of the excipients exert toxicity to the complex physiological environment in the vagina. Furthermore, our *in vitro* results proclaim that EBN formulation has the potential to exert antifungal activity against FLU-resistant yeast strains and to play an important role in antifungal treatments for immunocompromised women who experience recurrent VVC infections. Future studies will be aimed at determining the extent to which EBN inhibits VVC caused by FLU- resistant yeast strains.

Study limitations

We tested forty EB analogs in both FLU-sensitive and resistant strains *in vitro* and obtained five hits with different substituents. It is possible, however, that the active EB analogs will have cysteine modifying action like EB and may only be useful for topical administration. Further studies are needed to evaluate their chemical specificity beyond *in vitro*.

The S1 strain used for both *in vitro* and *in vivo* studies was isolated from an oral thrush of an HIV-infected individual. However, we used this strain to induce vaginal candidiasis. This strain, although isolated from a different region of infection, showed successful colonization in the vaginal tract. Since both oral and vaginal thrush are designated as mucocutaneous candidiasis, we speculate this why the S1 strain exhibits

virulence in the vagina. Also, testing the S1 strain was the optimal choice because the next step will be to test EBN on FLU-resistant S2 strain (genotyped). On the other hand, the strain 10231(FLU-resistant) procured from ATCC was isolated from a patient with bronchomycosis. We tested this strain for establishing the VVC model, however, this strain was not virulent enough at the test inoculation dose used to sustain fungal colonization throughout the study. Going further, we will use a clinically isolated strain from the vaginal tract for future studies.

We acknowledge the interspecies difference between human and mouse vaginal tract. A human vagina is disparate from mouse vaginal tract in certain morphological and anatomical ways but serves as a versatile structure with similar functions. The vaginal microbiome is profound and diverse in a human vagina and comprised of probiotic organisms such as *Lactobacilli.* The glycogen rich vaginal tract is a haven for these probiotics to grow and proliferate and metabolized to lactic acid creating an acidic environment. A human vagina is acidic (3.8-4.5) while a mouse vagina has higher pH (~6.5). This difference may have an impact on the intervention in the mouse VVC model. Therefore, we may need to test the formulation using a 3D vaginal model, an *in vitro* grown tissue from human ectocervical/vaginal tissue available from vendors such as MatTek (EpiVaginal™) and EpiSkin (SkinEthic™).

Vaginal candidiasis is often experienced in women of child-bearing age, those taking hormone-replacement therapy and pregnant women due to high estrogen levels. Other limitation of the formulation from the clinical point of view would be the use of EBN formulation during the menstrual shedding phase. But the estrogen levels are high before and low during shedding phase and reduces the chances of yeast infection during

menstruation. We did not encounter this problem in the *in vivo* study because the mice we used were estrogenized for the entire period of the study. Lastly, the ability of EBN to initiate the teratogenic effects remains unknown for use in pregnant women. The fact that uterus is in close proximity to the vagina points out the likelihood of drug reaching the former; however, an extensive study and evidence is required to understand the teratogenicity of EB, if any.

CONCLUSIONS

Based on the studies carried out, I accept the following hypothesis:

- **EB possesses antifungal activity against *C. glabrata,* a strain associated with VVC as well as *C. albicans* S1 (FLU-sensitive) and S2 (FLU- resistant) strains.**

These findings led us to formulate EB and test for VVC.

- **Novel organoselenium compounds possess antifungal activity against S1 and S2 strains.**

After screening the novel organoselenium compounds for fungicidal effect, a few compounds were selected which showed similar or superior activity to EB. Of all the forty compounds G20 and G30 exhibited superior antifungal activity than EB against S1 and S2 strains *in vitro*. In brief, the results point to investigating compounds with substitution of electron-withdrawing and a diphenylamine group in the parent molecule of EB. The active EB analogs will be further investigated for *in vivo* efficacy. The findings from medium acidification assays indicate that these active compounds may have an inhibitory effect on pumps other than H^+-ATPase.

- **EB-SNEP demonstrates potential antifungal treatment for VVC *in vivo*.**

EB was formulated in a self-nanoemulsifying preconcentrate (EB-SNEP) which upon intravaginal administration formed nanoemulsion (EBN) *in vivo*. With the vaginal fungal burden data, EB-SNEP (12.5 mg/kg) proved to be a reliable and superior formulation with an improved antifungal profile when compared to EB-suspension, MICO, and FLU.

- **EB-SNEP is safe in *in vitro* cells and *in vivo* mouse model of VVC.**

From the toxicological point of view, EB-SNEP is safe to the mammalian cells and probiotic organisms, while toxic to fungal cells *in vitro* and *in vivo*.

APPENDIX

Appendix 1: HPLC Analysis

Chromatographic separation of EB was performed using Waters alliance® HPLC equipped with 2998 Photodiode Array (PDA) detector and Hypersil® ODS column (250 mm × 4.6 mm, 5 μm). An optimum ratio of 60:40 Acetonitrile (CAN): HPLC grade water was used as the mobile phase. Injection volume and flow rate was set to 10 μL and 1 ml/min respectively. Column temperature was maintained at 25°C. Samples were injected and analysed using autosampler and output signal was detected using Empower 3 software at 265 nm. Retention time of EB was 4.65 ± 0.5 min.

Appendix 2: Detailed composition of EB-SNEP used in the mouse VVC study

Table 18: Composition of EB-SNEP used in the mouse VVC study

Components	Percentage (%)	Role of the components
EB	0.95 % w/v	Antifungal drug
Dimethylacetamide (DMA)	9.5 %	Co-solvent
Captex 300 EP/NF	25.79 %	Medium chain triglyceride (accounts for oily phase)
Kolliphor® ELP	36.10 %	Surfactant
Tea tree oil (TTO)	28.57 % v/v	Imparts stability to the formulation (accounts for oily phase) and possesses antifungal activity (Mertas *et al.*, 2015; Li *et al.*, 2017)

- **EB-SNEP (12.5 mg/kg):** 100 mg of EB (molecular weight: 274.17) was dissolved in 1000 µl of DMA as stock solution for 0.25 mg dose of EB. The pre-concentrate in the ratio 5:7 (Captex oil: Kolliphor ELP) was prepared separately. To the 130 µl of the preconcentrate, 20 µl of EB stock solution was added and vortexed resulting in EB preconcentrate (EB-SNEP). To this mixture, 60 µl of tea tree oil was added and vortexed well.
- **EB-SNEP (5 mg/kg):** 40 mg of EB was dissolved in 1000 µl of DMA as stock solution for 0.1 mg dose of EB in 27 µl. To the 130 µl of the preconcentrate, 20 µl of EB stock solution was added and vortexed resulting in EB-SNEP. To this mixture, 60 µl of tea tree oil was added and vortexed well.

- **Blank + TTO:** This solution comprised of 20 µl of DMA along with 130 µl of the preconcentrate (Captex and Kolliphor) and 60 µl of tea tree oil without EB. The Blank + TTO group was added to justify the antifungal effects of TTO, if any.
- **Blank:** This solution comprised of 20 µl of DMA along with 130 µl of the preconcentrate (Captex and Kolliphor). The Blank group was added to justify the antifungal effects of 147xcipients, if any.

Appendix 3: Summary of animal data in S1 intervention study

Table 19: Animal data in S1 intervention study

Batch No	Sr. No.	Randomized numer	Code	Body wt before Inj	Body wt after Inj	Date of Euthanization	Lavage fluid	Wt. of half vaginal tissue	Colonies	Dilution Factor	CFU/100 ul	Initial Inoculum dose	% change in Inoculum	% Inoculum remaining
B-1	1	1	PA-1	22 g	23 g	10/4/2019	100 ul	0.0172g	24	10	480.00	1400000.00	99.97	0.03
	2	2	PA-2	21 g	21 g	10/4/2019	100 ul	0.03 g	0	0	0.00	1400000.00	100.00	0.00
	3	29	MA-1	21 g	21g	10/4/2019	100 ul	0.0437 g	46	100	9200.00	1400000.00	99.34	0.66
	4	30	MA-2	23 g	22 g	10/4/2019	100 ul	0.0364 g	20	10	400.00	1400000.00	99.97	0.03
	5	64	NJ-1	22 g	23 g	10/4/2019	100 ul	0.0364 g	118	10	2360.00	1400000.00	99.83	0.17
	6	85	NY-1	20 g	22 g	10/4/2019	100 ul	0.0426 g	28	1000	22000.00	1400000.00	98.43	1.57
	7	86	NY-2	22 g	22 g	10/4/2019	100 ul	0.0219 g	28	100	56000.00	1400000.00	96.00	4.00
B-2	8	11	KS-2	20 g	20 g	12/19/2019	100 ul	0.0375 g	6	10	120.00	2800000.00	100.00	0.00
	9	24	KS-4	21 g	21 g	12/19/2019	100 ul	0.0367 g	28	1000	56000.00	2800000.00	98.00	2.00
	10	9	TN-3	20 g	20 g	12/19/2019	100 ul	0.0327 g	47	10,000	940000.00	2800000.00	66.43	33.57
	11	54	IA-5	20 g	18 g	12/19/2019	100 ul	0.0280 g	70	100	14000.00	2800000.00	99.50	0.50
	12	59	NV-3	20 g	20 g	12/19/2019	100 ul	0.0450 g	27	10,000	540000.00	2800000.00	80.71	19.29
	13	74	LA-4	20 g	20 g	12/19/2019	100 ul	0.0301 g	0	0	0.00	2800000.00	100.00	0.00
	14	88	NY-4	20 g	20 g	12/19/2019	100 ul	0.0249 g	26	10,000	520000.00	2800000.00	81.43	18.57
B-3	15	32	MA-4	20 g	21 g	12/20/2019	100 ul	0.0257 g	46	100	9200.00	480000.00	98.08	1.92
	16	33	MA-5	20 g	20 g	12/20/2019	100 ul	0.0392 g	40	10,000	800000.00	480000.00	-66.67	33.33
	17	25	TN-4	19g	21 g	12/20/2019	100 ul	0.0322 g	75	10,000	1500000.00	480000.00	-212.50	-112.50
	18	26	TN-5	20 g	21 g	12/20/2019	100 ul	0.0281 g	71	10,000	1420000.00	480000.00	-195.83	-95.83
	19	67	NJ-4	20 g	20 g	12/20/2019	100 ul	0.0233 g	40	100	80000.00	480000.00	83.33	16.67
	20	73	LA-3	20 g	20 g	12/20/2019	100 ul	0.0345 g	0	0	0.00	480000.00	100.00	0.00
	21	82	CA-5	20 g	20 g	12/20/2019	100 ul	0.0438 g	35	10,000	700000.00	480000.00	-45.83	54.17
B-4	22	8	KS-1	20 g	20 g	12/24/2019	100 ul	0.0264 g	103	100	20600.00	1440000.00	98.57	1.43
	23	14	KS-7	21g	22 g	12/24/2019	100 ul	0.0233 g	37	100	7400.00	1440000.00	99.49	0.51
	24	19	WA-5	20 g	21 g	12/24/2019	100 ul	0.0276 g	32	10000	640000.00	1440000.00	55.56	44.44
	25	57	NV-1	20 g	21 g	12/24/2019	100 ul	0.0267 g	35	10,000	700000.00	1440000.00	51.39	48.61
	26	61	NV-5	22 g	22 g	12/24/2019	100 ul	0.0307 g	175	100	35000.00	1440000.00	97.57	2.43
	27	62	NV-6	22 g	22 g	12/24/2019	100 ul	0.0262 g	122	10,000	2440000.00	1440000.00	-69.44	30.56
	28	77	LA-7	20 g	21 g	12/24/2019	100 ul	0.0508 g	0	0	0.00	1440000.00	100.00	0.00
B-5	29	6	PA-6	20 g	21 g	1/13/2020	100 ul	0.0346g	40	100	8000.00	720000.00	98.89	1.11
	30	23	TN-2	18 g	19 g	1/13/2020	100 ul	0.0404 g	78	10000	1560000.00	720000.00	-116.67	-16.67
	31	16	WA-2	19 g	21 g	1/13/2020	100 ul	0.0330 g	72	10000	1440000.00	720000.00	-100.00	0.00
	32	55	IA-6	20 g	20 g	1/13/2020	100 ul	0.0181 g	85	1000	170000.00	720000.00	76.39	23.61
	33	58	NV-2	20 g	20 g	1/13/2020	100 ul	0.0329 g	45	10000	900000.00	720000.00	-25.00	75.00
	34	79	CA-2	19 g	20 g	1/10/2020	100 ul	0.0197 g	44	10000	880000.00	720000.00	-22.22	77.78
	35	83	CA-6	19 g	19 g	1/10/2020	100 ul	0.0273 g	120	1000	240000.00	720000.00	66.67	33.33

B-6	36	13	KS-6	20g	19 g	1/15/2020	100 ul	0.0595g	41	1000	82000.00	1160000.00	92.93	7.07
	37	34	MA-6	20 g	21 g	1/15/2020	100 ul	0.0243 g	49	10000	980000.00	1160000.00	15.52	84.48
	38	50	IA-1	21 g	22 g	1/15/2020	100 ul	0.0361 g	74	1000	148000.00	1160000.00	87.24	12.76
	39	69	NJ-6	20 g	21 g	1/15/2020	100 ul	0.0296 g	31	10000	620000.00	1160000.00	46.55	53.45
	40	80	CA-3	19 g	20 g	1/12/2020	100 ul	0.0360 g	67	100	13400.00	1160000.00	98.84	1.16
	41	84	CA-7	20 g	21 g	1/12/2020	100 ul	0.0305 g	50	1000	100000.00	1160000.00	91.38	8.62
	42	90	NY-6	19 g	20 g	1/15/2020	100 ul	0.0236 g	45	100000	9000000.00	1160000.00	-675.86	-575.86
B-7	43	3	PA-3	19 g	21 g	2/2/2020	100 ul	0.0258 g	40	10	800.00	1360000.00	99.94	0.06
	44	10	KS-3	20 g	21 g	2/2/2020	100 ul	0.0340 g	22	10000	440000.00	1360000.00	67.65	32.35
	45	17	WA-3	20 g	22 g	2/2/2020	100 ul	0.0190 g	51	100	10200.00	1360000.00	99.25	0.75
	46	31	MA-3	21 g	22 g	2/2/2020	100 ul	0.0261 g	145	1000	290000.00	1360000.00	78.68	21.32
	47	51	IA-2	22 g	22 g	2/2/2020	100 ul	0.0389 g	25	1000	50000.00	1360000.00	96.32	3.68
	48	63	NV-7	21 g	22 g	2/2/2020	100 ul	0.0286 g	25	100000	5000000.00	1360000.00	-267.65	-167.65
	49	68	NJ-5	20 g	22 g	2/2/2020	100 ul	0.0276 g	40	100	8000.00	1360000.00	99.41	0.59
B-8	50	40	VA-5	19 g	19 g	2/3/2020	100 ul	0.0225 g	23	1000	46000.00	1000000.00	95.40	4.60
	51	39	VA-4	18 g	19 g	2/3/2020	100 ul	0.0333 g	37	1000	74000.00	1000000.00	92.60	7.40
	52	52	IA-3	21 g	21 g	2/3/2020	100 ul	0.0264 g	32	1000	60000.00	1000000.00	94.00	6.00
	53	60	NV-4	19 g	20 g	2/3/2020	100 ul	0.0325 g	78	10000	1560000.00	1000000.00	-56.00	44.00
	54	65	NJ-2	19 g	21 g	2/3/2020	100 ul	0.0265 g	30	1000	13000.00	1000000.00	98.70	1.30
	55	66	NJ-3	19 g	20 g	2/3/2020	100 ul	0.0260 g	34	1000	68000.00	1000000.00	93.20	6.80
	56	87	NY-3	20 g	23 g	2/3/2020	100 ul	0.0337 g	21	10000	420000.00	1000000.00	58.00	42.00
B-9	57	5	PA-5	21 g	22 g	2/19/2020	100 ul	0.0262 g	70	10	1400.00	840000.00	99.83	0.17
	58	12	KS-5	21 g	22 g	2/19/2020	100 ul	0.0296 g	50	1000	100000.00	840000.00	88.10	11.90
	59	15	WA-1	22 g	22 g	2/19/2020	100 ul	0.0268 g	51	1000	102000.00	840000.00	87.86	12.14
	60	70	NJ-7	22 g	23 g	2/19/2020	100 ul	0.0300 g	0	0	0.00	840000.00	100.00	0.00
	61	71	LA-1	21 g	22 g	2/19/2020	100 ul	0. 0354 g	0	0	0.00	840000.00	100.00	0.00
	62	78	CA-1	22 g	22 g	2/16/2020	100 ul	0.0268 g	40	1000	80000.00	840000.00	90.48	9.52
	63	89	NY-5	20 g	21 g	2/19/2020	100 ul	0.0288 g	65	10000	1300000.00	840000.00	-54.76	45.24
B-10	64	18	WA-4	21g	23 g	2/20/2020	100 ul	0.0212 g	50	10000	1000000.00	1200000.00	16.67	83.33
	65	20	WA-6	21 g	22 g	2/20/2020	100 ul	0.0331 g	45	10000	900000.00	1200000.00	25.00	75.00
	66	27	TN-6/KS-8	20 g	23 g	2/20/2020	100 ul	0.0198 g	32	10000	640000.00	1200000.00	46.67	53.33
	67	28	TN-7/KS-9	20 g	21 g	2/20/2020	100 ul	0.0267 g	57	1000	114000.00	1200000.00	90.50	9.50
	68	35	MA-7	20 g	23 g	2/20/2020	100 ul	0.0272 g	29	10000	580000.00	1200000.00	51.67	48.33
	69	91	NY-7	20 g	22 g	2/20/2020	100 ul	0.0253 g	60	10000	1200000.00	1200000.00	0.00	100.00
B-11	70	22	TN-1	20 g	22 g	9/6/2020	100 ul	0.0425 g	22	10,000	440000.00	288000.00	-52.78	47.22
	71	27	TN-6	18 g	21 g	9/6/2020	100 ul	0.0500 g	28	10,000	560000	288000.00	-94.44	5.56
	72	21	WA-7	19 g	21 g	9/6/2020	100 ul	0.0494 g	25	1000	50000	288000.00	82.64	17.36
	73	93	NY-8	20 g	21 g	9/6/2020	100 ul	0.0306 g	27	10,000	540000	288000.00	-87.50	12.50
	74	51	IA-2	21 g	22 g	9/6/2020	100 ul	0.0380 g	60	100	12000	288000.00	95.83	4.17
	75	53	IA-4	20 g	21 g	9/6/2020	100 ul	0.0457 g	27	100	5400	288000.00	98.13	1.88
	76	88	PA-4	20 g	22 g	9/6/2020	100 ul	0.0289 g	18	100	3600	288000.00	98.75	1.25
	77	74	PA-7	20 g	21 g	9/6/2020	100 ul	0.0586 g	22	100	4400	288000.00	98.47	1.53
	78	92	PA-8	19 g	21 g	9/6/2020	100 ul	0.0377 g	150	10	3000	288000.00	98.96	1.04
B12	79	Tox study	SM1	24 g	26 g	7/10/2020								
	80	Tox study	SM2	29 g	30 g	7/10/2020								
	81	Tox study	SM3	30 g	31 g	7/10/2020								
	82	Tox study	SM4	24 g	27 g	7/10/2020								
	83	Tox study	SM5	20 g	22 g	7/10/2020								
	84	Tox study	SM6	25 g	27 g	7/10/2020								
	85	Tox study	SM7	24 g	27 g	7/10/2020	This an acute toxicity study where the mice were not infected instead treated with formulations to understand their toxicity. Mice were out of the body weight range because of the Corona virus pandemic.							
	86	Tox study	SM8	24 g	26 g	7/10/2020								
	87	Tox study	SM9	29 g	31 g	7/10/2020								
	88	Tox study	SM10	29 g	31 g	7/10/2020								
	89	Tox study	SM11	23 g	25 g	7/10/2020								
	90	Tox study	SM12	24 g	25 g	7/10/2020								
	91	Tox study	SM13	24 g	26 g	7/10/2020								
	92	Tox study	SM14	23 g	25 g	7/10/2020								

***PA**- EB-SNEP (12.5 mg/kg); **MA**- EB suspension (12.5 mg/kg);

NJ- MICO (2% cream) **NY**- 6th day infected (Control);

KS- Blank + TTO; **TN**- Blank without TTO;

IA- FLU (25 mg/kg p.o.); **NV**- Vehicle for EB-suspension;

LA- Naive; **CA**- 3rd day infected;

WA- EB-SNEP (5 mg/kg); **VA**- G20 (12.5 mg/kg);

SM1- SM-4: EB-SNEP (12.5 mg/kg); **SM5- SM8**: Blank + TTO; **SM9 – SM11**: Estrogenized; **SM12 – SM14**: Non-estrogenized.

Table 20: Animal data in S1 and 10231 Pilot study

Sr. No.	Code	Body wt before Inj	Body wt after Inj	Date of Euthanization	Lavage fluid	Wt. of half vaginal tissue	Colonies	Dilution Factor	CFU/100 ul	Initial Inoculum dose
				S1 STRAIN						
1	3-1	21 g	21g	4/23/2019	100 ul	0	62	1000	124000.00	~5.5 x 10^5
2	3-2	20 g	20 g	4/23/2019	100 ul	0	30	1000	60000.00	~5.5 x 10^5
3	3-3	19 g	19 g	4/23/2019	100 ul	0	57	10,000	1140000.00	~5.5 x 10^5
4	3-4	20 g	20 g	4/23/2019	100 ul	0	9	100	1800.00	~5.5 x 10^5
5	6-1	20 g	20 g	4/26/2019	100 ul	0	124	1000	248000.00	~5.5 x 10^5
6	6-2	20 g	21 g	4/26/2019	100 ul	0	98	1000	196000.00	~5.5 x 10^5
7	6-3	19 g	20 g	4/26/2019	100 ul	0	86	1000	172000.00	~5.5 x 10^5
8	6-4	18 g	19 g	4/26/2019	100 ul	0	36	10	120.00	~5.5 x 10^5
9	9-1	18 g	20 g	4/29/2019	100 ul	0	130	1000	260000.00	~5.5 x 10^5
10	9-2	20 g	20 g	4/29/2019	100 ul	0	115	1,000	230000.00	~5.5 x 10^5
11	9-3	18 g	19 g	4/29/2019	100 ul	0	105	1000	210000.00	~5.5 x 10^5
12	9-4	15 g	15 g	4/29/2019	100 ul	0	0	0	0.00	~5.5 x 10^5
				10231 STRAIN						
1	3-1	18 g	20 g	8/3/2019	100 ul	0.071 g	24	10	480.00	~5.5 x 10^6
2	3-2	20 g	23 g	8/3/2019	100 ul	0.076 g	8	10	160.00	~5.5 x 10^6
3	3-3	18 g	21 g	8/3/2019	100 ul	0.113 g	95	10	1900.00	~5.5 x 10^6
4	3-4	21 g	23 g	8/3/2019	100 ul	0.119 g	0	0	0.00	~5.5 x 10^6
5	6-1	20 g	23 g	8/6/2019	100 ul	0.0868 g	78	100	15600.00	~5.5 x 10^6
6	6-2	20 g	23 g	8/6/2019	100 ul	0.0445 g	120	100	24000.00	~5.5 x 10^6
7	6-3	19 g	21 g	8/6/2019	100 ul	0.0493 g	105	100	21000.00	~5.5 x 10^6
8	6-4	18 g	21 g	8/6/2019	100 ul	0.0650 g	0	0	0.00	~5.5 x 10^6
9	9-1	21 g	23 g	8/9/2019	100 ul	0.1163 g	0	0	0.00	~5.5 x 10^6
10	9-2	21 g	22 g	8/10/2019	100 ul	0.0661 g	0	0	0.00	~5.5 x 10^6
11	9-3	21g	23 g	8/11/2019	100 ul	0.0515 g	0	0	0.00	~5.5 x 10^6
12	9-4	21 g	21 g	8/12/2019	100 ul	0.0700 g	0	0	0.00	~5.5 x 10^6

Day 3: 3-1, 3-2, 3-3, 3-4

Day 6:6-1, 6-2, 6-3, 6-4

Day 9:9-1, 9-2, 9-3, 9-4

Appendix 4: Gene expression analysis by the vaginal tissues from the mouse model of VVC.

Pioneering research works have shown a surge in levels of inflammatory mediators in the mouse model of VVC. It has been established that S100 alarmins increase during the VVC infection and is primarily mediated via a direct interaction with the epithelial cells and *Candida.* Since vaginal epithelial cells are the primary source of S100 alarmins following vaginal inoculation with *Candida,* we carried out gene expression analysis for S100A8 and S100A9 alarmins as well as IL-1β, and TLR4 from the mouse vaginal tissues from the following groups: (Naïve, 6^{th} day infected (control), Blank + TTO, EBN (12.5 mg/kg), EB-suspension, MICO and FLU.

Materials

For gene expression analysis, RNeasy mini kit was purchased from Qiagen (Germantown, MD; Cat # NC9677589), and SuperScript IV VILO mastermix was procured from ThermoFisher Scientific (Waltham, MA; cat #11756050). NanoDrop spectrophotometer (ThermoFisher Scientific) and QuantStudio-3 (Applied Biosystems) Real-Time PCR system was used. A microplate reader ELX 800MS (BioTek Instrument Inc., Vermont, USA) was used to read fluorescence.

Methods

Gene expression assay: Half of the vaginal tissue isolated after euthanization was preserved in RNAlater stabilization solution for 24h at 4℃, and then stored at -80℃ for later use. Total RNA extractions were performed using RNeasy Mini kit, with an additional on-column DNase digestion prior to extraction. Total RNA extracts were quantified using NanoDrop spectrophotometer. RT-qPCR was performed in two-step method, where synthesizing cDNA from total RNA was followed by RT-qPCR using TaqMan gene

expression assays for the genes IL-1 β, S100A8, S100A9, and TLR2). The cycle threshold (Ct) values of target genes were normalized using the Ct value of the endogenous control 18s rRNA content. Normalized data were used to quantify relative expression levels of IL-1 β, S100A8, S100A9, and TLR2 mRNA using the ΔΔCT method. The results are expressed as the fold change relative to the gene expression of estrogenized inoculated mice.

Results

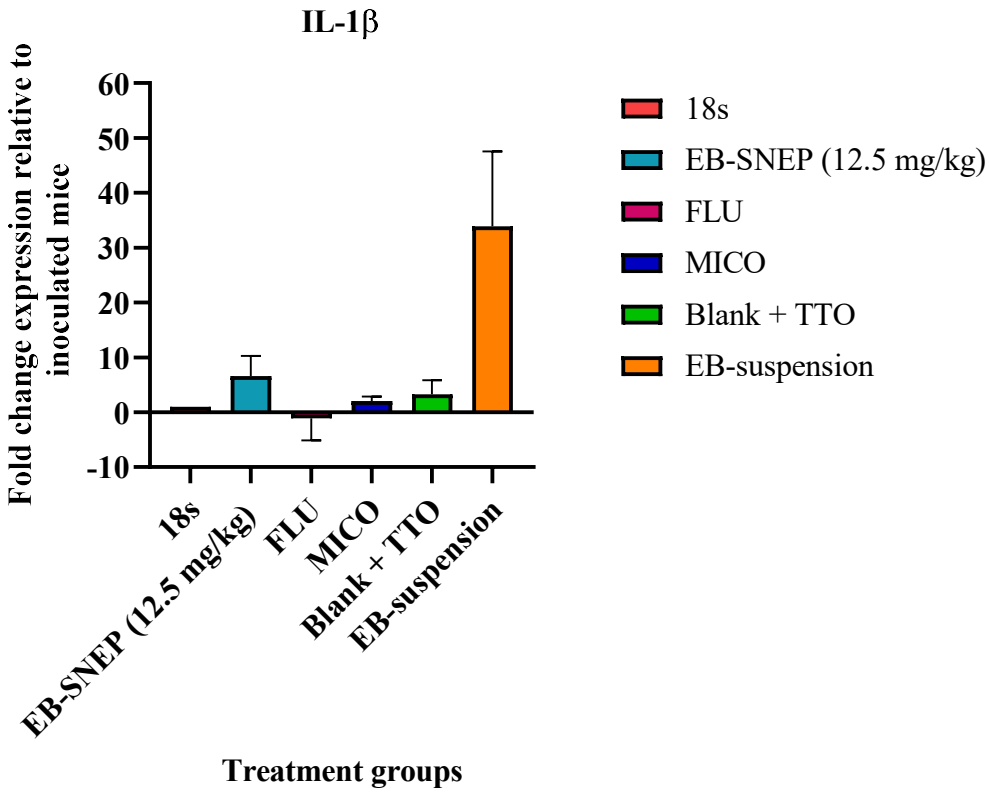

Figure 46: Gene expression of IL-1β by the mouse vaginal tissues. Mice were infected on day 0 and treated on day 3, 4, 5 and thereafter euthanized on day 6. Mouse vaginal tissues were excised, and total RNA was analyzed for each treatment groups with respect to control group (infected, untreated). Each bar represents the mean, and each vertical line represents the standard error of two representative experiments.

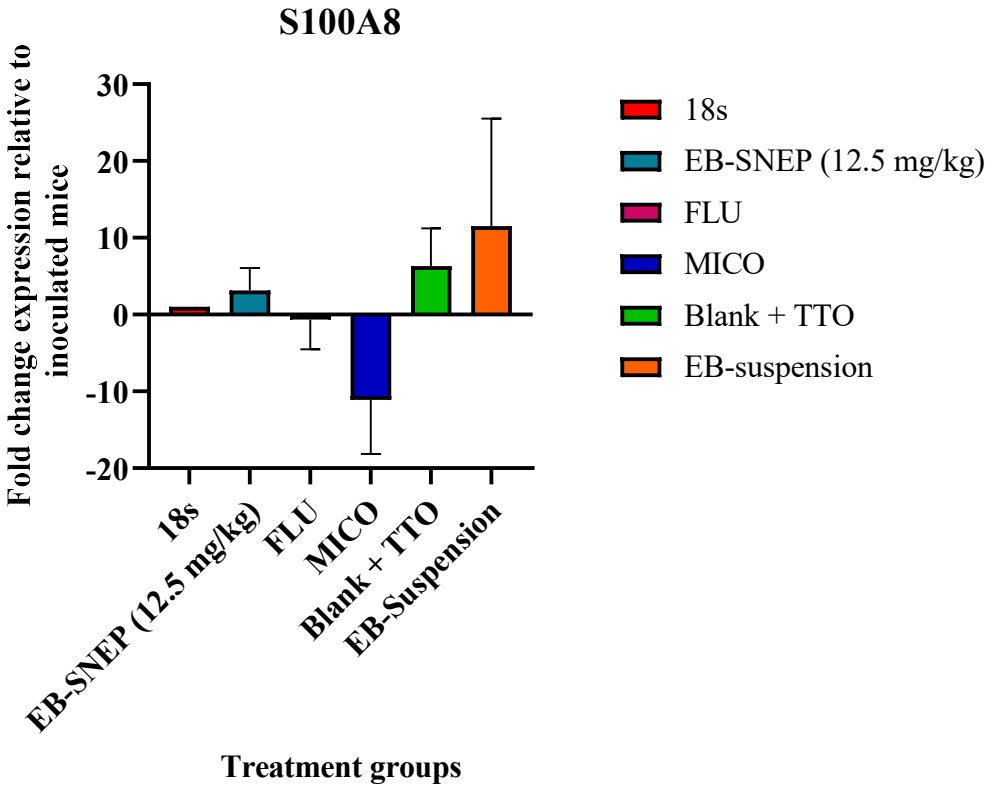

Figure 47:Gene expression of S100A8 by the mouse vaginal tissues. Mice were infected on day 0 and treated on day 3, 4, 5 and thereafter euthanized on day 6. Mouse vaginal tissues were excised, and total RNA was analyzed for each treatment groups with respect to control group (infected, untreated). Each bar represents the mean, and each vertical line represents the standard error of two representative experiments.

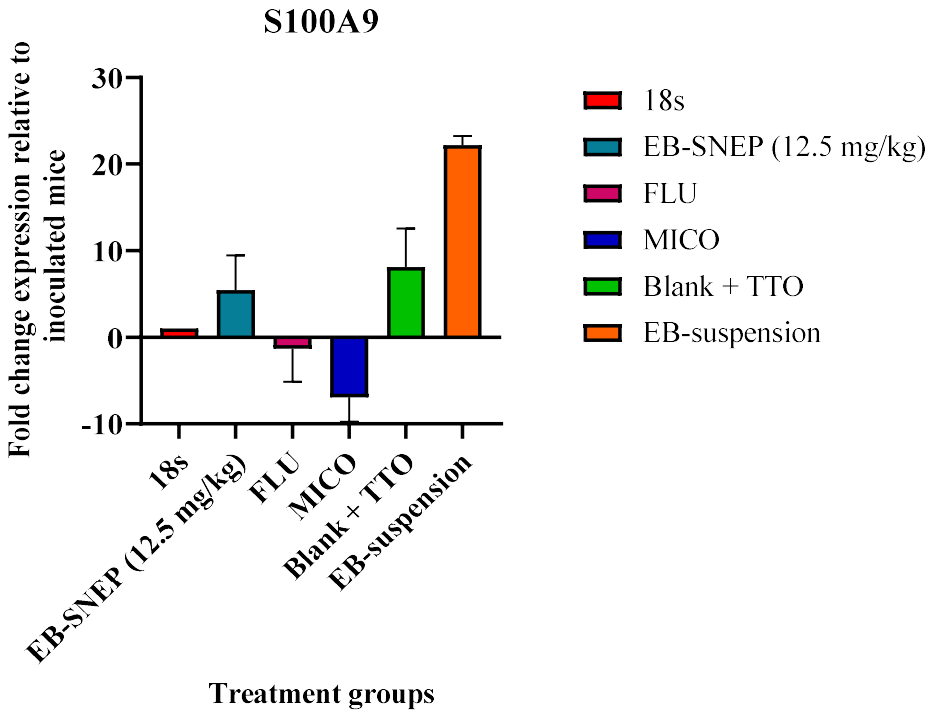

Figure 48:Gene expression of S100A9 by the mouse vaginal tissues. Mice were infected on day 0 and treated on day 3, 4, 5 and thereafter euthanized on day 6. Mouse vaginal tissues were excised, and total RNA was analyzed for each treatment groups with respect to control group (infected, untreated). Each bar represents the mean, and each vertical line represents the standard error of two representative experiments.

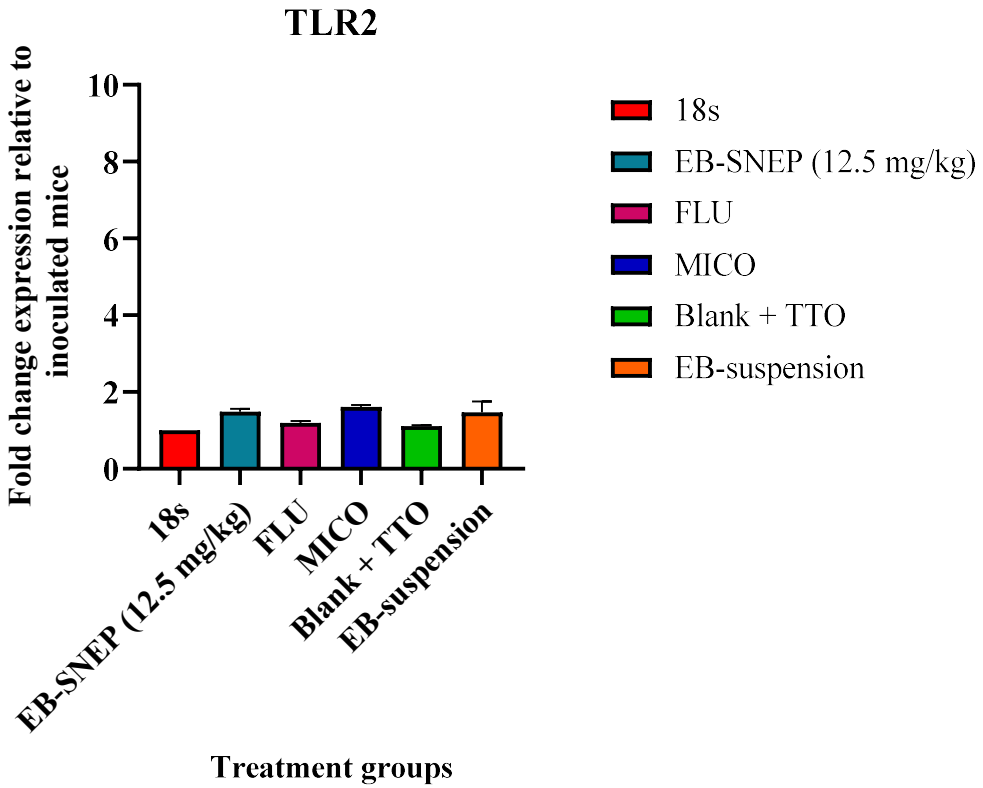

Figure 49:Gene expression of TLR2 by the mouse vaginal tissues. Mice were infected on day 0 and treated on day 3, 4, 5 and thereafter euthanized on day 6. Mouse vaginal tissues were excised, and total RNA was analyzed for each treatment groups with respect to control group (infected, untreated). Each bar represents the mean, and each vertical line represents the standard error of two representative experiments.

Appendix 5: *In vitro* and *in vivo* studies of G20 and G30

As per the *in vitro* studies conducted in our lab, EB analog G20 and G30 (provided by Dr. Magdalena Pietka-Ottlik, Wroclaw University, Poland), displayed superior antifungal activity compared to EB in both the test strains. Also, test compound G20 and G20 without chloro provided by Elizabeth Wojaczynska, Wroclaw University, Poland), were tested in S1 strain of *C. albicans*. We tested G20 and G30 in the mouse model of VVC. For this purpose, G20 and G30 SNEPs were prepared for intravaginal administration.

In vitro study using resazurin assay

This study was carried out with test compounds G20 and G20 without chloro group in S1 strain. The procedure for this assay can be found on Page 32 of this thesis in the Methods section.

Preparation of G20 and G30 SNEPs:

5 mg of drug (G20/G30) was dissolved in 40 µl of DMA. To this 460 µl of Captex: Kolliphor ELP (5:6) was added to prepare the final preconcentrate. Blank was prepared in the same way excluding the drug.

Blank was prepared by adding 40 µl DMA and 460 µl of Captex: Kolliphor ELP (5:6).

In vivo studies

Animal studies were carried out in the similar way as mentioned in the Methods for the intervention study.

Results

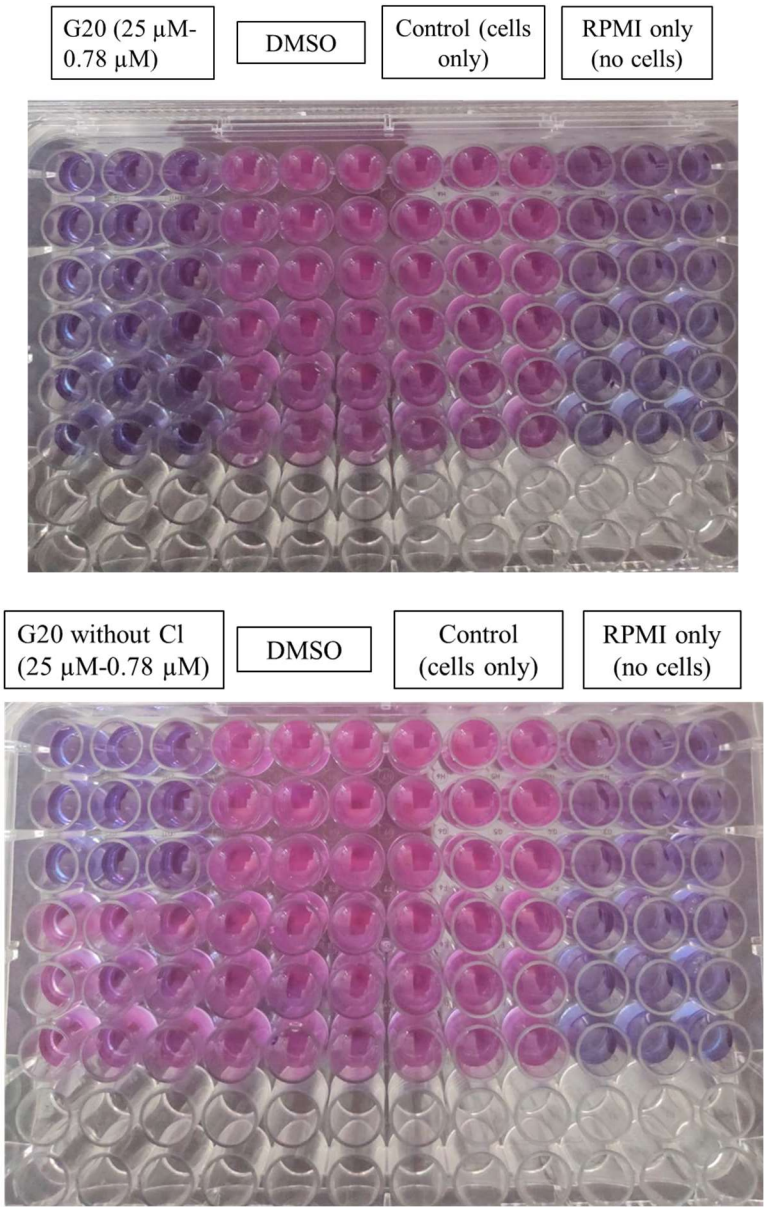

Figure 50: Representative image of resazurin assay for test compounds G20 and G20 without chloro with an equivalent MIC= 0.76 µM and 6.25 µM in S1 strain. Each plate represents experiments done in triplicate.

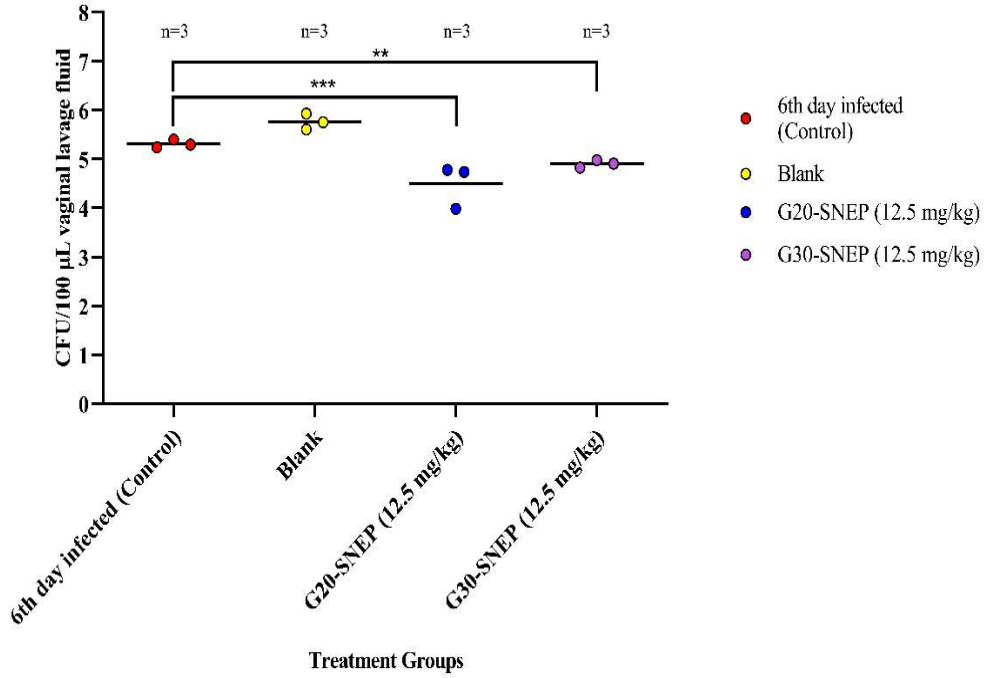

Figure 51: Efficacy of G20 and G30 (12.5 mg/kg) in the mouse model of VVC. On days 3, 4 and 5, mice with VVC received respective treatments via the intravaginal route once per day. Data shown are the CFUs obtained from each animal from the respective groups. The fungal burden of murine VVC was calculated on a scale of log10 (CFU/100 µL) in the vaginal lavage. Points on the curve represent individual mice, horizontal lines represent the geometric mean of each group.

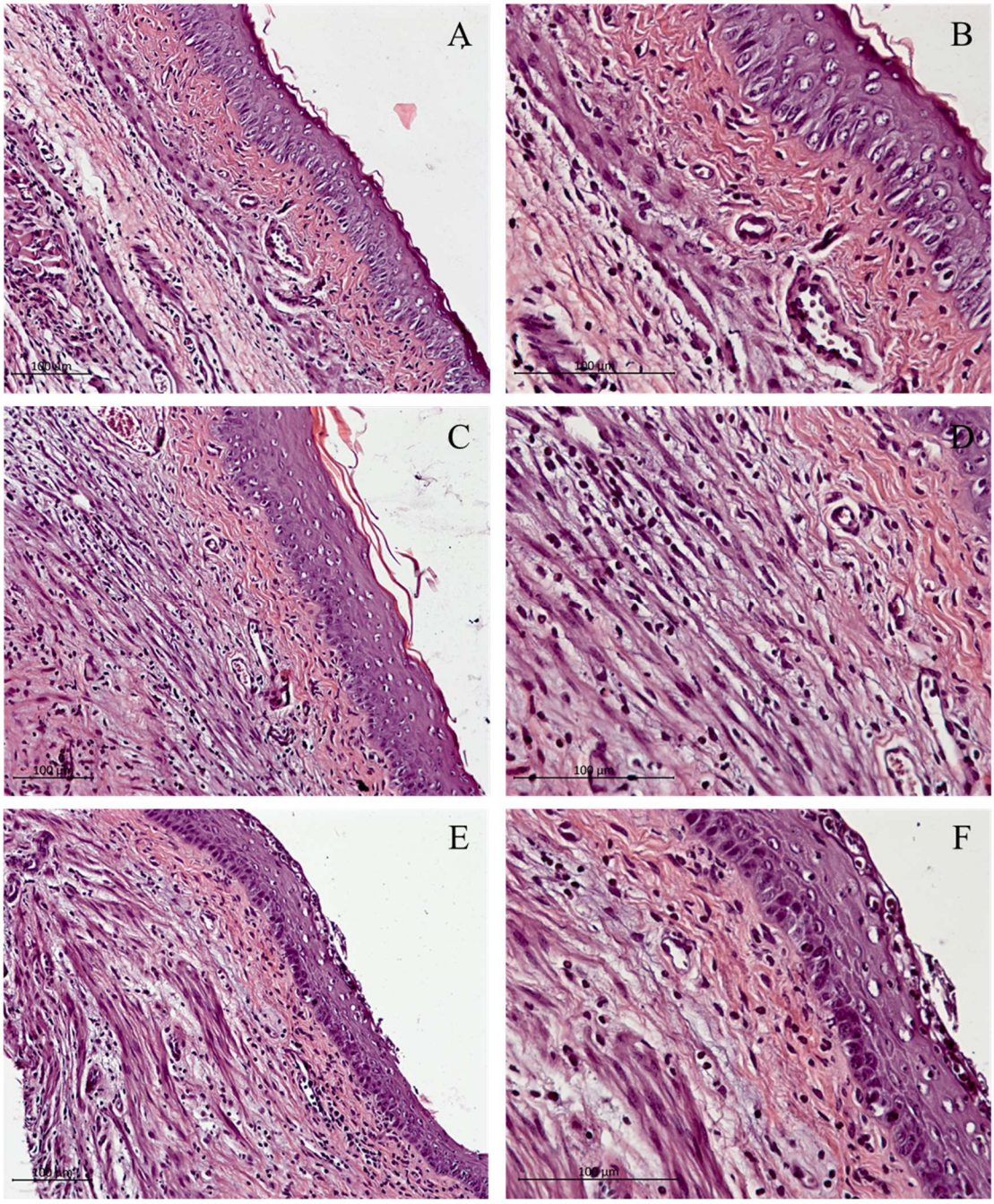

Figure 52: Representative light micrographs of H & E stained mouse vaginal tissues. (A) and (B) Blank group with edematous vaginal epithelial cells; (C) and (D) G20-SNEP (12.5 mg/kg) infected group showed intact keratin layer and slight epithelial hyperplasia; (E) and (F) G30-SNEP (12.5 mg/kg) group showed epithelial hyperplasia and epithelial layer sloughing. PMN infiltration were seen in the epithelial layer. Magnification used was 200x and 400x. Bars on the micrograph represent a length of 100 µm.

Table 21: Animal codes for *in vivo* study with test compounds G20 and G30

Sr. No.	Code	Body wt before Inj	Body wt after Inj	Date of Euthanization	Lavage fluid	Wt. of half vaginal tissue	Colonies	Dilution Factor	CFU/100 ul	Initial Inoculum dose
1	VA-5	19 g	19 g	2/3/2020	100 ul	0.0225 g	62	100	12400.00	1000000.00
2	VA-4	18 g	19 g	2/3/2020	100 ul	0.0333 g	37	1000	74000.00	1000000.00
3	RI-1	21 g	21g	9/17/2020	100 ul	0.0480 g	18	10	360.00	800000.00
4	RI-2	19 g	20 g	9/17/2020	100 ul	0.0425 g	28	100	5600.00	800000.00
5	RI-3	21 g	22 g	9/17/2020	100 ul	0.0453 g	4	10	80.00	800000.00
6	RI-4	20 g	22 g	9/17/2020	100 ul	0.0320 g	0	0	0.00	800000.00
7	RI-5	19 g	20g	9/17/2020	100 ul	0.0500 g	33	10	460.00	800000.00
8	RI-6	20 g	20 g	9/17/2020	100 ul	0.0480 g	71	100	14200.00	800000.00
9	RI-7	18 g	20 g	9/17/2020	100 ul	0.0300 g	55	100	11000.00	800000.00
10	RI-8	19 g	20 g	9/17/2020	100 ul	0.0320 g	60	1000	12000.00	800000.00
11	RI-9	20 g	21 g	9/17/2020	100 ul	0.0520 g	36	10,000	720000.00	800000.00
12	RI-10	19 g	21 g	9/17/2020	100 ul	0.0380 g	60	1000	120000.00	800000.00
13	R-11	20 g	22 g	9/17/2020	100 ul	0.0397 g	23	1000	46000.00	800000.00
14	RI-12	20 g	21 g	9/17/2020	100 ul	0.0448 g	45	10,000	900000.00	800000.00
15	Blk-7	22 g	23 g	10/10/2020	100 ul	Not done	42	10,000	840000.00	880000.00
16	Blk-8	21 g	21 g	10/10/2020	100 ul	Not done	28	10,000	560000.00	880000.00
17	Blk-9	21 g	22 g	10/10/2020	100 ul	Not done	20	10,000	400000.00	880000.00
18	VA-1	23 g	22 g	10/10/2020	100 ul	Not done	27	1000	54000.00	880000.00
19	VA-2	22 g	23 g	10/10/2020	100 ul	Not done	30	1000	60000.00	880000.00
20	VA-3	20 g	22 g	10/10/2020	100 ul	Not done	42	100	9600.00	880000.00
21	RI-13	20 g	22 g	10/10/2020	100 ul	Not done	40	1000	80000.00	880000.00
22	RI-14	20 g	21 g	10/10/2020	100 ul	Not done	47	1000	94000.00	880000.00
23	RI-15	19 g	20 g	10/10/2020	101 ul	Not done	33	1000	66000.00	880000.00

VA4 and VA-5: G20 suspension (12.5 mg/kg)

Study I: RI-1– RI-4: 0.25 mg G30
RI-5 – RI-8: 0.1 mg G30
RI-9 – RI-12: Blank

Study II: Blk-7 – Blk-9: Blank
VA-1 – VA-3: 0.25 mg G20
RI-13 – RI-15: 0.25 mg G30

REFERENCES

Alam MF., Safhi MM., Moni SS., and Jabeen A. (2016). *In vitro* antibacterial spectrum of sodium selenite against selected human pathogenic bacterial strains. *Scientifica*. 2016:9176273.

Amézqueta S., Subirats X., Fuguet E., Rosés M., and Ràfols C. (2020). Octanol-Water Partition Constant, in Handbooks in Separation Science: Liquid-Phase Extraction pp 183–208, Elsevier.

Arnér ESJ., and Holmgren A. (2000). Physiological functions of thioredoxin and thioredoxin reductase. *European Journal of Biochemistry*. 267:6102–6109.

Ayehunie S., Cannon C., Lamore S., Kubilus J., Anderson DJ., Pudney J., and Klausner M. (2006). Organotypic human vaginal-ectocervical tissue model for irritation studies of spermicides, microbicides, and feminine-care products. *Toxicology In Vitro.* 20:689–698.

Ayehunie S., Cannon C., LaRosa K., Pudney J., Anderson DJ., and Klausner M. (2011). Development of an *in vitro* alternative assay method for vaginal irritation. *Toxicology*. 279:130–138.

Barnett JA. (1998). A history of research on yeasts. 1: Work by chemists and biologists 1789–1850. *Yeast*. 14:1439–1451.

Barnett JA. (2000). A history of research on yeasts. 2: Louis Pasteur and his contemporaries, 1850–1880. *Yeast*. 16:755–771.

Benedict K., Jackson BR., Chiller T., and Beer KD. (2019). Estimation of direct healthcare costs of fungal diseases in the United States. *Clinical Infectious Diseases*. 68:1791–1797.

Billack B., Santoro M., and Lau-Cam C. (2009). Growth inhibitory action of ebselen on fluconazole-resistant *Candida albicans*: role of the plasma membrane H^+-ATPase. *Microbial Drug Resistance*. 15:77–83.

Billack B., Piętka-Ottlik M., Santoro M., Nicholson S., Młochowski J., and Lau-Cam C. (2010). Evaluation of the antifungal and plasma membrane H+-ATPase inhibitory action of ebselen and two ebselen analogs in *S. cerevisiae* cultures. *Journal of Enzyme Inhibition and Medicinal Chemistry*. 25:312–317.

Blackwell M. (2011). The fungi: 1, 2, 3 ... 5.1 million species? *American Journal of Botany*. 98:426–38.

Bondaryk M., Kurzątkowski W., and Staniszewska M. (2013). Antifungal agents commonly used in the superficial and mucosal candidiasis treatment: mode of action and resistance development. *Advances in Dermatology and Allergology*. 30:293–301.

Botstein D., Chervitz SA., and Cherry JM. (1997). Yeast as a model organism. *Science*. 277:1259–1260.

Botstein D., and Fink GR. (2011). Yeast: an experimental organism for 21st century biology. *Genetics*. 189:695–704.

Boyd K. L., Muehlenbachs A., Rendi M. H., Garcia R. L., and Gibson-Corley K. N. (2018). Female reproductive system, in *Comparative Anatomy and Histology: A Mouse and Human Atlas*. pp 303–334, Academic Press, San Diego.

Bradford L. L., and Ravel J. (2016). The vaginal mycobiome: a contemporary perspective on fungi in women's health and diseases. *Virulence* **8**:342–351.

Bruno V., Shetty A. C., Yano J., Fidel P., Noverr M., and Peters B. (2015). Transcriptomic analysis of vulvovaginal candidiasis identifies a role for the NLRP3 inflammasome. *American Society for Microbiology.* 6:e00182-15.

Burghoorn H. P., Soteropoulos P., Paderu P., Kashiwazaki R., and Perlin D. S. (2002). Molecular evaluation of the plasma membrane proton pump from *Aspergillus fumigatus*. *Antimicrobial Agents and Chemotherapy*. 46:615–624.

Cannon R. D., Lamping E., Holmes A. R., Niimi K., Baret P. V., Keniya M. V., Tanabe K., Niimi M., Goffeau A., and Monk B. C. (2009). Efflux-mediated antifungal drug resistance. *Clinical Microbiology Reviews*. 22:291–321.

Cassone A. (2015). Vulvovaginal *Candida albicans* infections: pathogenesis, immunity and vaccine prospects. *An International Journal of Obstetrics & Gynaecology*. 122:785–794.

Cassone A., and Sobel J. D. (2016). Experimental models of vaginal candidiasis and their relevance to human candidiasis. *Infection and Immunity*. 84:1255–1261.

Chan G., Hardej D., Santoro M., Lau-Cam C., and Billack B. (2007). Evaluation of the antimicrobial activity of ebselen: role of the yeast plasma membrane H+-ATPase. *Journal of Biochemical and Molecular Toxicology*. 21:252–264.

Chapple A. (2001). Vaginal thrush: perceptions and experiences of women of South Asian descent. *Health Education Research*. 16:9–19.

Chew P., Yuen D. Y. C., Stefanovic N., Pete J., Coughlan M. T., Jandeleit-Dahm K. A., Thomas M. C., Rosenfeldt F., Cooper M.E., and de Haan J.B. (2010). Antiatherosclerotic and renoprotective effects of ebselen in the diabetic apolipoprotein E/GPx1-double knockout mouse. *Diabetes*. 59:3198–3207.

Clinical and Laboratory Standards Institute. (2002). Reference method for broth dilution antifungal susceptibility testing of yeasts. Approved standard, 2nd edn. NCCLS document M27-A2. Wayne, PA: Clinical and Laboratory Standards Institute.

Collins K. B., Patterson B. K., Naus G. J., Landers D. V., and Gupta P. (2000). Development of an *in vitro* organ culture model to study transmission of HIV-1 in the female genital tract. *Nature Medicine*. 6:475–479.

Conti H. R., Huppler A. R., Whibley N., and Gaffen S. L. (2014). Animal models for candidiasis. *Current Protocols in Immunology*. 105:19.6.1-19.6.17.

Cotgreave I. A., Johansson U., Westergren G., Moldéus P. W., and Brattsand R. (1988). The anti-inflammatory activity of ebselen but not thiols in experimental alveolitis and bronchiolitis. *Agents Actions*. 24:313–319.

D'Cruz O. J., Yiv S. H., Waurzyniak B., and Uckun F. M. (2001). Contraceptive efficacy and safety studies of a novel microemulsion-based lipophilic vaginal spermicide. *Fertility and Sterility*. 75:115–124, Elsevier.

Dadar M., Tiwari R., Karthik K., Chakraborty S., Shahali Y., and Dhama K. (2018). *Candida albicans*- Biology, molecular characterization, pathogenicity, and advances in diagnosis and control – An update. *Microbial Pathogenesis*. 117:128–138.

da Silva Dantas A., Lee K. K., Raziunaite I., Schaefer K., Wagener J., Yadav B., and Gow N. (2016). Cell biology of *Candida albicans*-host interactions. *Current Opinion in Microbiology*. 34:111–118.

De Nollin S., and Borgers M. (1975). Scanning Electron Microscopy of *Candida albicans* after *in vitro* treatment with miconazole. *Antimicrobial Agents and Chemotherapy*. 7:704–711.

Donders G. G., Grinceviciene S., Ruban K., and Bellen G. (2020). Vaginal pH and microbiota during fluconazole maintenance treatment for recurrent vulvovaginal candidosis (RVVC). *Diagnostic Microbiology and Infectious Disease*. 97:115024.

Duan S. F., Han P. J., Wang Q. M., Liu W. Q., Shi J. Y., Li K., Zhang X. L., and Bai F. Y. (2018). The origin and adaptive evolution of domesticated populations of yeast from Far East Asia. *Natural Communications*. 9:2690.

El-Hammadi M. M., and Arias J. L. (2020). Nanotechnology for vaginal drug delivery and targeting, in *Nanoengineered Biomaterials for Advanced Drug Delivery* pp 647–682, Elsevier.

Fidel P. L., Vazquez J. A., and Sobel J. D. (1999). *Candida glabrata*: Review of epidemiology, pathogenesis, and clinical disease with comparison to *C. albicans*. *Clinical Microbiology Reviews*. 12:80–96.

Fidel P. L., Cutright J., and Steele C. (2000). Effects of reproductive hormones on experimental vaginal candidiasis. *Infection and Immunity.* 68:651–657.

Fidel P. L., Barousse M., Espinosa T., Ficarra M., Sturtevant J., Martin D. H., Quayle A. J., and Dunlap K. (2004). An intravaginal live *Candida* Challenge in humans leads to new hypotheses for the immunopathogenesis of vulvovaginal candidiasis. *Infection and Immunity*. 72:2939–2946.

Fisher M. C., Gurr S. J., Cuomo C. A., Blehert D. S., Jin H., Stukenbrock E. H., Stajich J. E., Kahmann R., Boone C., Denning D. W., Gow N., Klein B. S., Kronstad J. W., Sheppard D. C., Taylor J. W., Wright G. D., Heitman J., Casadevall A., and Cowen L. E. (2020). Threats Posed by the Fungal Kingdom to Humans, Wildlife, and Agriculture. *Mbio*. 11:e00449-20.

Franz R., Ruhnke M., and Morschhäuser J. (1999). Molecular aspects of fluconazole resistance development in *Candida albicans*. *Mycoses*. 42:453–458.

Ghose A. K., Viswanadhan V. N., and Wendoloski J. J. (1998). Prediction of hydrophobic (lipophilic) properties of small organic molecules using fragmental methods: An

analysis of ALOGP and CLOGP Methods. *The Journal of Physical Chemistry A* 102:3762–3772.

Giusto K., Patki M., Koya J., Ashby C. R., Munnangi S., and Patel K. (2019). A vaginal nanoformulation of a SphK inhibitor attenuates lipopolysaccharide-induced preterm birth in mice. *Nanomedicine*. 14:2835-2851.

Griffiths H. R., Dowling E, J., Sahinoglu T., Blake D. R., Parnham M., and Lunec J. (1992). The selective protection afforded by ebselen against lipid peroxidation in an ROS-dependent model of inflammation. *Agents Actions*. 36:107–111.

Gurpreet K., and Singh S. K. (2018). Review of nanoemulsion formulation and characterization techniques. *Indian Journal of Pharmaceutical Sciences* 80:781–789.

Gurtovenko A. A., and Anwar J. (2007). Modulating the structure and properties of cell membranes: The mechanism of action of dimethyl sulfoxide. *The Journal of Physical Chemistry B*. 111:10453–10460.

Harriott M. M., Lilly E. A., Rodriguez T. E., Fidel P. L., and Noverr M. C. (2010). *Candida albicans* forms biofilms on the vaginal mucosa. *Microbiology*. 156:3635–3644.

Hayashi M., and Slater T. F. (1986). Inhibitory effects of ebselen on lipid peroxidation in rat liver microsomes. *Free Radical Research*. 2:179–185.

Hitchcock C. A. (1993). Resistance of *Candida albicans* to azole antifungal agents. *Biochemical Society Transactions*. 21:1039–1047.

Irving G., Miller D., Robinson A., Reynolds S., and Copas A. J. (1998). Psychological factors associated with recurrent vaginal candidiasis: a preliminary study. *Sexually Transmitted Infections*. 74:334–338.

Jaromin A., Zarnowski R., Piętka-Ottlik M., Andes D. R., and Gubernator J. (2018). Topical delivery of ebselen encapsulated in biopolymeric nanocapsules: drug repurposing enhanced antifungal activity. *Nanomedicine*. 13:1139–1155.

Kil J., Pierce C., Tran H., Gu R., and Lynch E. D. (2007). Ebselen treatment reduces noise induced hearing loss via the mimicry and induction of glutathione peroxidase. *Hearing Research*. 226:44–51.

Koga-Ito C. Y., Lyon J. P., and de Resende M. A. (2008). Comparison between E-test and CLSI broth microdilution method for antifungal susceptibility testing of *Candida albicans* oral isolates. *Revista do Instituto de Medicina Tropical*. 50:7–10.

Kollerup Madsen B., Hilscher M., Zetner D., and Rosenberg J. (2019). Adverse reactions of dimethyl sulfoxide in humans: a systematic review. *F1000Res* 7:1746. doi: 10.12688/f1000research.16642.2

Kovács R., Czudar A., Horváth L., Szakács L., Majoros L., and Kónya J. (2014). Serum interleukin-6 levels in murine models of *Candida albicans* infection. *Acta Microbiologica et Immunologica Hungarica*. 61:61–69.

Kühbacher A., Burger-Kentischer A., and Rupp S. (2017). Interaction of *Candida* species with the skin. *Microorganisms*. 5:32. doi: 10.3390/microorganisms5020032

Kumar R., Saraswat D., Tati S., and Edgerton M. (2015). Novel aggregation properties of *Candida albicans* secreted aspartyl proteinase Sap6 mediate virulence in oral candidiasis. *Infection and Immunity*. 83:2614–2626. doi: 10.1128/IAI.00282-15

Lara H. H., Romero-Urbina D. G., Pierce C., Lopez-Ribot J. L., Arellano-Jiménez M. J., and Jose-Yacaman M. (2015). Effect of silver nanoparticles on *Candida albicans* biofilms: an ultrastructural study. *Journal of Nanobiotechnology*. 13:91. doi: 10.1186/s12951-015-0147-8

Larkin E., Hager C., Chandra J., Mukherjee P. K., Retuerto M., Salem I., Long L., Isham N., Kovanda L., Borroto-Esoda K., Wring S., Angulo D., and Ghannoum M. (2017). The emerging pathogen *Candida auris*: growth phenotype, virulence factors, activity of antifungals, and effect of scy-078, a novel glucan synthesis inhibitor, on growth morphology and biofilm formation. *Antimicrobial Agents* and *Chemotherapy*. 61:e02396. doi: 10.1128/AAC.02396-16

Liao H., Liu S., Wang H., Su H., and Liu Z. (2017). Efficacy of histatin5 in a murine model of vulvovaginal candidiasis caused by *Candida albicans*. *Pathogens and Disease*. 75. doi: 10.1093/femspd/ftx072

Malík I., Bukovský M., Andriamainty F., and Gališinová J. (2012). Antimicrobial activity of meta-alkoxyphenylcarbamates containing substituted N-phenylpiperazine fragment. *Brazilian Journal of Microbiology*. 43:959–965.

Mannaa M., and Kim K. D. (2018). Effect of temperature and relative humidity on growth of *Aspergillus* and *Penicillium* spp. and biocontrol activity of *Pseudomonas*

protegens AS15 against Aflatoxigenic *Aspergillus flavus* in stored rice grains. *Mycobiology*. 46:287–295.

Martinez R. C., Franceschini S. A., Patta M. C., Quintana S. M., Candido R. C., Ferreira J. C., Martinis E. C., and Reid G. (2009). Improved treatment of vulvovaginal candidiasis with fluconazole plus probiotic *Lactobacillus rhamnosu*s GR-1 and *Lactobacillus reuteri* RC-14. *Letters in Applied Microbiology*. 48:269–274.

McAleer W. J., Buynak E. B., Maigetter R. Z., Wampler D. E., Miller W. J., and Hilleman M. R. (1984). Human hepatitis B vaccine from recombinant yeast. *Nature*. 307:178–180.

Menéndez C. A., Byléhn F., Perez-Lemus G. R., Alvarado W., and de Pablo J. J. (2020). Molecular characterization of ebselen binding activity to SARS-CoV-2 main protease. *Science Advances*. 6:eabd3045. doi: 10.1126/sciadv.abd0345.

Merkhofer R. M., and Klein B. S. (2020). Advances in understanding human genetic variations that influence innate immunity to fungi. *Frontiers in Cellular and Infection Microbiology*. 10:69. doi: 10.3389/fcimb.2020.00069

Miller E. A., Beasley D. E., Dunn R. R., and Archie E. A. (2016). *Lactobacilli* dominance and vaginal pH: why is the human vaginal microbiome unique? *Frontiers in Microbiology*. 7: 1936. doi: 10.3389/fmicb.2016.01936

Mirza M. A., Ahmad S., Mallick M. N., Manzoor N., Talegaonkar S., and Iqbal Z. (2013). Development of a novel synergistic thermosensitive gel for vaginal candidiasis: An *in vitro*, *in vivo* evaluation. *Colloids and Surfaces B: Biointerfaces*. 103:275–282.

Missall T. A., and Lodge J. K. (2005). Thioredoxin reductase is essential for viability in the fungal pathogen *Cryptococcus neoformans*. *Eukaryotic Cell*. 4:487–489.

Monk B. C., Niimi K., Lin S., Knight A., Kardos T. B., Cannon R. D., Parshot R., King A., Lun D., and Harding D. R. (2005). Surface-active fungicidal D-peptide inhibitors of the plasma membrane proton pump that block azole resistance. *Antimicrobial Agents and Chemotherapy*. 49:57–70.

Morschhäuser J. (2002). The genetic basis of fluconazole resistance development in *Candida albicans*. *Biochimica et Biophysica Acta*. 1587:240–248.

Mouithys-Mickalad A., Faez J. M., Chistiaens L., Kohnen S., Deby C., Hoebeke M., Lamy M., and Deby-Dupont G. (2004). *In vitro* evaluation of glutathione peroxidase (GPx)-like activity and antioxidant properties of some Ebselen analogues. *Redox Report*. 9:81–87.

Mousavi B., Hedayati M., Hedayati N., Ilkit M., and Syedmousavi S. (2016). Aspergillus species in indoor environments and their possible occupational and public health hazards. *Current Medical Mycology*. 2:36–42.

Naglik J. R., Fidel P. L., and Odds F. C. (2008). Animal models of mucosal *Candida* infection. *FEMS Microbiology Letters*. 283:129–139.

Nakamura Y., Feng Q., Kumagai T., Torikai K., Ohigashi H., Osawa T., Noguchi N., Niki E., and Uchida K. (2002). Ebselen, a glutathione peroxidase mimetic seleno-organic compound, as a multifunctional antioxidant. Implication for inflammation-associated carcinogenesis. *Journal of Biological Chemistry.* 277:2687–2694.

Nazzaro F., Fratianni F., Coppola R., and De Feo V. (2017). Essential oils and antifungal activity. *Pharmaceuticals*. 10:86.

Nobile C. J., and Johnson A. D. (2015). *Candida albicans* biofilms and human disease. *Annual Review of Microbiology*. 69:71–92.

Nozawa R., Arai M., Kuruto R., Motohashi T., and Masayasu H. (1996). Susceptibility of mice to bacterial and fungal infections after intragastric administration of ebselen. *Journal of Pharmacy and Pharmacology* 48:64–67.

Orie N. N., Warren A. R., Basaric J., Lau-Cam C., Piętka-Ottlik M., Młochowski J., and Billack B. (2017). *In vitro* assessment of the growth and plasma membrane H^+-ATPase inhibitory activity of ebselen and structurally related selenium- and sulfur-containing compounds in *Candida albicans*. *Journal of Biochemical and Molecular Toxicology*. 31.

Pankhurst C. L. (2009). Candidiasis (oropharyngeal). *BMJ Clinical Evidence*. 2009:1304**.**

Pappas P. G., Lionakis M. S., Arendrup M. C., Ostrosky-Zeichner L., and Kullberg B. J. (2018). Invasive candidiasis. *Nature Reviews Disease Primers*. 4:1–20.

Parnham M., and Sies H. (2000). Ebselen: prospective therapy for cerebral ischaemia. *Expert Opinion on Investigational Drugs*. 9:607–619.

Perlin D. S., Brown C. L., and Haber J. E. (1988). Membrane potential defect in hygromycin B-resistant pma1 mutants of *Saccharomyces cerevisiae*. *Journal of Biological Chemistry*. 263:18118–18122.

Qu S., Chen L., Tian H., Wang Z., Wang F., Wang L., Li J., Ji H., Xi L., Feng Z., Tian J., and Feng Z. (2019). Effect of perillaldehyde on prophylaxis and treatment of vaginal candidiasis in a murine model. *Frontiers in Microbiology*. 10:1466.

Radhakrishna M., Sharadamma C., Vagdevi M., Abhilekha M., Rubeena S., and Nischal K. (2010). Synthesis and antibacterial activity of novel organoselenium compounds. *International Journal of Chemistry*. 2:149-154.

Ray A., Ray S., George A. T., and Swaminathan N. (2011). Interventions for prevention and treatment of vulvovaginal candidiasis in women with HIV infection. The *Cochrane Database of Systematic Reviews*. CD008739.

Ren X., Zou L., Lu J., and Holmgren A. (2018). Selenocysteine in mammalian thioredoxin reductase and application of ebselen as a therapeutic. *Free Radical Biology and Medicine*. 127:238–247.

Rossato L., and Colombo A. L. (2018). *Candida auris*: what have we learned about its mechanisms of pathogenicity? *Frontiers in Microbiology*. 9:3081.

Segal E., and Frenkel M. (2018). Experimental *in vivo* models of candidiasis. *Journal of Fungi*. 4:21.

Sies H. (1993). Ebselen, a selenoorganic compound as glutathione peroxidase mimic. *Free Radical Biology and Medicine*. 14:313–323.

Singh N., Halliday A. C., Thomas J. M., Kuznetsova O. V., Baldwin R., Woon ECY, Aley PK, Antoniadou I, Sharp T, Vasudevan SR, and Churchill GC (2013). A safe lithium mimetic for bipolar disorder. *Nature Communications*. 4:1332.

Singh N., Sharpley A. L., Emir U. E., Masaki C., Herzallah M. M., Gluck M. A., Sharp T., Harmer C. J., Vasudevan S. R., Cowen P. J., and Churchill G. C. (2016). Effect of the putative lithium mimetic ebselen on brain myo -inositol, sleep, and emotional processing in humans. *Neuropsychopharmacology*. 41:1768–1778.

Soteropoulos P., Vaz T., Santangelo R., Paderu P., Huang D. Y., Tamás M. J., and Perlin D. S. (2000). Molecular characterization of the plasma membrane H+-ATPase, an antifungal target in *Cryptococcus neoformans*. *Antimicrobial Agents and Chemotherapy*. 44:2349–2355.

Southwell I. A., Freeman S., and Rubel D. (1997). Skin irritancy of tea tree oil. *Journal of Essential Oil Research* 9:47–52.

Spampinato C., and Leonardi D. (2013). *Candida* infections, causes, targets, and resistance mechanisms: traditional and alternative antifungal agents. *Biomed Research International*. 2013:204237.

Superti F., and De Seta F. (2020). Warding off recurrent yeast and bacterial vaginal infections: lactoferrin and *lactobacilli*. *Microorganisms*. 8:130.

Tumu H., Cuffari B. J., Pino M. A., Palus J., Piętka-Ottlik M., and Billack B. (2020). Ebselen oxide attenuates mechlorethamine dermatotoxicity in the mouse ear vesicant model. *Drug and Chemical Toxicology*. 43:335–346.

Vandeputte P., Ferrari S., and Coste A. T. (2012). Antifungal resistance and new strategies to control fungal infections. *International Journal of Microbiology*. 2012:713687.

Vartak R., Patki M., Menon S., Jablonski J., Mediouni S., Fu Y., Valente S. T., Billack B., and Patel K. (2020). β-cyclodextrin polymer/Soluplus® encapsulated ebselen ternary complex (EβpolySol) as a potential therapy for vaginal candidiasis and pre-exposure prophylactic for HIV. *International Journal of Pharmaceutics*. 589:119863.

Vartak R., Menon S., Patki M., Billack B., and Patel K. (2020b) Ebselen nanoemulgel for the treatment of topical fungal infection. *European Journal of Pharmaceutical Sciences* 148:105323.

de Vasconcelos L. C., Sampaio F. C., Albuquerque A., and Vasconcelos L. C. (2014). Cell viability of *Candida albicans* against the antifungal activity of thymol. *Brazilian Dental Journal*. 25:277–281.

Vermani K., and Garg S. (2000). The scope and potential of vaginal drug delivery. *Pharmaceutical Science & Technology Today*. 3:359–364.

Walzl A., Unger C., Kramer N., Unterleuthner D., Scherzer M., Hengstschläger M., Schwanzer P. D., and Dolznig H. (2014). The resazurin reduction assay can distinguish cytotoxic from cytostatic compounds in spheroid screening assays. *Journal of Biomolecular Screening*. 19:1047–1059.

Wang X., Bing J., Zheng Q., Zhang F., Liu J., Yue H., Tao L., Du H., Wang Y., Wang H., and Huang G. (2018). The first isolate of *Candida auris* in China: clinical and biological aspects. *Emerging Microbes and Infections*. 7:93.

Watts C. J., Wagner D. K., and Sohnle P. G. (2009). Fungal infections, cutaneous, in *Encyclopedia of Microbiology (Third Edition)* pp 382–388, Academic Press, Oxford.

Willems H. M. E., Ahmed S. S., Liu J., Xu Z., and Peters B. M. (2020). Vulvovaginal candidiasis: a current understanding and burning questions. *Journal of Fungi*. 6:27.

Witkin S. S., and Linhares I. M. (2017). Why do lactobacilli dominate the human vaginal microbiota? *An International Journal of Obstetrics & Gynaecology*. 124:606–611.

Wu X., Zhang S., Li H., Shen L., Dong C., Sun Y., Chen H., Xu B., Zhuang W., Deighton M., and Qu Y. (2020). Biofilm formation of *Candida albicans* facilitates fungal infiltration and persister cell formation in vaginal candidiasis. *Frontiers in Microbiology*. 11:1117.

Yamaguchi T., Sano K., Takakura K., Saito I., Shinohara Y., Asano T., and Yasuhara H. (1998). Ebselen in acute ischemic stroke. *Stroke*. 29:12–17.

Yang B., and Rao R. (2018). Emerging pathogens of the *Candida* species, in *Candida Albicans*, IntechOpen.

Yano J., Lilly E., Barousse M., and Fidel P. L. (2010). Epithelial cell-derived S100 calcium-binding proteins as key mediators in the hallmark acute neutrophil response during *Candida* vaginitis. *Infection and Immunity*. 78:5126–5137.

Yano J., and Fidel, Jr. P. L. (2011). Protocols for vaginal inoculation and sample collection in the experimental mouse model of *Candida* vaginitis. *Journal of Visualized Experiments*. 58:3382.

Yano J., Kolls J. K., Happel K. I., Wormley F., Wozniak K. L., and Fidel P. L. (2012). The acute neutrophil response mediated by S100 alarmins during vaginal *Candida* infections is independent of the Th17-pathway. *PLoS One* 7:e46311. doi: 10.1371/journal.pone.0046311

Yano J., Peters B. M., Noverr M. C., and Fidel P. L. Jr. (2018). Novel mechanism behind the immunopathogenesis of vulvovaginal candidiasis: "Neutrophil anergy". *Infection and Immunity*. 86: e00684-17. doi: 10.1128/IAI.00684-17

Zangl I., Pap I. J., Aspöck C., and Schüller C. (2020). The role of lactobacillus species in the control of *Candida* via biotrophic interactions. *Microbial Cell*. **7**:1–14.

Zeng Y., Qian Y., Ma L., and Gu H. (2007). Genome-wide expression profiling of the response to terbinafine in *Candida albicans* using a cDNA microarray analysis. *Chinese Medical Journal*. 120:807–813.

Zhang J. E., Luo D., Chen R. Y., Yang Y. P., Zhou Y., and Fan Y. M. (2013). Feasibility of histological scoring and colony count for evaluating infective severity in mouse vaginal candidiasis. *Experimental Animals*. 62:205–210.

Zhang X., Li T., Chen X., Wang S., and Liu Z. (2018). Nystatin enhances the immune response against *Candida albicans* and protects the ultrastructure of the vaginal epithelium in a rat model of vulvovaginal candidiasis. *BioMed Central Microbiology*. 18:166.

Zou L., Lu J., Wang J., Ren X., Zhang L., Gao Y., Rottenberg M. E., and Holmgren A. (2017). Synergistic antibacterial effect of silver and ebselen against multidrug-resistant Gram-negative bacterial infections. *EMBO Molecular Medicine*. 9:1165–1178.

VITA

Name:	*Suvidha M. Menon*
Master's Degree	*Master of Pharmacology*
	NMIMS University,
	Mumbai, India
	Major: Pharmacology
Date Graduated:	*August 2013*
Baccalaureate Degree:	*Bachelor of Pharmacy*
	Mumbai University, India
	Major: Pharmacy
Date Graduated:	*June 2010*